PERMEABILITY MODELING OF SYMMETRIC GRAPHITE EPOXY LAMINATES WITH ARBITRARY PLY ORIENTATIONS

By

ABHIJEET UTTURKAR

Bachelor of Engineering

University of Pune

Pune, India

(June, 2001)

Submitted to the Faculty of the
Graduate College of the
Oklahoma State University
in partial fulfillment of
the requirements for
the Degree of
MASTER OF SCIENCE
May, 2005

PERMEABILITY MODELING OF SYMMETRIC GRAPHITE EPOXY LAMINATES WITH ARBITRARY PLY ORIENTATIONS

Thesis approved:

Dr. Samit Roy

Thesis Adviser

Dr. Hong Bing Lu

Dr. Ronald Delahoussaye

Dr. A. Gordon Emslie

Dean of the Graduate College

ACKNOWLEDGEMENTS

I wish to express my gratitude to my parents for their confidence in me. I would like to thank them for their consistent encouragement and love. I would like to express my gratitude to my sister for her inspiration and support. My special thanks are due to my roommates for their motivation and support during my studies.

I would like to express my sincere thanks to my adviser, Dr. Samit Roy for his supervision, constructive guidance, financial support and inspiration throughout the study. I would like to thank him for providing me with sophisticated and friendly work environment. My master's studies under him was a wonderful experience. I would also like to extend my sincere appreciation to Dr. R. D. Delahoussaye and Dr. Hongbing Lu for providing invaluable guidance and encouragement throughout this study. I would also like to thank Dr. Ghajar for his help and guidance.

This project has been funded by the grant (NAG-1-02016) from the National Aeronautics and Space Administration (NASA), Langley, VA. I would like to thank Dr. Thomas Gates for his interest and support of this work.

I wish to express my sincere gratitude to Mr. Michael Putti-Benjamin for his co-operation, discussions and friendship in this study. I wish to extend my gratitude to Mr. Abilash Nair for discussions on first order shear deformation theory and analytical model during this study. I would like to thank my research colleagues for their constant help and encouragement.

Finally, I would like to thank the Department of Mechanical and Aerospace Engineering for providing me with the opportunity to pursue M.S. at Oklahoma State University.

TABLE OF CONTENTS

Chapter **Page**

1. INTRODUCTION……...…..1

1.1 Introduction……..……...…...1

1.2 Thesis outline….……...……...…..4

2. LITERATURE REVIEW……..6

3. OBJECTIVE AND APPROACH ……...……...12

4. ANALYTICAL SOLUTION FOR DCOD USING FIVE LAYER MODEL.……14

4.1 Introduction……..……..…….……...……...…..14

4.2 Analytical expression for Five Layer Model...…..…….16

5. ANALYTICAL SOLUTION FOR DCOD USING THREE LAYER MODEL…….21

5.1 Introduction……..……..…….……....……...…..21

5.2 Analytical expression for Three Layer Model....…..……..….23

6. IN-SITU DAMAGE EFFECTIVE FUNCTION…….....27

6.1 Introduction……..…..……..…….……....……...……....27

6.2 IDEF calculation……..29

6.2.1 For Five layer model…….29

6.2.2 For Three layer model……...29

6.3 Total strain energy calculation approach…….30

6.3.1 For Five layer model…….…….30

6.3.2 For Three layer model……....30

6.4 Strain energy release rate calculation approach …….31

6.4.1 SERR for matrix cracking……....31

6.4.2 SERR for delamination growth……....33

7. FINITE ELEMENT MODELING……..…….....35

8. RESULTS AND DISCUSSION…….…….....39

8.1 FLM – FEA comparison ……...……39

8.2 Effect of crack density on DCOD…..……...……...….…....50

8.3 Effect of delamination length on DCOD……..54

8.4 Effect of mechanical force on DCOD……62

8.5 Effect of temperature difference on DCOD……...……64

8.6 Combined effect of mechanical and thermal load on DCOD……...…….66

8.7 Permeability model results….……68

8.8 Damage growth prediction……...……..72

9. CONLUSIONS……...…….....75

REFERENCES.....77

APPENDICES……..…….80

Appendix A : Five layer model laminate analysis ....……81

Appendix B : Three layer model laminate analysis….……..……96

Appendix C : Constants in Three layer model analysis….……..107

LIST OF TABLES

Table **Page**

1.1 Material properties of IM7/PETI-5…...……..…...……...……..4

LIST OF FIGURES

Figure **Page**

1.1 Cross-ply laminate subjected to uniaxial loading and resulting damage...……..2

1.2 Permeation path at overlap of transverse cracks in arbitrary orientation plies…....3

2.1 Micro-crack in 90º ply block of a [0/90]2S specimen [17] …….…….…….10

4.1 Transverse crack and delaminations under uniaxial tensile load in Five Layer Model……..…15

4.2 Crack spacing and delaminations length in Five Layer Model……..16

4.3 One quarter of repeating interval of five layer model case ...……..…..17

5.1 Transverse crack and delaminations under uniaxial tensile load in a Three Layer Model ……..……..22

5.2 One quarter of repeating interval of three layer model case ……23

7.1 2-D FEA model of Case1 (Five Layer Model) for [0/90/0]s ……37

7.2 2-D FEA model of Case2 (Three Layer Model) for [0/90/0]s ……..……38

7.3 3-D FEA model mesh with 3-D 8 node brick elements, length X=0.5 inch, width Z=1 inch, thickness of half laminate Y=0.024 inch ……..38

8.1 $[0/90/0]_s$ laminate, crack in 90˚ layer FLM-FEA comparison, Mechanical Load ……... 40

8.2 $[45/0/-45/90]_s$ laminate crack in 0˚ layer FLM-FEA comparison DCOD (TOP) Mechanical load …….…….. 40

8.3 $[45/0/-45/90]_s$ laminate with crack in 0˚ layer FLM-FEA comparison S=0.25”and L=0.01”, DCOD (BOTTOM) Mechanical load ……..… 41

8.4 $[45/0/-45/90]_s$ laminate with crack in 0˚ layer FLM-FEA comparison S=0.25”and L=0.01”, DCOD (TOP) Thermal load ……...…….. 41

8.5 $[45/0/-45/90]_s$ laminate with crack in 0˚ layer FLM-FEA comparison S=0.25”and L=0.01”, DCOD (BOTTOM) Thermal load ……...……. 42

8.6 $[45/0/-45/90]_s$ laminate with crack in -45˚ layer FLM-FEA comparison S=0.25”and L=0.01”, DCOD (TOP) Mechanical load ……...……. 42

8.7 $[45/0/-45/90]_s$ laminate with crack in -45˚ layer FLM-FEA comparison S=0.25”and L=0.01”, DCOD (BOTTOM) Mechanical load ……..……. 43

8.8 $[45/0/-45/90]_s$ laminate with crack in -45˚ layer FLM-FEA comparison S=0.25” and L=0.01”, DCOD (TOP) Thermal load …….. 43

8.9 $[45/0/-45/90]_s$ laminate with crack in -45˚ layer FLM-FEA comparison S=0.25” and L=0.01”, DCOD (BOTTOM) Thermal load …… 44

8.10 $[45/0/-45/90]_s$ laminate with crack in 0˚ layer FLM-FEA crack shape comparison, S=0.25”and L=0.01” ΔT = -495˚F …….. 45

8.11 $[45/0/-45/90]_s$ laminate with crack in 0˚ layer FLM-FEA crack shape comparison, S=0.25”and L=0.01” N_m=1000 lb/in …….…….. 45

8.12 $[45/0/-45/90]_s$ laminate with crack in -45˚ layer FLM-FEA crack shape comparison, S=0.25”and L=0.01” ΔT = -495˚F …….. 46

8.13 $[45/0/-45/90]_s$ laminate with crack in -45˚ layer FLM-FEA crack shape comparison, S=0.25”and L=0.01” N_m=1000 lb/in …….. 46

8.14 $[45/0/-45/90]_s$ laminate with crack in 45˚ layer TLM-FEA crack profile comparison, S=0.25”and L=0.01”, N_m=1000 lb/in…….. 47

8.15 $[45/0/-45/90]_s$ laminate with crack in 45˚ layer TLM-FEA crack profile comparison, S=0.25”and L=0.01”, ΔT = -495˚F ..…….. 47

8.16 $[45/0/-45/90]_s$ laminate with crack in 90˚ layer TLM-FEA crack profile comparison, S=0.25”and L=0.01”, N_m=1000 lb/in …….. 48

8.17 $[45/0/-45/90]_s$ laminate with crack in 90˚ layer TLM-FEA crack profile comparison, S=0.25”and L=0.01”, ΔT = -495˚F....…….. 48

8.18 $[45/0/-45/90]_s$ laminate with crack in layers FLM-FEA DCOD comparison, S=0.25”and L=0.01”, N_m=1000 lb/in ……...…….. 49

8.19 $[45/0/-45/90]_s$ laminate with crack in layers FLM-FEA DCOD comparison, S=0.25”and L=0.01”, ΔT = -495˚F……....…….. 49

8.20 $[0/90/0]_s$ laminate with crack in 90˚ layer (FLM) for ΔT = -495˚F, =0.01”…..…50

8.21 $[0/90/0]_s$ laminate with crack in 90˚ layer (FLM) for N_m = 1000 lb/in, L=0.01”..51

8.22 $[45/0/-45/90]_s$ laminate with crack in -45˚ layer (FLM) for ΔT = -495˚F and L=0.01” …… 51

8.23 $[45/0/-45/90]_s$ laminate with crack in -45˚ layer (FLM) for N_m = 1000 lb/in and L=0.01” …….....52

8.24 $[45/0/-45/90]_s$ laminate with crack in -45˚ layer (FLM) for ΔT = -495˚F and L=0.01” ……..…….. 52

8.25 45/0/-45/90]$_s$ laminate with crack in -45˚ layer (FLM) for N_m = 1000 lb/in and L=0.01” …… 53

8.26 [45/0/-45/90]$_s$ laminate with crack in top 45˚ layer (TLM) for ΔT = -495˚F and L=0.01” …… 53

8.27 [45/0/-45/90]$_s$ laminate with crack in top 45˚ layer (TLM) for N_m = 1000 lb/in and L=0.01” ……..…….. 54

8.28 [0/90/0]$_s$ laminate with crack in 90˚ layer (FLM) for ΔT = -495˚F and S=0.25” …….....…… 55

8.29 [0/90/0]$_s$ laminate with crack in 90˚ layer (FLM) for N_m = 1000 lb/in and S=0.25” ……..…… 55

8.30 [0/90/0]$_s$ laminate with crack in 90˚ layer (FLM) for ΔT = -495˚F and S=2.2” …….……. 56

8.31 [0/90/0]$_s$ laminate with crack in 90˚ layer (FLM) for N_m = 1000 lb/in and S=2.2” ……..… 56

8.32 [45/0/-45/90]$_s$ laminate with crack in -45˚ layer (FLM) for ΔT = -495˚F and S=0.25” ……..…….. 57

8.33 [45/0/-45/90]$_s$ laminate with crack in -45˚ layer (FLM) for N_m = 1000 lb/in and S=0.25” …… 57

8.34 [45/0/-45/90]$_s$ laminate with crack in -45˚ layer (FLM) for ΔT = -495˚F and S=2.2” ……..…… 58

8.35 [45/0/-45/90]$_s$ laminate with crack in -45˚ layer (FLM) for N_m = 1000 lb/in and S=2.2” …….……. 58

8.36 $[45/0/-45/90]_s$ laminate with crack in 0˚ layer (FLM) for ΔT = -495˚F and S=0.25” ……..…….. 59

8.37 $[45/0/-45/90]_s$ laminate with crack in 0˚ layer (FLM) for N_m = 1000 lb/in and S=0.25 ……..…… 59

8.38 $[45/0/-45/90]_s$ laminate with crack in 0˚ layer (FLM) for ΔT = -495˚F and S=2.2” …….. 60

8.39 $[45/0/-45/90]_s$ laminate with crack in 0˚ layer (FLM) for N_m = 1000 lb/in and S=2.2” …….. 60

8.40 $[45/0/-45/90]_s$ laminate with crack in 45˚ layer (TLM) for ΔT = -495˚F and S=0.25” ……...……. 61

8.41 $[45/0/-45/90]_s$ laminate with crack in 45˚ layer (TLM) for N_m = 1000 lb/in and S=0.25” ……...……. 61

8.42 $[45/0/-45/90]_s$ laminate with crack in -45˚ layer (FLM) for S=0.25”and L=0.01”, no thermal load ……..….. 62

8.43 $[45/0/-45/90]_s$ laminate with crack in 0˚ layer (FLM) for S=0.25”and L=0.01”, no thermal load ……...…….. 63

8.44 $[45/0/-45/90]_s$ laminate with crack in 45˚ layer (TLM) for S=0.25”and L=0.01”, no thermal load ……...……. 63

8.45 $[45/0/-45/90]_s$ laminate with crack in -45˚ layer (FLM) for S=0.25”and L=0.01”, no mechanical load …….……. 64

8.46 $[45/0/-45/90]_s$ laminate with crack in 0˚ layer (FLM) for S=0.25”and L=0.01”, no mechanical load …….…….. 65

8.47 $[45/0/-45/90]_s$ laminate with crack in 45˚ layer (TLM) for S=0.25”and L=0.01”, no mechanical load …….…….…… 65

8.48 $[45/0/-45/90]_s$ laminate with crack in -45˚ layer (FLM) for S=0.25”and L=0.01”, mechanical load N_m=1000 lb/in …….….. 66

8.49 $[45/0/-45/90]_s$ laminate with crack in 0˚ layer (FLM) for S=0.25”and L=0.01”, mechanical load N_m=1000 lb/in ……..……. 67

8.50 $[45/0/-45/90]_s$ laminate with crack in 45˚ layer (TLM) for S=0.25”and L=0.01”, mechanical load N_m=1000 lb/in ……...…… 67

8.51 $[45/0/-45/90]_s$ laminate S=0.25”and L=0.01” Effect of mechanical load on permeability …….....……..…….. 68

8.52 Effect of thermal load on normalized permeability for $[45/0/-45/90]_s$ laminate S=0.25” and L=0.01” …….….. 69

8.53 Effect of crack density on normalized permeability for $[45/0/-45/90]_s$ laminate L=0.01”, N_m=1000 lb/in …….. 70

8.54 $[45/0/-45/90]_s$ laminate L=0.01”, N_m=1000 lb/in, Effect of crack density on crack opening volume COV …….. 71

8.55 Effect of delaminations length on normalized permeability for $[45/0/-45/90]_s$ laminate S=0.25” …….…… 71

8.56 $[45/0/-45/90]_s$ laminate L=0.01”, N_m=1000 lb/in Effect of crack density on maximum tensile stress in undamaged layers …….…….…… 72

8.57 Effect of mechanical tensile load on crack density …….…….…… 73

8.58 Effect of thermal load on crack density …….…….…… 73

8.59 Effect of mechanical tensile load on delamination length ..…….…… 74

8.60 Effect of thermal load on delamination length …….……..…… 74

NOMENCLATURE

DCOD	Delaminated crack opening displacement
$A_{**}^{(k)}$	Extension and shear extension coupling stiffness of kth sublaminate
$B_{**}^{(k)}$	Extension and shear extension coupling stiffness of kth sublaminate
$D_{**}^{(k)}$	Bending torsion coupling stiffness of kth sublaminate
IDEF	In-situ damage effective factor
ε_y	Axial strain
ΔT	Temperature difference (°F)
N_m	Mechanical force
N_T	Thermal load
FLM	Five Layer Model
TLM	Three Layer Model

CHAPTER 1

INTRODUCTION

1.1 Introduction

Composites are one of the most advanced materials specialized to achieve the best of the properties of constituent materials. They offer a number of advantages over metals and other conventional materials in the aerospace and many other applications. For the next generation space vehicles, composite materials are ideal for applications such as fuel tanks. For reusable launch vehicles (RLVs) as well as expendable launch vehicles (ELVs), composites are used to reduce the payload and increase fatigue life under thermal and mechanical loading conditions for various structural parts. Materials with high strength-to-weight and stiffness-to-weight ratios are essential and composites exactly satisfy the needs. However, due to very high temperature variations in addition to structural loads during the operation of space vehicles, composites are susceptible to transverse matrix cracks. Difference in coefficient of thermal expansion and mismatch of Poisson's ratio between the adjacent plies can be one of the main reasons for the

initiation and propagation of matrix cracks. These cracks in the polymer matrix can lead to the permeation of cryogenic fuel in fuel tank, which eventually might become a cause of an accident. These matrix cracks typically tend to form and grow in direction parallel to fibers through the thickness of ply direction. Along with the transverse cracks, there are inter-laminar delaminations originating from the tips of these cracks due to stress concentration.

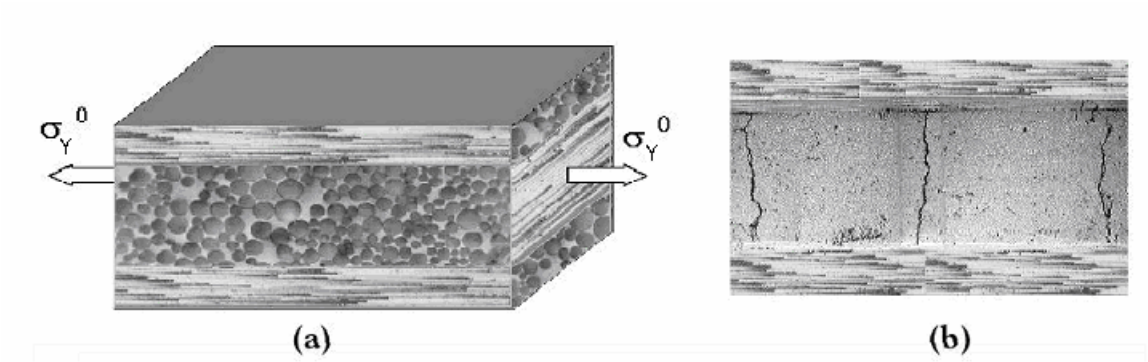

Fig.1.1 Cross-ply laminate subjected to uniaxial loading and resulting damage.

A typical cross section of a cross ply laminate shows fibers and matrix in Fig. 1.1(a) with application of uniaxial load in Y direction (along the 0º ply direction). Fig. 1.1(b) depicts the cracks formed in middle 90º ply along with delaminations produced at the crack tips.

Delaminations and cracks may form an intersecting network of leak passages through which high pressure cryogenic fuel can permeate. Fig. 1.2 shows how the cracks in successive layers of a laminate interact to form a network of passages. As depicted by the schematic in Fig.1.2, the crack opening displacements associated with the delaminated transverse matrix cracks, when subjected to thermal and/or mechanical loading, form a path through the entire thickness of the arbitrarily oriented ply laminate, thereby allowing cryogenic fuel to permeate. To study the permeation problem, an

analytical solution is necessary to predict the delaminated crack opening displacement (DCOD) developed in each of the plies, as later it will be shown that DCOD and crack density are the two important factors which decide the permeability of a composite laminate. After obtaining the solutions for DCOD, a mathematical model for predicting permeability of symmetric cross-ply and arbitrarily oriented ply graphite-epoxy laminates can be established. Cracks can exist not only in outermost (top) ply and the middle (central/symmetric) ply but also in the intermediate plies. Generally ply laminates with different arbitrarily oriented plies are used for optimizing the properties and strength to weight ratio of structures and therefore it is necessary to develop a solution for DCOD developed in the intermediate plies of such different orientation ply laminate.

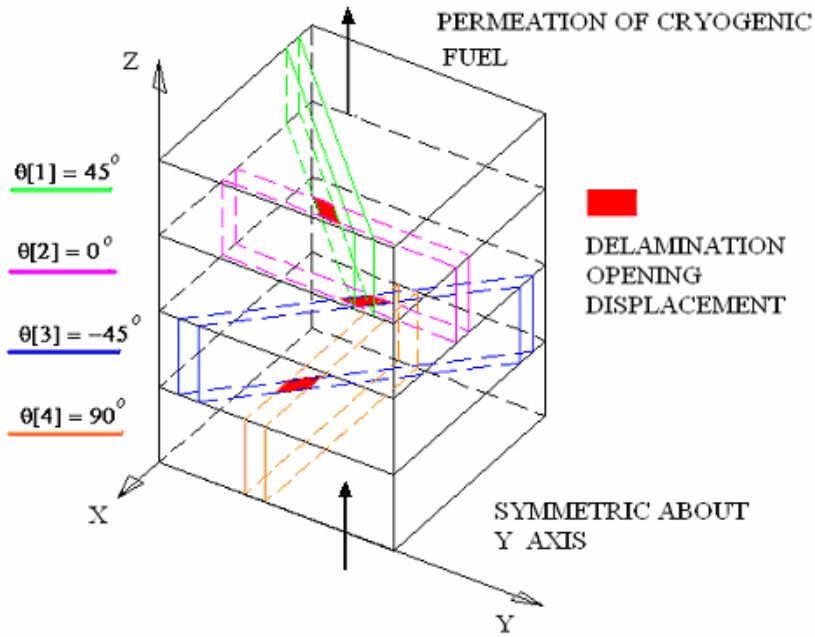

Fig.1.2 Permeation path at overlap of transverse cracks in arbitrary orientation plies

The representative volume element (RVE) of a [45/0/-45/90]s laminate shown in Fig.1.2 has cracks in various oriented layers. The ply orientation angles are measured with respect to the Y axis. Due to the different orientations of layers in arbitrarily orientated ply laminate, the delaminated opening displacement of each ply under thermal and mechanical loads is different and therefore has to be predicted individually. The shaded region shows the overlap of cracks through which permeation can occur.

The composite material under consideration here is graphite epoxy IM7/PETI-5. The properties of IM7/PETI-5 are as shown in Table 1.1 and are obtained from mechanical characterization work performed by Gates et al [7].

Table 1.1. Material Properties of IM-7/PETI-5 Room Temperature (75ºF)

E_{11}	E_{22} (Msi)	E_{33}	G_{12}	G_{13} (Msi)	G_{23}	ν_{12}	ν_{13}	ν_{23}	α_1 (X 10^{-6} ε/ºF)	α_2
24.20	1.28	1.28	0.73	0.73	0.48	0.3	0.3	0.34	-0.722	10.80

1.2 Thesis Outline

In Chapter 1, an introduction to the permeation problem in graphite-epoxy laminate system used in cryogenic fuel tanks of reusable launch vehicles is presented along with an outline of the thesis. Chapter 2 is comprised of literature review of work done previously by other researchers. Chapter 3 gives the problem statement and scope and objective of the thesis. Chapter 4 presents a development of solution for finding the crack opening displacement associated with delaminations in arbitrarily oriented ply laminates using five-layer model. Chapter 5 includes the use of a Three Layer model to calculate cracks in the outermost layer. Chapter 6 presents an approach to predict the in situ damage effective function (IDEF) and strain energy release rate. Chapter 7 discusses

the finite element models used to verify the results obtained from Five Layer and Three Layer models. Chapter 8 discusses results obtained from Five Layer and Three Layer models. Chapter 9 lists the conclusions based on the current study and the scope for future study.

CHAPTER 2

LITERATURE REVIEW

The problem of high pressure cryogenic fuel permeation through delaminated crack opening of composite laminates has been a matter of concern for a while due to highly critical and potentially dangerous consequences. If permeation persists, the use of composites as fuel tank material would be hazardous. Many researchers have studied the phenomenon of permeation of cryogenic fuel through composite laminates. Experimental as well as analytical and simulations studies have been performed.

McManus et al [1,2] observed that the permeability is strongly influenced by loading conditions, crack density and ply orientation. They analytically predicted matrix cracks in a composite laminate, together with the resulting degradations of laminate properties, as functions of temperature or thermal cycles. A simple shear-lag solution for the stresses in the vicinity of cracks and a fracture mechanics crack formation criterion were used to predict matrix crack initiation and evolution. Experimentally, crack

densities were measured in a variety of laminates exposed to decreasing temperatures using X-ray radiography and microscopic inspection.

Varna et al [3] experimentally investigated the transverse cracks in cross-ply laminates to reveal the essential characteristics of their opening displacement under tensile loads. The average crack opening displacement was studied as a function of the longitudinal overall strain and the effects of matrix toughness and transverse ply thickness on this parameter were examined. They predicted the average COD based on shear-lag model and variational approach and found that the stiffness reduction in the uncracked layer influences the COD of the interior layer.

Hong et al [4,5] used a modified shear lag model taking into account the concept of interlaminar shear layer to predict the onset of a transverse crack and multiple transverse cracking as well as stiffness reduction due to the effect of transverse cracks on the thermomechanical properties of cross-ply laminated composites. They showed the dependence of the degradation of thermomechanical properties on the laminate configuration.

Nairn [6,7] used a variational energy approach to determine the two-dimensional thermoelastic stress state in cross-ply laminates of type $(0_m/90_n)_s$ and $(90_m/0_n)_s$. The stress analysis was used to calculate the energy release rate due to formation of a new microcrack. Further development of same model to include effects of delaminations with transverse matrix cracks was used to calculate the energy release rate for the initiation and growth of a delamination induced by a matrix microcrack. He concluded that at low crack densities, $((S)/90_n)_s$ laminates are expected to fail by microcracking and to show little or no delaminations whereas after a certain critical value of crack density, which is a

function of laminate structure and material properties, the energy release rate for delamination exceeds that for microcracking and delamination is predicted to dominate over microcracking.

Roy and Benjamin [8] developed a simple expression for calculating the COD based on shear lag analysis. A major limitation of shear lag analysis is that the constraining layers are assumed as a homogenous medium without taking into account the stacking sequence effects, and shear deformations within a cracked layer are ignored. Also, it can be seen from Fig.1.2 that the increase in crack opening displacement due to delamination plays an important role in determining the amount of permeation of cryogenic fuel, which is not included in the standard shear lag model.

Berthelot and Corre [9,10] developed a shear lag theory based analytical model for transverse cracking with delamination in cross-ply laminates subjected to tensile loading to evaluate strain and stress distribution. In the portion of laminate without delamination, the analytical model is based on a displacement approach which considers that the longitudinal displacement depends on the longitudinal and transverse coordinates in each layer. In the delaminated part, the analytical approach is reduced to the usual one-dimensional analysis. They concluded that complete parabolic shear-lag analysis yields a fairly good approximation of the strain and stress distributions obtained by finite element analysis.

Noh and Whitcomb [11,12] developed an expression for calculating the crack opening volume (COV) based on changes in the effective moduli of a cracked ply. They studied the effect of various parameters such as adjacent ply orientation, material properties of adjacent plies, initial properties of the cracked ply and cracks in adjacent ply

on COV. They observed that the crack opening could be predicted using two-dimensional models when crack-tip delaminations are fully developed, and that interaction effects on COD due to matrix cracks in adjacent plies can be ignored.

Zhang et al [13,14] analytically studied the delaminated transverse matrix cracking of CFRP laminates under uniaxial tension. The model was based on first order shear deformable laminate theory, applying force, moment and shear stress constitutive equations to each sublaminate and analyzing the system using load and displacement boundary conditions. They found that a Five Layer model was able to predict the crack opening displacement in mid-layers, whereas a Three Layer model was useful for prediction of cracks in outermost layers. They also developed the concept of an in situ damage effective function (IDEF) for reducing stiffness of laminate as a function of damage growth.

Gates et al [15] studied the effect of cryogenic temperature on materials properties of IM7/PETI-5 and found that temperature, loading mode and aging time can all have significant influence on residual strength and stiffness of the laminate, and this influence is a strong function of laminate stacking sequence. They also observed that certain material properties, such as laminate moduli, are not only nonlinear but they may also be non-monotonic functions of temperature.

Bechel et al [16,17] developed an apparatus to experimentally observe the damage development in graphite epoxy laminates. IM7/3K, IM7/5250-4 carbon/bismaleimide cross-ply ([0/90]2S and [90/0/90/0/90/0/90/0/90]) and quasi-isotropic ([0/45/-45/90]s) laminates were submerged in liquid nitrogen (LN2) and returned to room temperature for various number of cycles. They observed that samples with ply thickness reduced by 30%

had lower surface cracks upto 200 cycles but at 1000 cycles, surface crack densities were equal regardless of ply thickness. Fig. 2.1 shows cross section of laminate in which crack in 90º layer (middle) is evident [16].

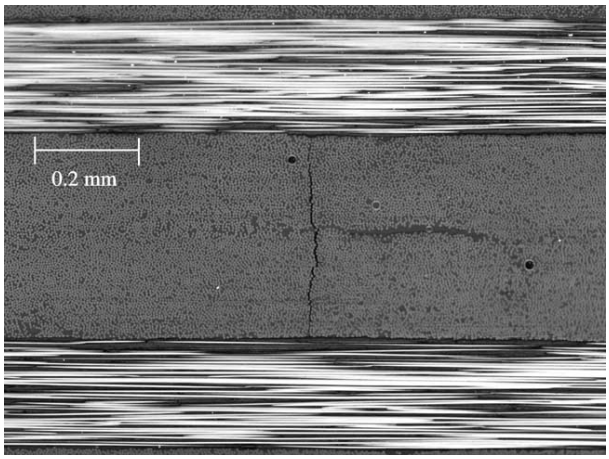

Fig. 2.1. Micro-crack in 90º ply block of a [0/90]2S specimen [17]

Roy and Benjamin [18] developed an analytical solution for predicting permeation due to crack opening displacement and delaminations in graphite epoxy systems IM7/PETI-5 cross ply laminates. This model is based on first-order shear laminate theory embodied in a Five Layer and a Three Layer model. Using this approach, the DCOD can be calculated for a cross-ply laminate with a given delamination length, crack density and loading conditions. Prediction of permeability is achieved by using Darcy's law for isothermal, viscous flow of gases through porous media. The results obtained from both five-layer and three-layer model are used as input to the permeability model. Using this model, the permeability is calculated for an orthotropic laminate lay-up for a given delamination length, crack density and loading conditions. The model is restricted to the analysis of orthotropic cross ply laminates and cracks present in middle (central) plies and the outermost (top) plies.

It is evident that in order to comprehensively study the permeability problem, it is necessary to develop a mathematical model to find the opening displacement associated with matrix cracks in the presence of delaminations. For any arbitrary ply orientation, using the analytical solution for matrix crack opening displacement associated with delaminations, an expression for permeability will be derived and verified using experimental data.

CHAPTER 3

OBJECTIVE & APPROACH

As described in previous sections, in order to be able to develop a mathematical model for prediction of permeability in graphite-epoxy laminates it is first necessary to predict the crack opening displacement associated with delaminations in every layer of arbitrary orientation that forms a path through the entire thickness of the laminate as shown in Fig.1.2. Once the crack opening displacement is known for given set of thermal and/or mechanical loads, the permeability can be predicted by modifying the model previously developed by Roy and Benjamin [18].

In this study, an analytical methodology based on first-order shear laminate theory [13] is applied to predict opening displacement associated with delaminations in $[0/90/0]_s$ cross-ply and $[45/0/-45/90]_s$ angle-ply laminate systems in a graphite-epoxy laminate (IM-7/PETI-5) subject to thermal and mechanical loading conditions. Delamination length and crack density are specified as input in the interest of simplicity. The Five Layer and Three Layer models presented in this study are developed further from the

work originally presented by Zhang et al [13] and Roy and Benjamin [18]. The five-layer model is used to predict DCOD in the intermediate layers where as the Three Layer model is used to predict DCOD in outermost (top) layer. The DCOD obtained using five-layer and Three Layer models are verified using two-dimensional and three dimensional finite element analysis. A mathematical model to predict permeability in graphite-epoxy laminate system [18] is used with the help of Darcy's law for isothermal, viscous flow of gases through porous media. The results obtained from five-layer model are used as input to the permeability model. An approach to calculate the stiffness reduction factor is presented as in situ damage effective function (IDEF), a function of crack spacing and delamination length along with material properties.

CHAPTER 4

ANALYTICAL SOLUTION FOR DCOD USING FIVE LAYER MODEL

4.1 Introduction to Five Layer Model

In this chapter, an analytical model has been developed to determine the delaminated crack opening displacement (DCOD) in the intermediate plies of a symmetric laminate with arbitrarily oriented plies. The model is based on first order shear deformation theory. The load conditions considered here are mechanical uniaxial tensile loading and thermal loading. Each layer is individually analyzed for crack assuming that the other layers are intact. It can be easily understood that plies with fibers perpendicular to load direction, i.e. 90º layer, are more susceptible to damage initiation. As the transverse matrix cracks are studied in this model, layers with orientations other than 90º are analyzed by resolving the applied forces into components parallel and perpendicular to the fiber direction. This is done considering the rotation of co-ordinate system accordingly to view those layers as having orientation of 90º. Appropriate

transformations in loads and properties are applied to full RVE for analysis of the particular layer under consideration.

The damage mode in such 90º plies is transverse matrix cracks. These type of cracks increase with increase in axial load. Along with transverse matrix cracks, there are delaminations at the crack tips due to stress concentrations. Such matrix cracking with delaminations in adjacent plies cause the openings called delaminated crack opening displacement (DCOD), which are spaced through out the thickness of the laminate. These DCOD are responsible for the permeation of cryogenic fuel through the laminates. A representative schematic of such DCOD in a laminate is shown in fig. 4.1. The cracked 90º layer is shown with transverse crack and delaminations at the ends of the crack. The laminate is considered symmetric about Y axis.

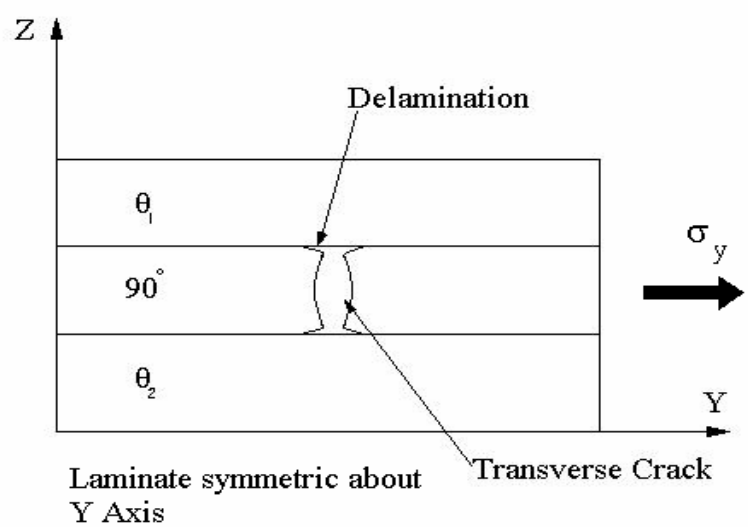

Fig. 4.1. Transverse crack and delaminations under uniaxial tensile load in a Five Layer Model

4.2 Analytical Expression for Five Layer Model

In this section, the expression for delaminated crack opening displacement in the Five Layer Model is developed for a general laminate configuration of $[\Phi/../\theta/90/\varphi/..\psi]_s$. As shown in Fig. 4.2, the RVE has a uniform crack spacing of '2S' and local delamination length of '2L'. The layers with arbitrary orientations $\Phi/../\theta$ and $\varphi/..\psi$ are not damaged, whereas the crack exists in 90º layer.

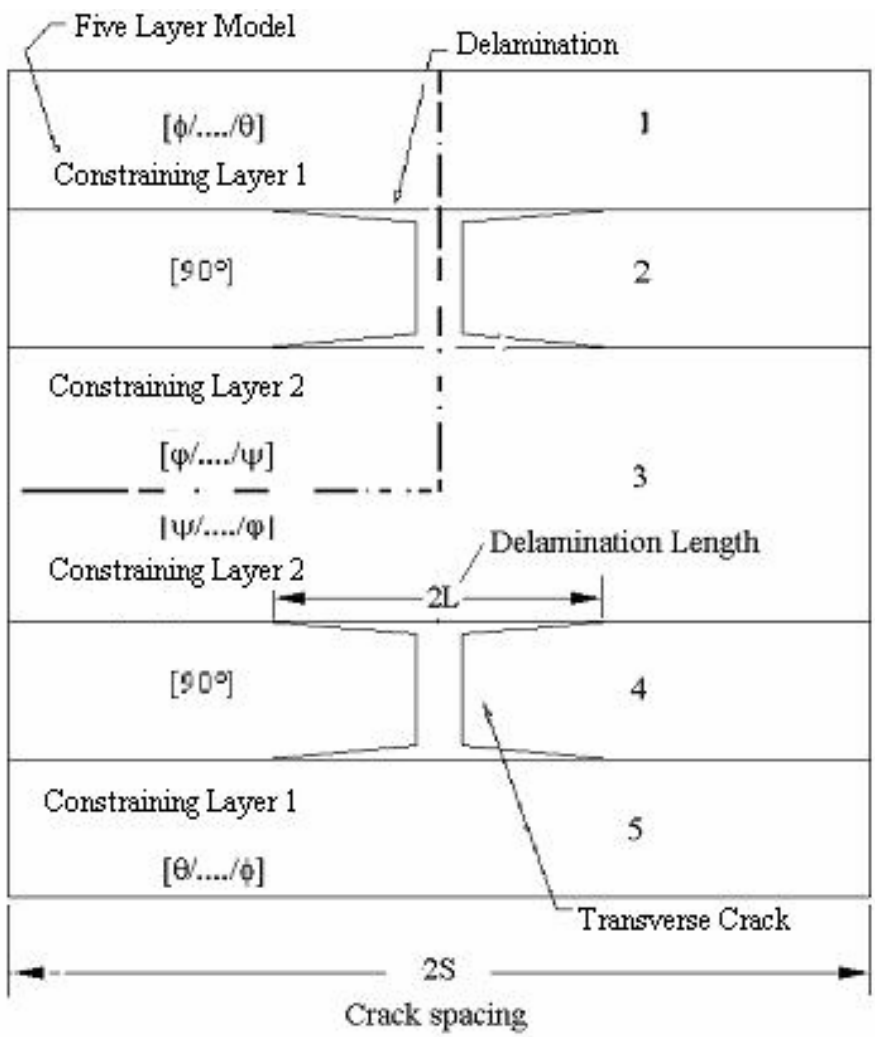

Fig. 4.2. Crack spacing and delamination length in Five Layer Model

Considering symmetry of laminate about Y axis and about crack, as well as symmetry of loading, only one-quarter of this Five Layer laminate is modeled as shown in Fig. 4.3. The modeled portion of laminate is divided into 6 different parts called sublaminates. Sublaminates 1,2 and 3 are in the undamaged region of 'y' (S-L) whereas sublaminates 4, 5 and 6 are in the damaged portion of 'y' (L).

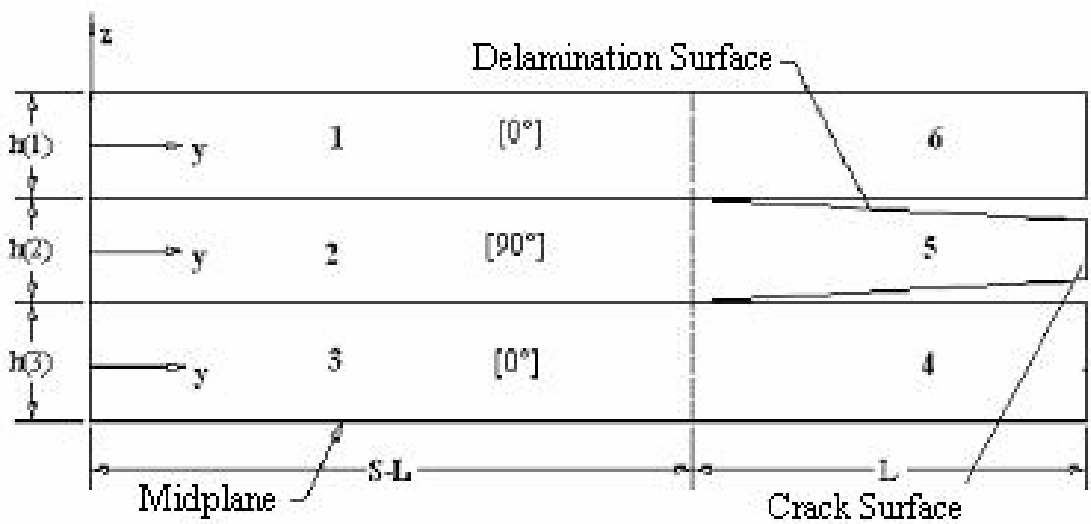

Fig. 4.3. One-quarter of repeating interval of a Five Layer model case

Assuming that the displacements in y and z directions within each sublaminate can be given by,

$$v(y,z) = V(y) + z\beta(y) \tag{4.1}$$

$$w = W(y) \tag{4.2}$$

Where, V(y) is the y displacement of mid-surface of the sublaminate.

β(y) is the slope of the sublaminate mid-surface in y direction.

W(y) is the z displacement of mid-surface of the sublaminate.

The force and moment equilibrium equations for each sub-laminate are,

$$N,_y + T_t - T_b = 0 \tag{4.3}$$

$$M,_y - Q + \frac{h}{2}\left(T_t + T_b\right) = 0 \tag{4.4}$$

$$Q,_y + P_t - P_b = 0 \tag{4.5}$$

where N, Q and M are axial force, shear force and bending moment resultants, P and T denote interlaminar peel and shear stresses with subscripts t and b denoting top and bottom surfaces. Combining the strain-displacement relations with Equations (4.1, 4.2) and the in-plane stress-strain relationships of a lamina, the force-displacement relationships of a sublaminate are,

$$N_M = A_{22}V,_y + B_{22}\beta,_y - \bar{Q}_{22}h\int_{T_{ref}}^{T_f} \alpha_y dT \tag{4.6}$$

$$M_M = B_{22}V,_y + D_{22}\beta,_y - \bar{Q}_{22}h\bar{Z}\int_{T_{ref}}^{T_f} \alpha_y dT \tag{4.7}$$

$$Q = A_{44}(\beta + W,_y) \tag{4.8}$$

where, A_{22}, B_{22}, D_{22} and A_{44} are components of the A, B and D stiffness matrices from classical lamination theory; T_{ref} and T_f are reference and final temperatures; h is the thickness of the lamina; $\bar{Z}$ is centroidal distance of the lamina from laminate midplane; α_y is the coefficient of thermal expansion in y-direction and is given by the nonlinear function $C_0+C_1T+C_2T^2$. In the above equations, non-linear material properties with respect to temperature T are used in calculating the thermal forces and moments. The components of A, B, D and $\bar{Q}$ matrix are assumed to be nonlinear functions of temperature T. It should be noted that for a two-dimensional orthotropic model the other

stiffness components of the anisotropic sublaminate do not appear in the constitutive equations due to the assumption of plane strain with respect to the width of the specimen. By modifying the procedure given by Zhang et al [13] for applying it to present case, the solutions for displacement in 'y' direction of sublaminate 4, 5 and 6 are derived as,

$$v^{(4)}(y,z) = V^{(4)}(y) + z^{(3)}\beta^{(4)}(y) \tag{4.9}$$

$$v^{(5)}(y,z) = V^{(5)}(y) + z^{(2)}\beta^{(5)}(y) \tag{4.10}$$

$$v^{(6)}(y,z) = V^{(6)}(y) + z^{(2)}\beta^{(6)}(y) \tag{4.11}$$

Where,

$$V^{(4)} = -\frac{B_{22}^{(3)}}{A_{22}^{(3)}}(\psi_1 e^{\omega y} + \psi_2 e^{-\omega y}) + \psi_3 y + \psi_4 \tag{4.12}$$

$$V^{(5)} = \theta_3 y + \theta_4 \tag{4.13}$$

$$V^{(6)} = \theta_7 y + \theta_8 \tag{4.14}$$

$$\beta^{(4)} = \psi_1 e^{\omega y} + \psi_2 e^{-\omega y} \tag{4.15}$$

$$\beta^{(5)} = \theta_1 e^{\omega_1 y} + \theta_2 e^{-\omega_1 y} \tag{4.16}$$

$$\beta^{(6)} = \theta_5 y + \theta_6 \tag{4.17}$$

The detailed procedure for obtaining laminate constants θ_i, ψ_i, ω and ω_1 for the case of pure mechanical loading is given in Zhang et al [13]. Detailed analytical derivations including thermal and mechanical loading are given in Appendix A.

From Equations (4.12-4.17), the delaminated crack opening displacement (DCOD) calculated at the interface of sublaminate 4 and 5 at y=S for a given delamination length L and crack density 1/2S is given by,

$$DCOD_{top} = v^{(6)}(S, \frac{-h^{(3)}}{2}) - v^{(5)}(S, \frac{h^{(2)}}{2}) \tag{4.18}$$

$$DCOD_{bottom} = v^{(4)}(S, \frac{h^{(3)}}{2}) - v^{(5)}(S, \frac{-h^{(2)}}{2}) \tag{4.19}$$

Using Equations (4.15), DCOD for a given delamination length, crack density and symmetric loading (mechanical and /or thermal) condition can be obtained for the Case 1 laminate configuration.

CHAPTER 5

ANALYTICAL SOLUTION FOR DCOD USING THREE LAYER MODEL

5.1 Introduction to Three Layer Model

In this chapter, an analytical model is developed to determine the delaminated crack opening displacement (DCOD) in the outermost ply of arbitrarily oriented symmetric laminate. The model derived depends on first order shear deformation theory. The load conditions considered here are mechanical uniaxial tensile loading and thermal loading. The top layer is individually analyzed for a matrix crack assuming that the other layers are intact. It can be easily understood that plies with fibers perpendicular to load direction, i.e. 90º layer, are more susceptible to damage initiation. As the transverse matrix cracks are studied in this model, top layers with orientations other than 90º are analyzed by resolving the applied forces into components parallel and perpendicular to the fiber direction. This is done by considering the rotation of co-ordinate system

accordingly to view those layers as having orientation of 90º. Appropriate transformations in loads and properties are applied to full RVE for analysis.

The delaminated crack opening in the top layer is similar to that in intermediate layers, except the top surface is traction-free. Matrix cracking with delaminations in adjacent plies results in delaminated crack opening displacements (DCOD), which are assumed to be equally spaced through out the thickness of the laminate. These DCOD are responsible for the permeation of cryogenic fuel through the laminates. Representative schematic of such DCOD in a laminate is shown in fig. 5.1. The cracked top 90º layer is shown with transverse crack and delaminations at the end of the crack. The laminate is considered symmetric about X axis.

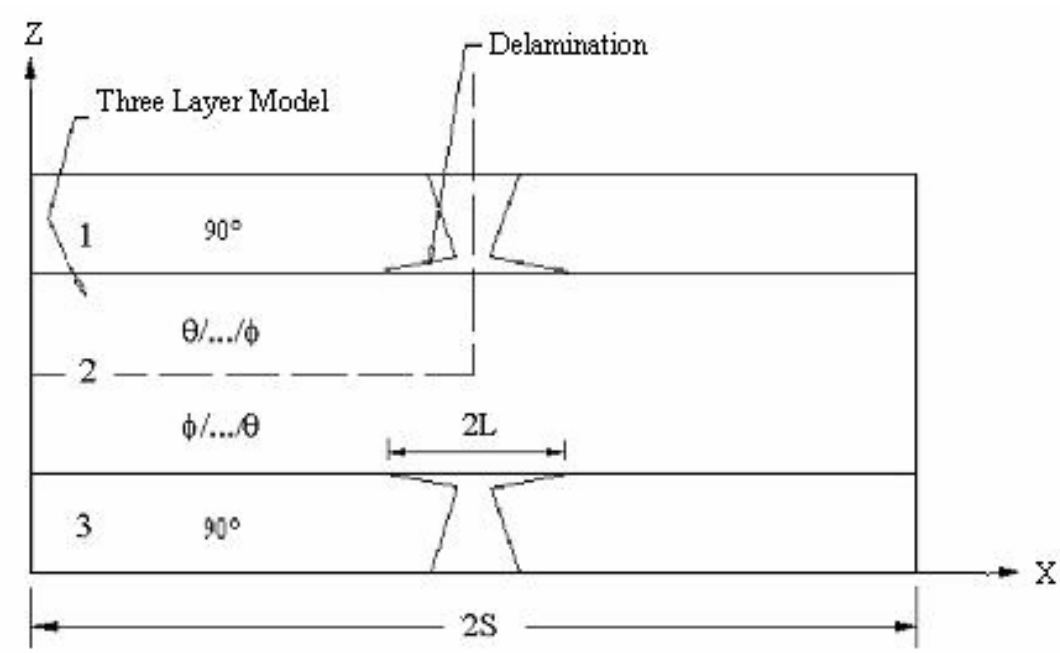

Fig. 5.1. Transverse crack and delaminations under uniaxial tensile load in a Three Layer Model.

5.2 Analytical Expression for Three Layer Model

In this section, the expression for delaminated crack opening displacement in a Three Layer model is developed for laminate configuration of $[90/\theta/\ldots/\Phi]_s$. As seen in Fig. 5.1, the above schematic is developed into RVE with crack spacing of '2S' and local delamination length of '2L', the similar to the Five Layer model. The layers with arbitrary orientations $\theta/\ldots/\Phi$ are assumed to be undamaged, whereas the crack exists in the 90º layer.

Considering symmetry of laminate about X axis and about crack, as well as symmetry of loading, only one-quarter of this Three Layer laminate is modeled as shown in Fig. 5.2. The modeled portion of laminate is divided into 4 different parts called sublaminates. Sublaminates 1 and 2 are undamaged region of 'x' (S-L) whereas sublaminates 3 and 4 are in damaged portion of 'x' (L).

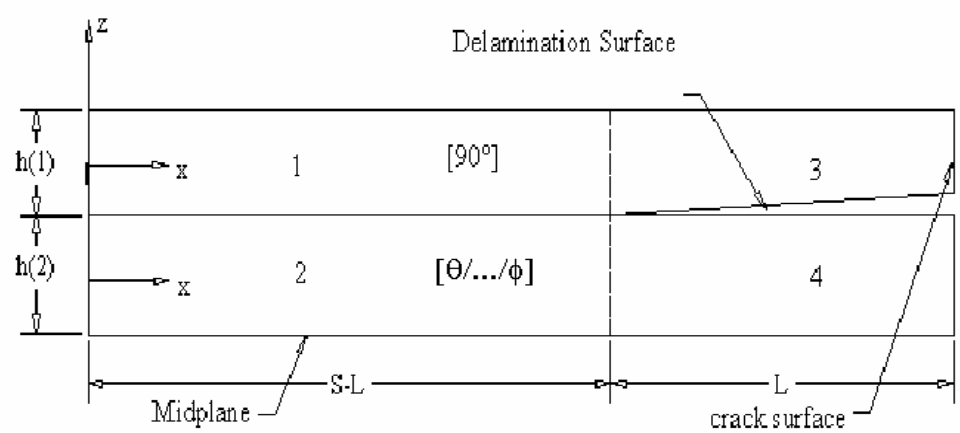

Fig. 5.2. One-quarter of repeating interval of a Three Layer model case

Assuming that the displacements in x and z directions within each sublaminate can be given by,

$$u(x,z) = U(x) + z\beta(x) \tag{5.1}$$

$$w = W(x) \tag{5.2}$$

Where, U(x) is the x displacement of mid-surface of the sublaminate.

β(x) is the slope of the sublaminate mid-surface in x direction.

W(x) is the z displacement of mid-surface of the sublaminate.

The force and moment equilibrium equations for each sub-laminate are,

$$N_{,x} + T_t - T_b = 0 \tag{5.3}$$

$$M_{,x} - Q + \frac{h}{2}\left(T_t + T_b\right) = 0 \tag{5.4}$$

$$Q_{,x} + P_t - P_b = 0 \tag{5.5}$$

where N, Q and M are axial force, shear force and bending moment resultants, P and T denote interlaminar peel and shear stresses with subscripts t and b denoting top and bottom surfaces. Combining the strain-displacement relations with Equations (5.1, 5.2) and the in-plane stress-strain relationships of a lamina, the force-displacement relationships of a sublaminate are,

$$N_M = A_{11}U_{,x} + B_{11}\beta_{,x} - \bar{Q}_{11}h\int_{T_{ref}}^{T_f} \alpha_x dT \tag{5.6}$$

$$M_M = B_{11}U_{,x} + D_{11}\beta_{,x} - \bar{Q}_{11}h\bar{Z}\int_{T_{ref}}^{T_f} \alpha_x dT \tag{5.7}$$

$$Q = A_{44}(\beta + W_{,x}) \tag{5.8}$$

where, as in Case 1, A_{11}, B_{11}, D_{11} and A_{44} are components of the A, B and D stiffness matrices from classical lamination theory; T_{ref} and T_f are reference and final temperatures respectively; h is the thickness of the lamina; $\overline{Z}$ is centroidal distance of the lamina from laminate midplane; α_x is the coefficient of thermal expansion in x-direction and is given by the nonlinear function $C_0+C_1T+C_2T^2$. In the above equations, non-linear material properties with respect to temperature T are used in calculating the thermal forces and moments. The components of A, B, D and $\overline{Q}$ matrix are assumed to be nonlinear functions of temperature T. For the two-dimensional orthotropic model the other stiffness components of the anisotropic sublaminate do not appear in the constitutive equations due to the assumption of plane strain with respect to the width direction. By modifying the procedure given by Zhang et al [13] for the present laminate, the solutions for displacement in x direction of sublaminate 3 and 4 are derived as,

$$u^{(3)}(x,z) = U^{(3)}(x) + z^{(1)}\beta^{(3)}(x) \tag{5.9}$$

$$u^{(4)}(x,z) = U^{(4)}(x) + z^{(2)}\beta^{(4)}(x) \tag{5.10}$$

Where,

$$U^{(3)} = \psi_2 x + \psi_3 \tag{5.11}$$

$$U^{(4)} = \theta_3 x + \theta_4 \tag{5.12}$$

$$\beta^{(3)} = \psi_1 \tag{5.13}$$

$$\beta^{(4)} = \theta_1 x + \theta_2 \tag{5.14}$$

A detailed analytical derivation including thermal loading is given in Appendix B

The DCOD calculated at the interface of sublaminate 3 and 4 at x=S for a given delamination length L and crack density 1/2S is given by,

$$DOD = u^{(4)}(S, \frac{h^{(2)}}{2}) - u^{(3)}(S, \frac{-h^{(1)}}{2}) \tag{5.15}$$

Using Equation (5.15), DCOD for a given delamination length, crack density and symmetric loading condition (mechanical and/or thermal) can be obtained for the Case 2 laminate configuration.

CHAPTER 6

IN-SITU DAMAGE EFFECTIVE FUNCTION

6.1 Introduction

Composite laminates are macroscopically inhomogeneous materials as they consist of layers of different orientations. But the individual layer can be considered as a homogeneous anisotropic solid phase with a distribution of micro-cracks. In this section, characterization of extension stiffness reduction of the constrained 90˚layers is explicitly expressed in terms of delamination length and transverse crack spacing by using the obtained stress field in Five Layer and Three Layer models. The reduced stiffness of the 90˚ ply group normalized by the stiffness of an intact lamina was introduced by Zhang et al [13,14] and is termed as IDEF. The model developed by Zhang et al [13,14] has been modified to apply the present boundary and load conditions. In-situ damage effective function (IDEF) has been defined for considering the changes in in-plane stiffness of damaged laminate. Equivalent constrained models (ECM) such as Five Layer Model and

Three Layer Model are used for stiffness degradation calculations. The stiffness reduction in the laminate due to transverse cracking and its induced delaminations is assumed to be attributed to the loss of the load carrying capacity of 90˚ plies. IDEF has been determined by assuming that the stiffness of an "equivalent" laminate where the degraded 90˚ plies are perfectly bonded is equal to that of the real cracked and delaminated laminate. IDEF happens to be a function of transverse crack spacing as well as delamination length and the in-situ constraining conditions of 90˚ plies.

The significance of IDEF is due to the fact that the strain energy release rate can be developed as a function of IDEF by calculating the potential energy of damaged laminate element with a finite gauge length of crack spacing (2S) and unit width under conditions of plain strain in the width direction. Potential energy can be found out by subtracting the external work done due to tensile load from total elastic strain energy (U) stored in a laminate element. Zhang et al [13,14] calculated total strain energy by integrating the strain energy over laminate due to normal stress and strain. The shear strains generated in the laminate were not considered. In this derivation, shear strain energy is also included in calculating the total strain energy of the laminate.

6.2 IDEF calculation

The axial strain ε_y produced in the laminate can be found out as given by Zhang et al [14]. As the rotation of the end-section of constraining layers in both FLM and TLM is zero, overall average axial strain in laminate is given as follows.

6.2.1 For Five Layer Model

$$\varepsilon_y = \frac{(V^{(6)}(s) + V^{(4)}(s))/2}{S} = \frac{(\psi_3 S + \psi_4 + \theta_7 S + \theta_8)/2}{S} \tag{6.1}$$

Therefore the extension stiffness of a damaged laminate in Y direction can be given as

$$A_{22}^d = \frac{N + N_T}{\varepsilon_y} \tag{6.2}$$

The IDEF can be found out as given by Zhang et al [13,14]

$$\Lambda_{22} = \frac{A_{22} - A_{22}^d}{2A_{22}^{(2)}} \tag{6.3}$$

6.2.2 For Three Layer Model

Using definitions of constants as defined in Three Layer model,

$$\varepsilon_y = \frac{U^{(4)}(s)}{S} = \frac{\theta_3 S + \theta_4}{S} \tag{6.4}$$

$$A_{22}^{d} = \frac{N + N_T}{\varepsilon_y} \tag{6.5}$$

$$\Lambda_{22} = \frac{A_{22} - A_{22}^{d}}{2A_{22}^{(1)}} \tag{6.6}$$

6.3 Total strain energy calculation approach

6.3.1 For Five Layer Model

Potential energy (PE) is

$$PE = U - N\varepsilon_y 2S \tag{6.7}$$

where U is strain energy of the laminate.

$$U = SA_{22}^{d}\varepsilon_y{}^2 + \frac{1}{2}\int_0^{2S} A_{44}^{d}\left((\beta^{(6)} + W_{,y}^{(6)})^2 + (\beta^{(4)} + W_{,y}^{(4)})^2\right)dy \tag{6.8}$$

A_{44}^{d} has been defined by Zhang et al [13] as stiffness of damaged laminate in shear. By substituting the values obtained from FLM (Appendix A), the resulting expression is

$$U = SA_{22}^{d}\varepsilon_y{}^2 + \frac{1}{2\omega}A_{44}^{d}\psi_1^2\left(e^{4\omega S} - 4\omega S e^{2\omega S} - 1\right) \tag{6.9}$$

6.3.2 For Three Layer Model

Potential energy (PE) is

$$PE = U - N\varepsilon_y 2S \tag{6.10}$$

where U is strain energy of the laminate.

$$U = SA_{22}^{d}\varepsilon_y{}^2 + \frac{1}{2}\int_0^{2S} A_{44}^{d}(\beta^{(4)} + W_{,y}^{(4)})^2 dy \tag{6.11}$$

By substituting the values obtained from TLM (Appendix B), the resulting expression is

$$U = SA_{22}^{d}\varepsilon_y{}^2 + \frac{1}{2}A_{44}^{d}\theta_1^2\left(e^{4\omega S} - 4\omega S e^{2\omega S} - 1\right) \tag{6.12}$$

6.4 Strain energy release rate calculation approach

6.4.1 SERR for Matrix cracking

Using the potential energy expression obtained in section 6.3.1 for initial crack spacing of '2S' and after formation of new cracks with crack spacing of 'S', approach followed by McManus et al [1,2] was used. By Griffith's energy approach, first partial derivative of potential energy with respect to crack length gives the strain energy release rate as

$$G^{MC} = \frac{\partial \pi}{\partial a} \tag{6.13}$$

where G^{MC} is the strain energy release rate due to matrix cracking, 'π' is total potential energy and 'a' is the crack length. Substituting and solving equations (6.7, 6.9) and combining with the constants derived in Appendix A, we get

$$PE = (N + N^T)\left\{S\left[\sum_{j=1}^{3}\alpha_j(\sinh(\lambda_j(S-L))(\gamma_j^{(3)} + \frac{B_{22}^{(3)}}{A_{22}^{(3)}} + p_j^{(1)}\frac{B_{22}^{(1)}}{A_{22}^{(1)}} + \gamma_j^{(1)})\right.\right.$$

$$+\eta_j^{(3)} L\left(\frac{1}{A_{22}^{(3)}} - \frac{1}{A_{22}^{(1)}}\right)\cosh(\lambda_j(S-L)) + \frac{N+N^T}{A_{22}}\left(2S - L + (L^2 - SL)\frac{A_{22}^{(3)}}{A_{22}^{(1)}}\right)$$

$$+\frac{L}{2A_{22}^{(1)}}\left(N + N^T - 2\overline{Q}_{22}^{(2)} h^{(2)} \int_{T_{ref}}^{T_f} \alpha_y^{(2)} dT\right)\Bigg]$$

$$+\left[\sum_{j=1}^{3} \alpha_j \sinh(\lambda_j(S-L)) \frac{(e^{4\omega S} - 4\omega S e^{2\omega S} - 1)}{(e^{\omega(S-L)} - e^{\omega(S+L)})(2e^{\omega S} - e^{\omega(S-L)} - e^{\omega(S+L)})}\right]\Bigg\}$$

(6.14)

Solving for G^{MC}, we get

$$G^{MC} = (N+N^T)\Bigg\{\Bigg[\sum_{j=1}^{3} \alpha_j (\sinh(\lambda_j(S-L))(\gamma_j^{(3)} + \frac{B_{22}^{(3)}}{A_{22}^{(3)}} + p_j^{(1)} \frac{B_{22}^{(1)}}{A_{22}^{(1)}} + \gamma_j^{(1)})$$

$$+\eta_j^{(3)} L\left(\frac{1}{A_{22}^{(3)}} - \frac{1}{A_{22}^{(1)}}\right)\cosh(\lambda_j(S-L)) + \frac{N+N^T}{A_{22}}\left(2S - L + (L^2 - SL)\frac{A_{22}^{(3)}}{A_{22}^{(1)}}\right)$$

$$+\frac{L}{2A_{22}^{(1)}}\left(N + N^T - 2\overline{Q}_{22}^{(2)} h^{(2)} \int_{T_{ref}}^{T_f} \alpha_y^{(2)} dT\right)\Bigg]$$

$$+S\sum_{j=1}^{3} \alpha_j (\lambda_j \cosh(\lambda_j(S-L))(\gamma_j^{(3)} + \frac{B_{22}^{(3)}}{A_{22}^{(3)}} + p_j^{(1)} \frac{B_{22}^{(1)}}{A_{22}^{(1)}} + \gamma_j^{(1)})$$

$$+S\eta_j^{(3)} L\left(\frac{1}{A_{22}^{(3)}} - \frac{1}{A_{22}^{(1)}}\right)\lambda_j \sinh(\lambda_j(S-L)) + S\frac{N+N^T}{A_{22}}(2-L)\frac{A_{22}^{(3)}}{A_{22}^{(1)}}$$

$$+\frac{(e^{\omega(S-L)} - e^{\omega(S+L)})(2e^{\omega S} - e^{\omega(S-L)} - e^{\omega(S+L)})(4\omega e^{4\omega S} - 8\omega^2 S e^{2\omega S} - 4\omega e^{2\omega S})}{(e^{\omega(S-L)} - e^{\omega(S+L)})^2 (2e^{\omega S} - e^{\omega(S-L)} - e^{\omega(S+L)})^2}\Bigg\}$$

(6.15)

6.4.2 SERR for delamination growth

Using the potential energy expression obtained in section 6.3.1 for initial crack spacing of '2S' and after formation of new cracks with crack spacing of 'S', approach followed by Zhang et al [13,14] was used. First partial derivative of potential energy with respect to delamination length gives the strain energy release rate as

$$G^{DL} = \frac{\partial \pi}{\partial L} \tag{6.16}$$

where GL^{DL} is the strain energy release rate due to delaminations, 'π' is total potential energy and 'L' is the half delamination length. Substituting and solving equations (6.7, 6.9) and combining with the constants derived in Appendix A, we get

$$\begin{aligned} PE = (N+N^T)\Bigg\{ S\Bigg[& \sum_{j=1}^{3} \alpha_j (\sinh(\lambda_j(S-L))(\gamma_j^{(3)} + \frac{B_{22}^{(3)}}{A_{22}^{(3)}} + p_j^{(1)} \frac{B_{22}^{(1)}}{A_{22}^{(1)}} + \gamma_j^{(1)}) \\ & + \eta_j^{(3)} L(\frac{1}{A_{22}^{(3)}} - \frac{1}{A_{22}^{(1)}}) \cosh(\lambda_j(S-L)) + \frac{N+N^T}{A_{22}} (2S - L + (L^2 - SL)\frac{A_{22}^{(3)}}{A_{22}^{(1)}}) \\ & + \frac{L}{2A_{22}^{(1)}} (N + N^T - 2\overline{Q}_{22}^{(2)} h^{(2)} \int_{T_{ref}}^{T_f} \alpha_y^{(2)} dT) \Bigg] \\ & + \Bigg[\sum_{j=1}^{3} \alpha_j \sinh(\lambda_j(S-L)) \frac{(e^{4\omega S} - 4\omega S e^{2\omega S} - 1)}{(e^{\omega(S-L)} - e^{\omega(S+L)})(2e^{\omega S} - e^{\omega(S-L)} - e^{\omega(S+L)})} \Bigg] \Bigg\} \end{aligned} \tag{6.17}$$

Solving for G^{DL}, we get

$$G^{DL} = (N + N^T)\Bigg\{ S\Bigg[\sum_{j=1}^{3} \alpha_j(-\lambda_j \cosh(\lambda_j(S-L))(\gamma_j^{(3)} + \frac{B_{22}^{(3)}}{A_{22}^{(3)}} + p_j^{(1)} \frac{B_{22}^{(1)}}{A_{22}^{(1)}} + \gamma_j^{(1)})$$

$$+\eta_j^{(3)}(\frac{1}{A_{22}^{(3)}} - \frac{1}{A_{22}^{(1)}})\cosh(\lambda_j(S-L)) - \eta_j^{(3)}\lambda_j L(\frac{1}{A_{22}^{(3)}} - \frac{1}{A_{22}^{(1)}})\sinh(\lambda_j(S-L))$$

$$+\frac{1}{2A_{22}^{(1)}}(N + N^T - 2\overline{Q}_{22}^{(2)} h^{(2)} \int_{T_{ref}}^{T_f} \alpha_y^{(2)} dT) + \frac{N + N^T}{A_{22}}(-1 + 2L - S)\frac{A_{22}^{(3)}}{A_{22}^{(1)}} \Bigg]$$

$$+\sum_{j=1}^{3} \alpha_j(-\lambda_j \cosh(\lambda_j(S-L))(e^{4\omega S} - 4\omega S e^{2\omega S} - 1)$$

$$\times\Bigg(\frac{(e^{\omega(S-L)} - e^{\omega(S+L)})(\omega e^{\omega(S-L)} - \omega e^{\omega(S+L)})}{(e^{\omega(S-L)} - e^{\omega(S+L)})^2 (2e^{\omega S} - e^{\omega(S-L)} - e^{\omega(S+L)})^2}$$

$$-\frac{(\omega e^{\omega(S-L)} + \omega e^{\omega(S+L)})(2e^{\omega S} - e^{\omega(S-L)} - e^{\omega(S+L)})}{(e^{\omega(S-L)} - e^{\omega(S+L)})^2 (2e^{\omega S} - e^{\omega(S-L)} - e^{\omega(S+L)})^2} \Bigg)\Bigg\} \tag{6.18}$$

CHAPTER 7

FINITE ELEMENT MODELING

For the verification of the analytically obtained results, 2-D and 3-D finite element models are constructed. A two dimensional model was constructed to compute the delaminated crack opening displacement occurring in laminates due to thermal and mechanical loadings for given crack spacing and delamination length. Finite element analysis was performed using commercial software ABAQUS, versions 6.3 and 6.4. Due to symmetry of laminate geometry and loading conditions, only half of the laminate representative volume element with single crack is analyzed. A plane strain assumption is made in X-Z plane and a two dimensional mesh with 8 node plane strain element is used.

Two dimensional finite element was done on [0/90/0]s IM7/PETI-5 laminate as shown in Fig. 7.1. The delaminated crack opening displacement was calculated from the computed displacement of nodes at the delaminated 0º-90º layer interface. The crack spacing considered is 4.4 inch and delamination length is 0.16 inch. This is verification of Case1 (Five Layer Model). Also, two dimensional analysis was performed on top layer of

[0/90/0]s laminate for Case2 (Three Layer Model) as shown in Fig. 7.2 with same crack spacing and delamination length as that of Case1.

Three dimensional analysis was performed on [0/90/0]s and [45/0/-45/90]s laminates using a model as shown in Fig. 7.3. A three dimensional quadratic 20 node brick element was used to create the mesh. Crack was modeled by creating extra nodes as per the requirement in corresponding elements and thus, connectivity was also changed for those elements. A crack spacing of 0.5 inches was used with delamination length of 0.01 inches. A considerably wide model (1 inch in Z direction and 0.5 inches in X direction) was created to avoid the edge effects, for considering plain strain equivalence in analytical model for X direction. Thickness of the full laminate is 0.048 inches (in Y direction).

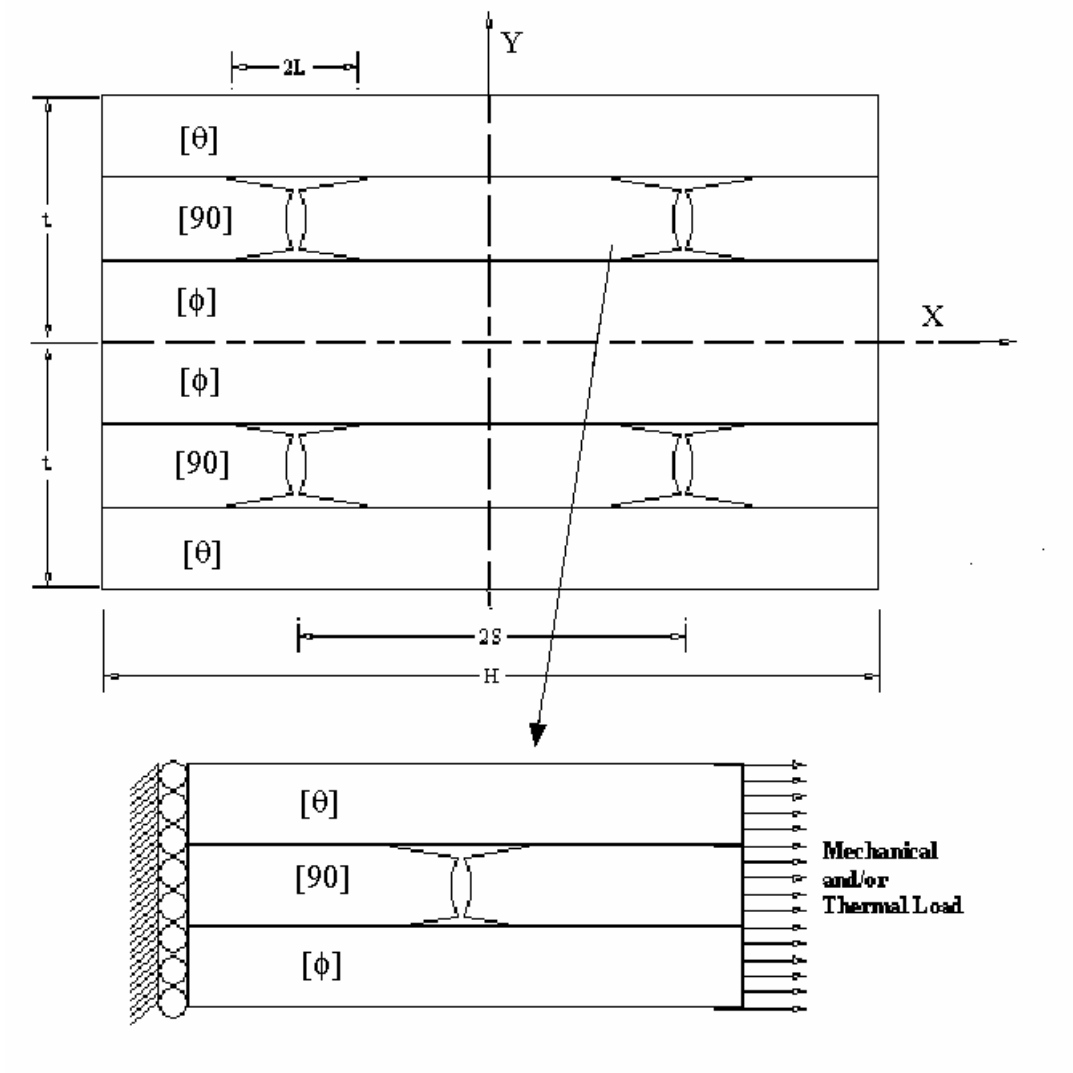

Fig. 7.1. 2-D FEA model of Case1 (Five Layer Model) for [0/90/0]s

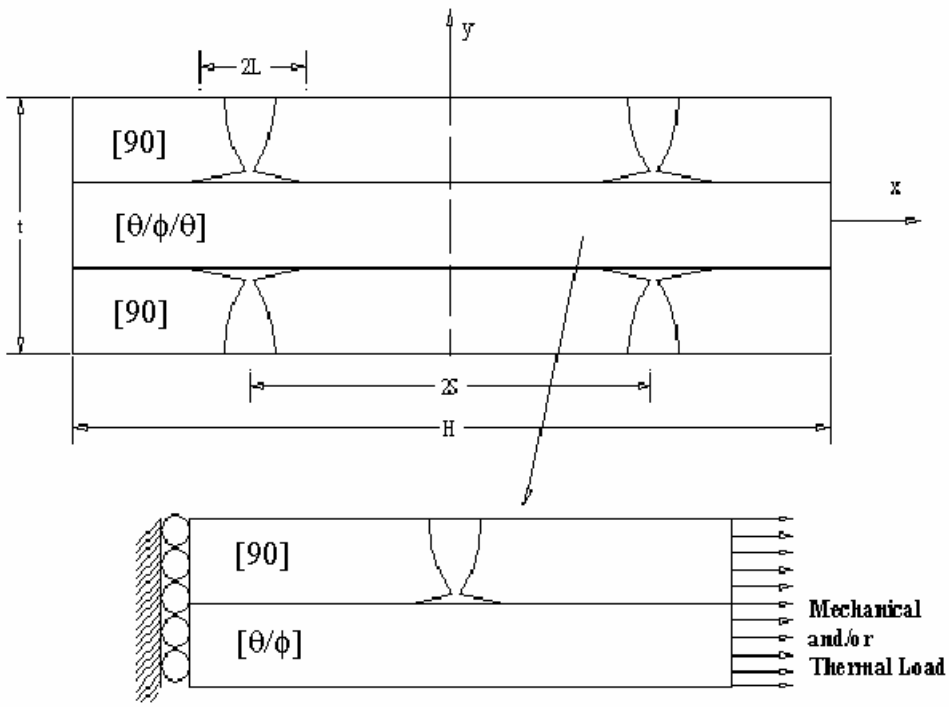

Fig. 7.2. 2-D FEA model of Case2 (Three Layer Model) for [0/90/0]s

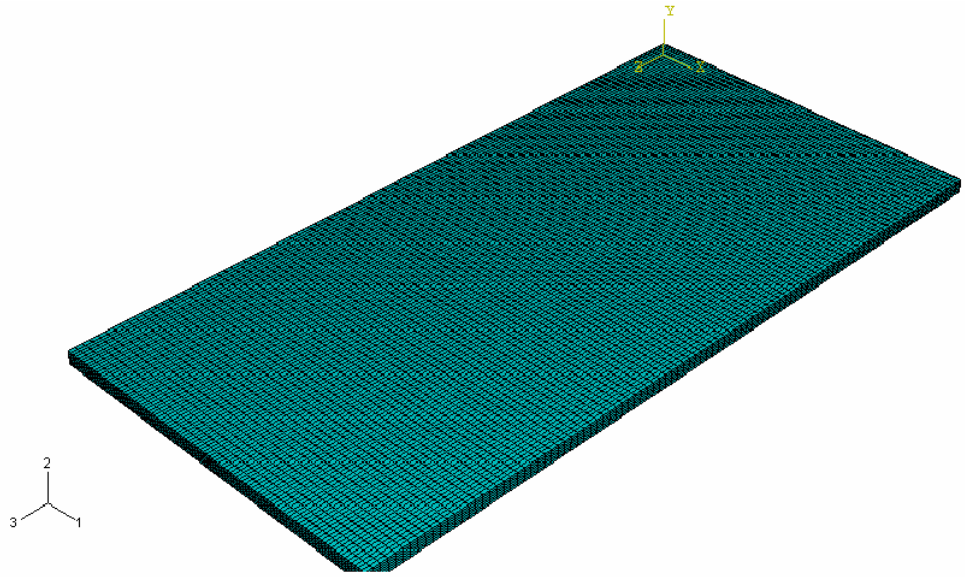

Fig. 7.3. 3-D FEA model mesh with quadratic 3-D 20 node brick elements, length X=0.5 inches, width Z=1 inch, thickness of half laminate Y=0.024 inches

CHAPTER 8

RESULTS AND DISCUSSION

From the analytical solutions of Three and Five Layer models for various configurations of IM-7/PETI-5 graphite epoxy laminates, following results are observed.

8.1 FLM – FEM comparison

The results from the Five Layer Model were compared to Finite Element model results as discussed in Chapter 7. It can be seen from the Fig.8.1 through Fig.8.9 that the analytical model shows reasonable agreement with the 2D and 3D FEA results for arbitrarily oriented ply laminates. Laminate configurations of $[0/90/0]_s$ and $[45/0/-45/90]_s$ are used for comparison.

First $[0/90/0]_s$ laminate is compared with 2D FEA solutions. The error observed is as low as 1%. Fig.8.32 shows that the lines representing FLM and FEA solutions almost match exactly.

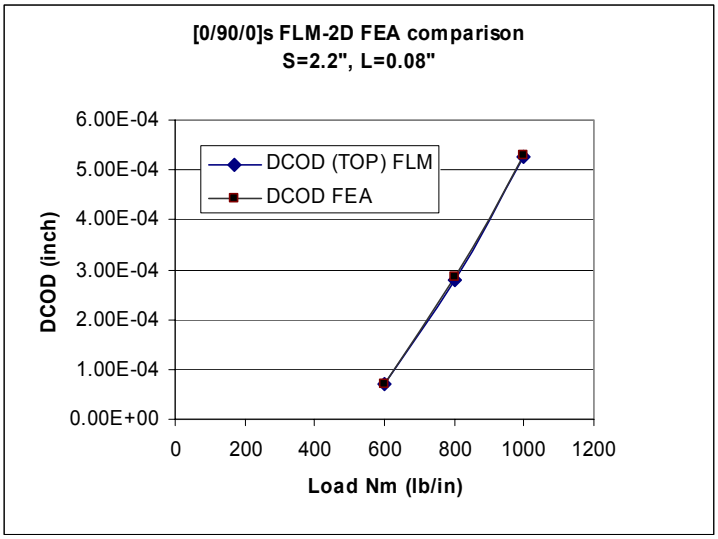

Fig.8.1 $[0/90/0]_s$ laminate, crack in 90˚ layer FLM-FEA comparison, mechanical load

For 3D FEA benchmark comparison, $[45/0/-45/90]_s$ laminate configuration is used. The analytical model results are in reasonable agreement with the finite element solutions with error ranging from 4% to 7% in various damaged layers for mechanical and thermal load conditions.

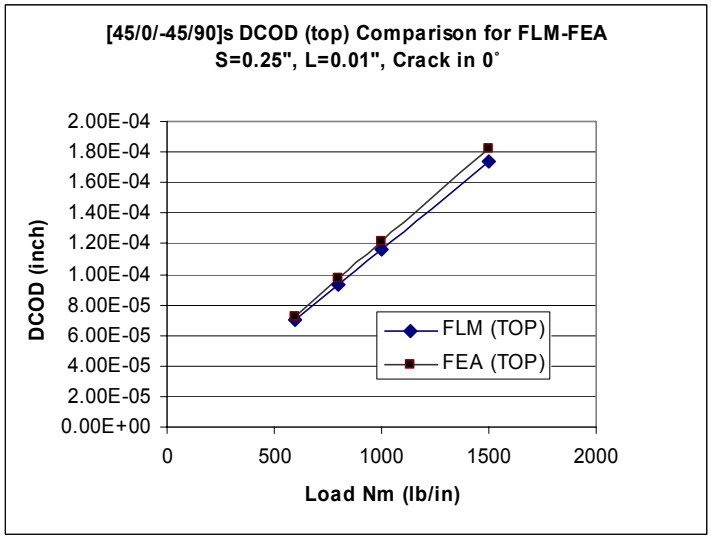

Fig.8.2 $[45/0/-45/90]_s$ laminate crack in 0˚ layer FLM-FEA comparison

DCOD (TOP) mechanical load

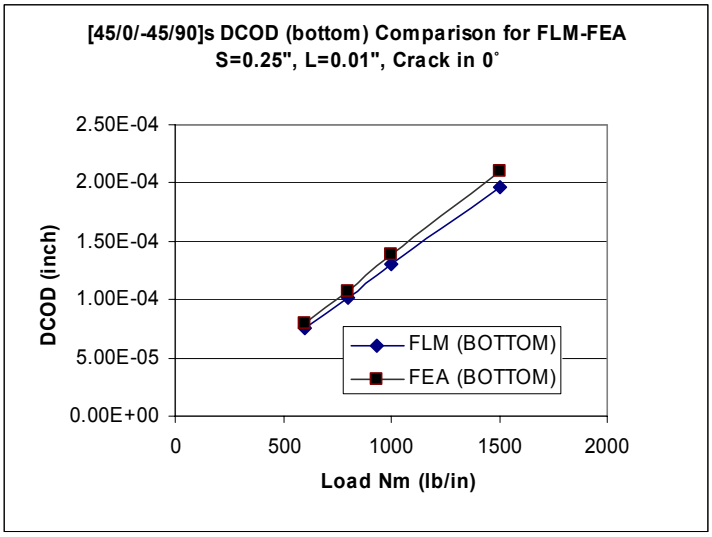

Fig.8.3 $[45/0/-45/90]_s$ laminate with crack in 0˚ layer FLM-FEA comparison S=0.25”and L=0.01”, DCOD (BOTTOM) mechanical load

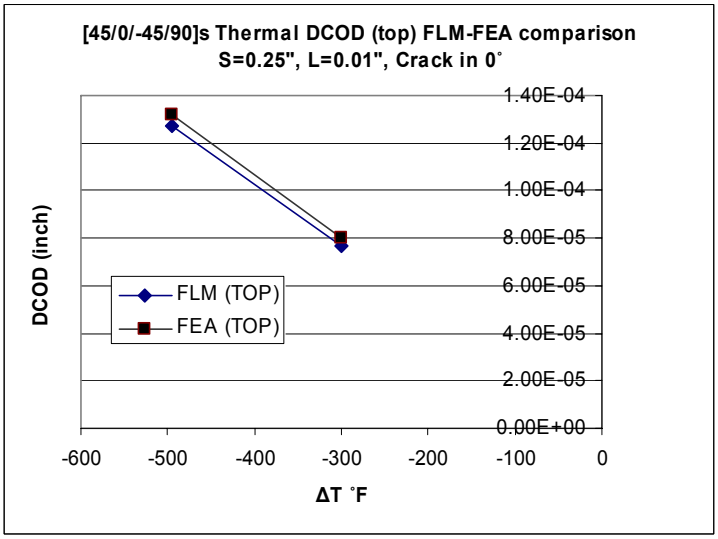

Fig.8.4 $[45/0/-45/90]_s$ laminate with crack in 0˚ layer FLM-FEA comparison S=0.25”and L=0.01”, DCOD (TOP) thermal load

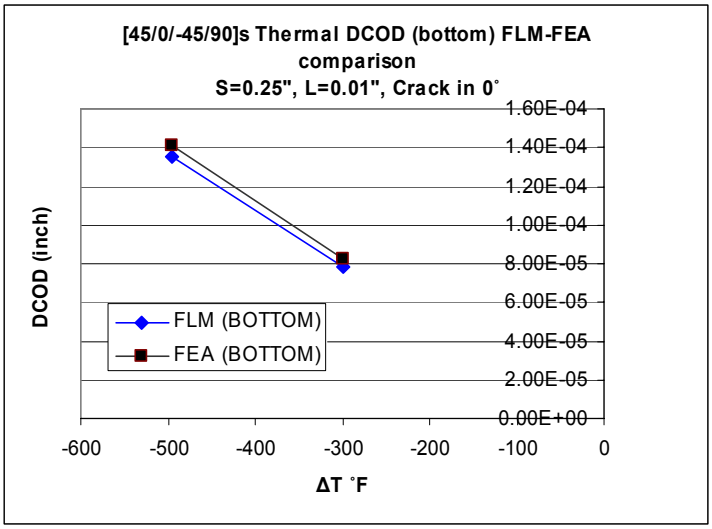

Fig.8.5 $[45/0/-45/90]_s$ laminate with crack in 0˚ layer FLM-FEA comparison

S=0.25”and L=0.01”, DCOD (BOTTOM) thermal load

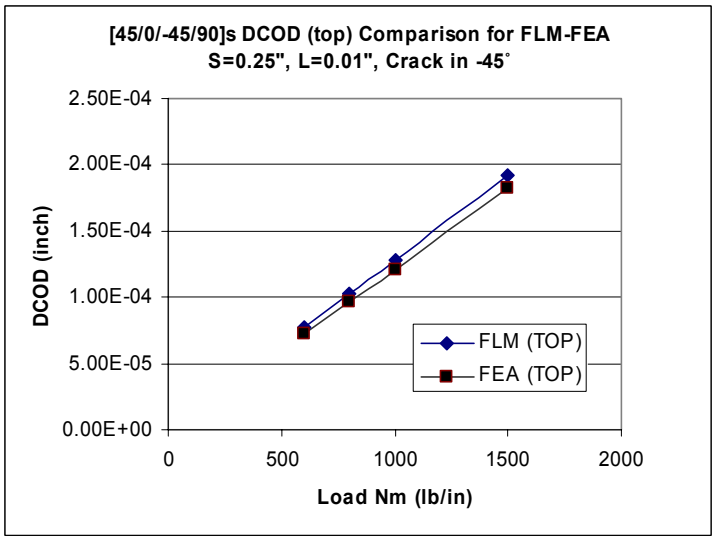

Fig.8.6 $[45/0/-45/90]_s$ laminate with crack in -45˚ layer FLM-FEA comparison

S=0.25”and L=0.01”, DCOD (TOP) mechanical load

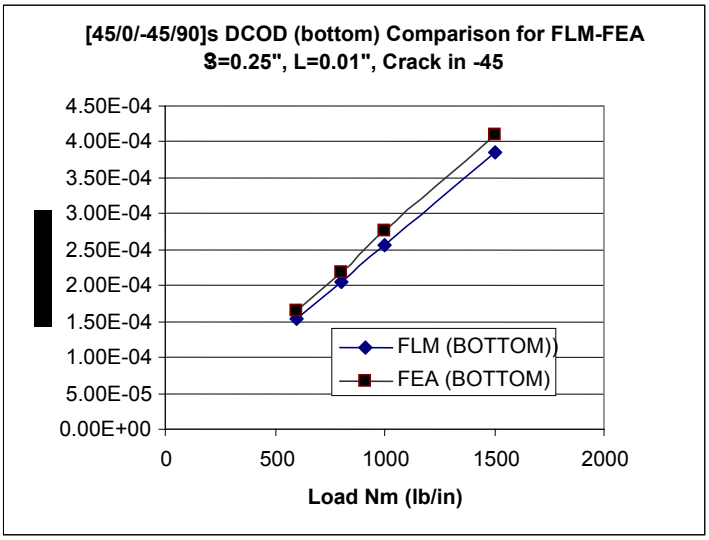

Fig.8.7 $[45/0/-45/90]_s$ laminate with crack in -45˚ layer FLM-FEA comparison S=0.25”and L=0.01”, DCOD (BOTTOM) mechanical load

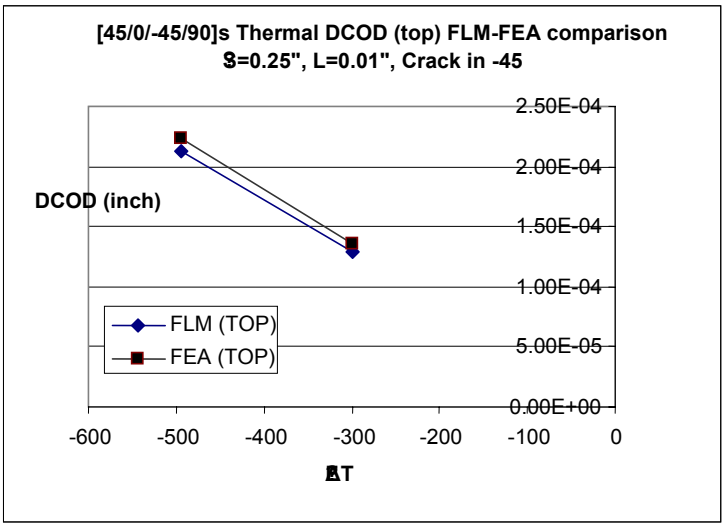

Fig.8.8 $[45/0/-45/90]_s$ laminate with crack in -45˚ layer FLM-FEA comparison S=0.25”and L=0.01”, DCOD (TOP) thermal load

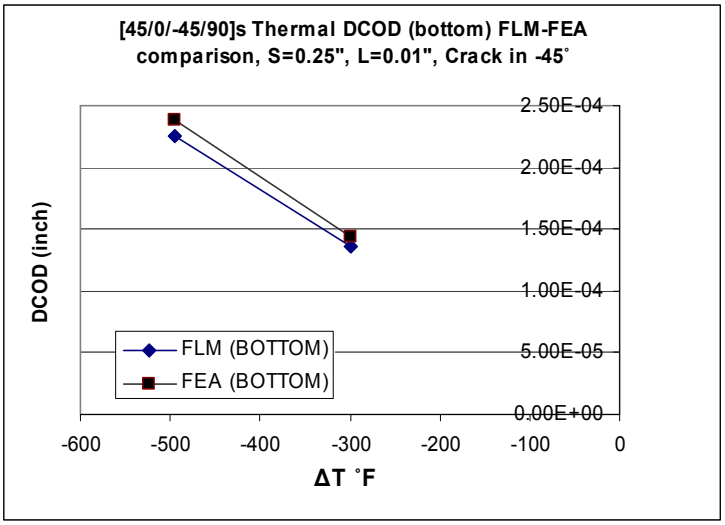

Fig.8.9 $[45/0/-45/90]_s$ laminate with crack in -45˚ layer FLM-FEA comparison S=0.25”and L=0.01”, DCOD (BOTTOM) thermal load

The crack shapes obtained from FLM and FEA are also compared. It can be seen from Fig.8.10 through Fig.8.17 that FEA predicts a “V” shape DCOD while FLM/TLM give a straight line for crack shape as FLM/TLM models are based on first order shear deformation theory where only linear variation of displacement is considered through each layer.

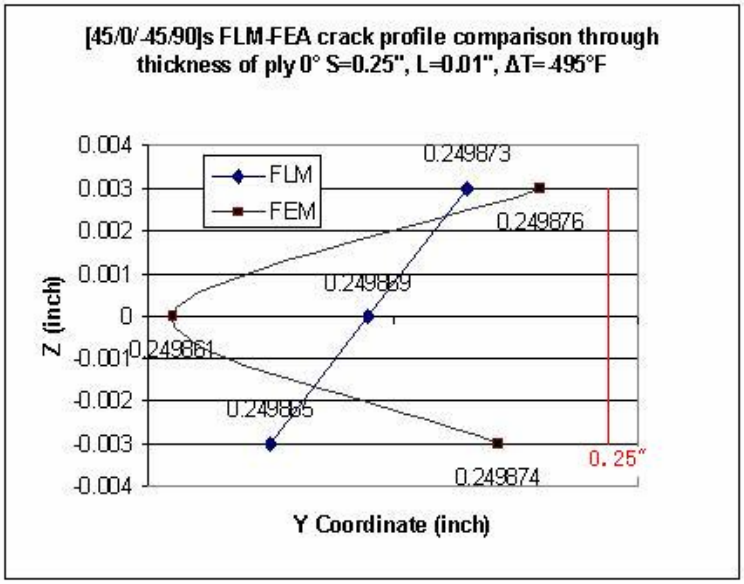

Fig.8.10 $[45/0/-45/90]_s$ laminate with crack in 0˚ layer FLM-FEA crack shape comparison, S=0.25”and L=0.01” ΔT = -495˚F

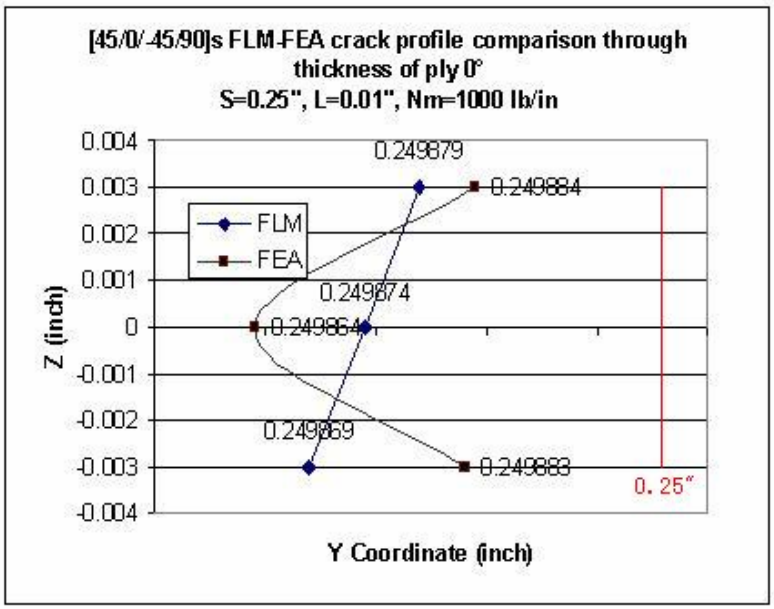

Fig.8.11 $[45/0/-45/90]_s$ laminate with crack in 0˚ layer FLM-FEA crack shape comparison, S=0.25”and L=0.01” N_m=1000 lb/in

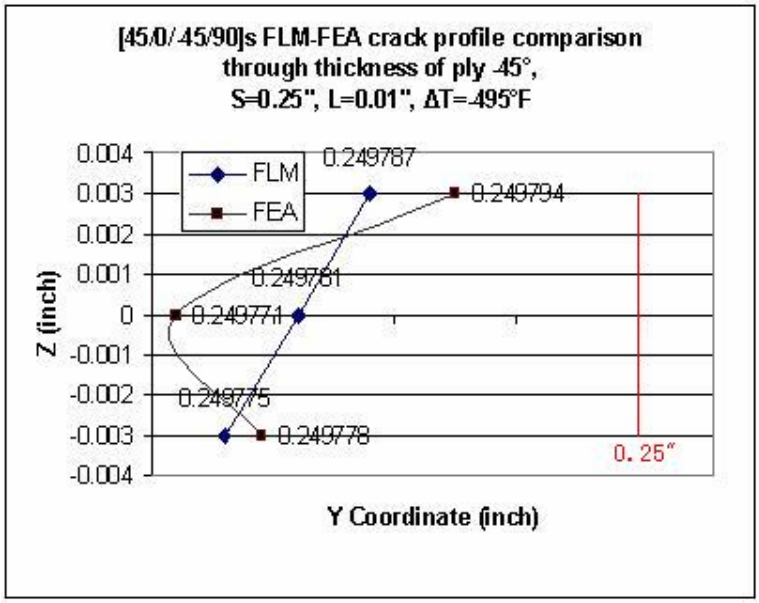

Fig.8.12 $[45/0/-45/90]_s$ laminate with crack in -45˚ layer FLM-FEA crack shape comparison, S=0.25”and L=0.01” ΔT = -495˚F

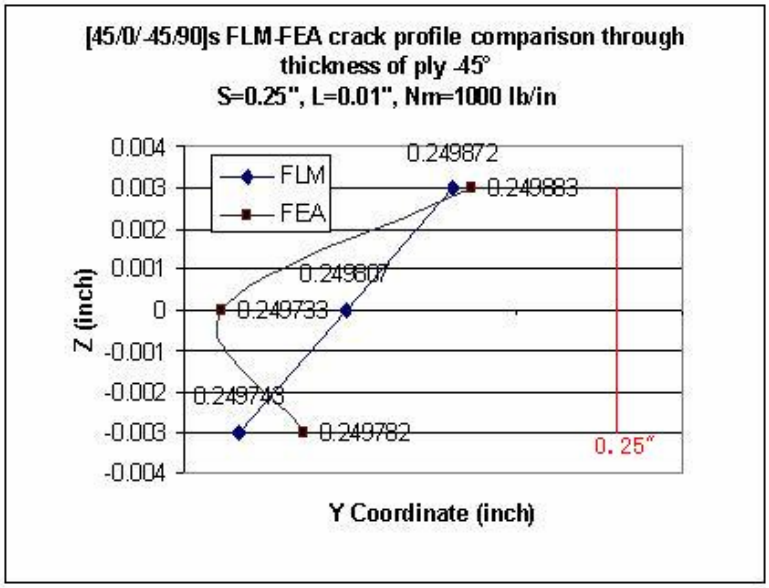

Fig.8.13 $[45/0/-45/90]_s$ laminate with crack in -45˚ layer FLM-FEA crack shape comparison, S=0.25”and L=0.01”, N_m=1000 lb/in

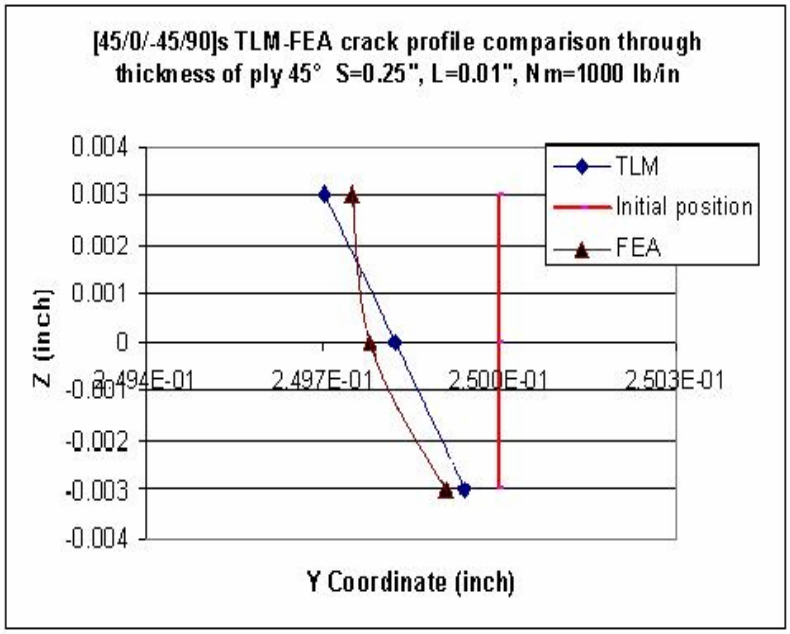

Fig.8.14 $[45/0/-45/90]_s$ laminate with crack in 45˚ layer TLM-FEA crack profile comparison, S=0.25”and L=0.01”, N_m=1000 lb/in

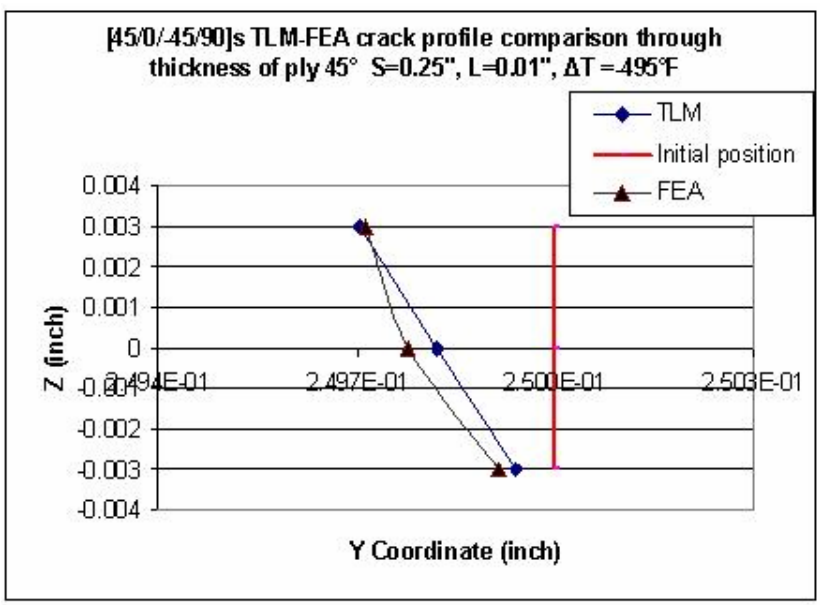

Fig.8.15 $[45/0/-45/90]_s$ laminate with crack in 45˚ layer TLM-FEA crack profile comparison, S=0.25”and L=0.01”, ΔT = -495˚F

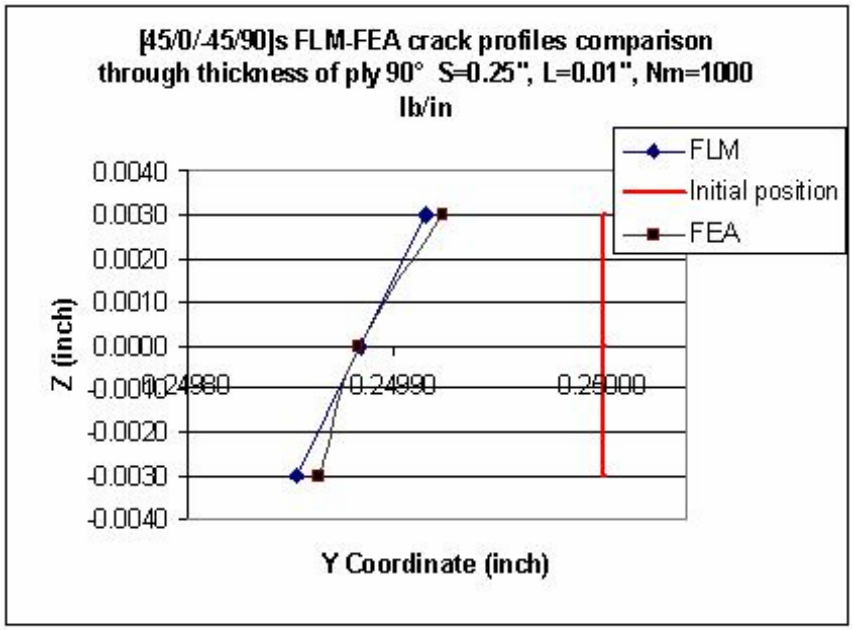

Fig.8.16 $[45/0/-45/90]_s$ laminate with crack in 90˚ layer TLM-FEA crack profile comparison, S=0.25”and L=0.01”, N_m=1000 lb/in

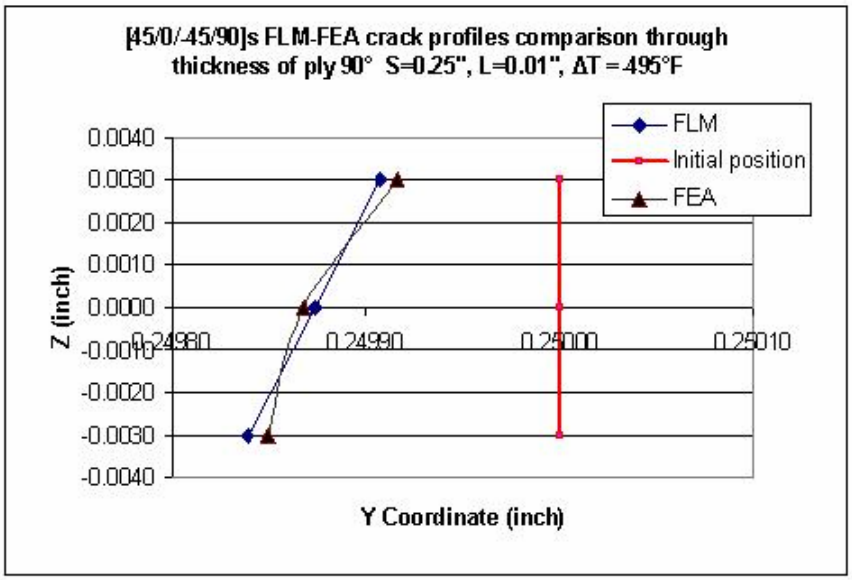

Fig.8.17 $[45/0/-45/90]_s$ laminate with crack in 90˚ layer TLM-FEA crack profile comparison, S=0.25”and L=0.01”, ΔT = -495˚F

Fig. 8.18 and Fig. 8.19 give the comparison between FLM/TLM and FEA results in form of % error for mechanical and thermal loads.

[45/0/-45/90]s		S	0.25	inch	
		L	0.01	inch	
Nm		1000 lb/in			
Layer		FLM DCOD inch	3D FEA DCOD inch	% error	
0°	top	1.16E-04	1.21E-04	4.29	FLM
0°	bottom	1.31E-04	1.39E-04	5.62	FLM
-45°	top	1.28E-04	1.21E-04	5.79	FLM
-45°	bottom	2.57E-04	2.76E-04	6.61	FLM
45°	bottom	5.81E-05	5.72E-05	1.61	TLM

Fig.8.18 $[45/0/-45/90]_s$ laminate with crack in layers FLM-FEA DCOD comparison, S=0.25”and L=0.01”, N_m=1000 lb/in

[45/0/-45/90]s		S	0.25	inch	
		L	0.01	inch	
ΔT		-495	°F		
Layer		FLM DCOD inch	3D FEA DCOD inch	% error	
0°	top	1.27E-04	1.32E-04	3.79	FLM
0°	bottom	1.35E-04	1.41E-04	4.26	FLM
-45°	top	2.13E-04	2.23E-04	4.48	FLM
-45°	bottom	2.25E-04	2.38E-04	5.29	FLM
45°	bottom	1.16E-04	1.14E-04	1.80	TLM

Fig.8.19 $[45/0/-45/90]_s$ laminate with crack in layers FLM-FEA DCOD comparison, S=0.25”and L=0.01”, ΔT = -495˚F

8.2 Effect of crack density on DCOD

A $[0/90/0]_s$ configuration is considered using delamination length as 0.01 inch and crack spacing S (or crack density CD) is varied as CD=1/2S, under a thermal load of -495˚F. Keeping the same delamination length, various load conditions are also applied as mechanical force of 1000 lb/in. Also, another laminate configuration $[45/0/-45/90]_s$ is observed under similar load conditions for different cases of cracks in 0˚, -45˚ and 45˚ layers separately. Results in Fig.8.20 through Fig.8.27 show that up to crack density of 5 cracks per inch, the DCOD remains constant and then decreases with increasing crack density. The higher the value for half crack spacing, the lower the crack density. Therefore, the effect of delaminated crack opening remains constant for lower crack density values. This can be attributed to the fact that as number of cracks per inch increases, maximum normal tensile stress in the cracked layer decreases because the crack spacing is less than the critical length necessary for complete load transfer from the undamaged plies. This is observed in FLM as well as TLM solutions.

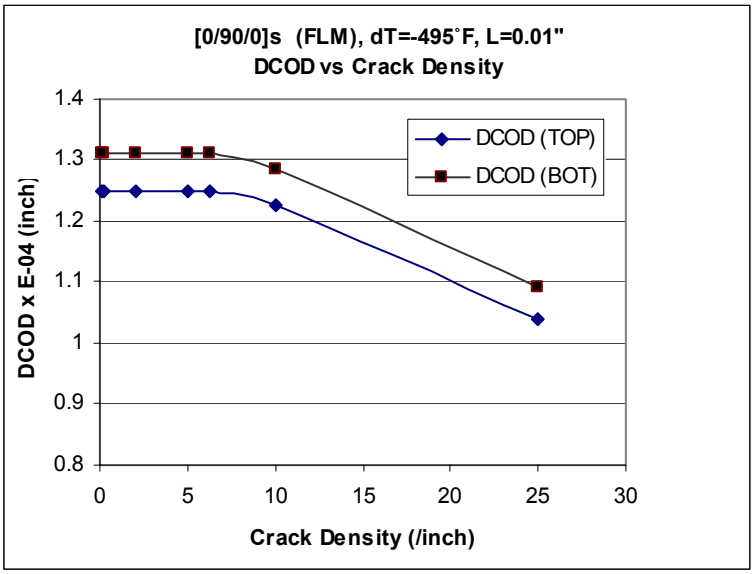

Fig.8.20 $[0/90/0]_s$ laminate with crack in 90˚ layer (FLM) for ΔT = -495˚F, L=0.01”

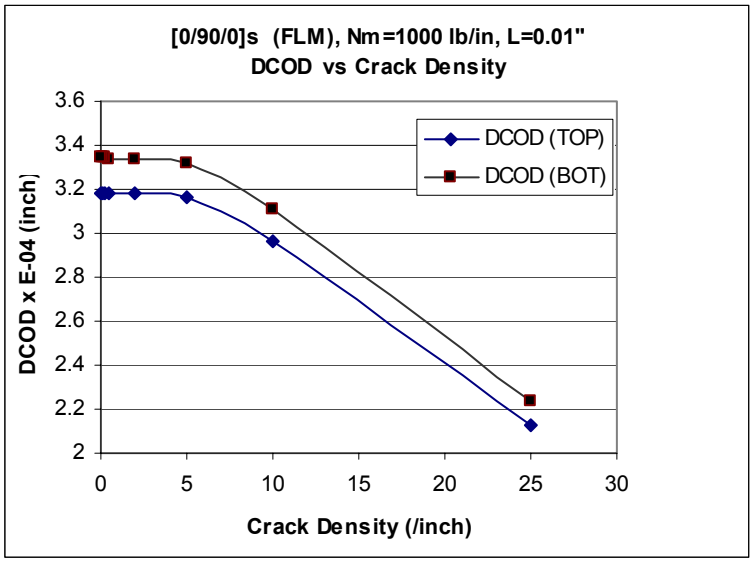

Fig.8.21 $[0/90/0]_s$ laminate with crack in 90˚ layer (FLM) for N_m = 1000 lb/in, L=0.01”

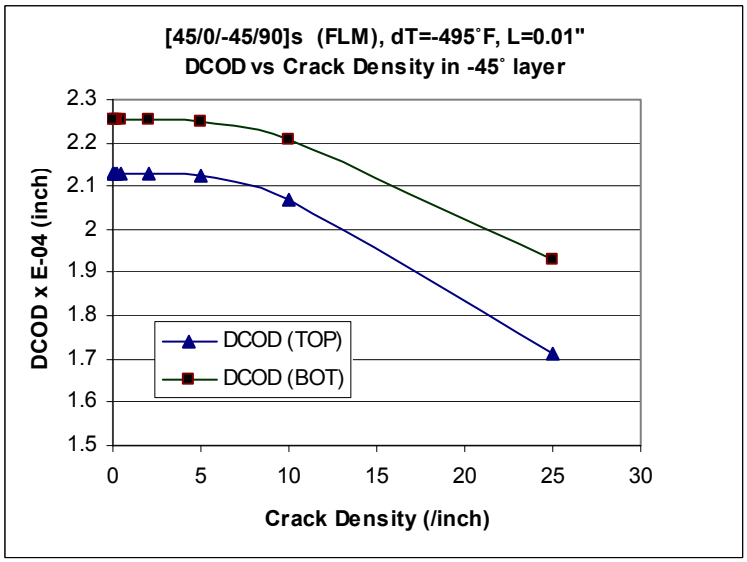

Fig.8.22 $[45/0/-45/90]_s$ laminate with crack in -45˚ layer (FLM) for

ΔT = -495˚F and L=0.01”

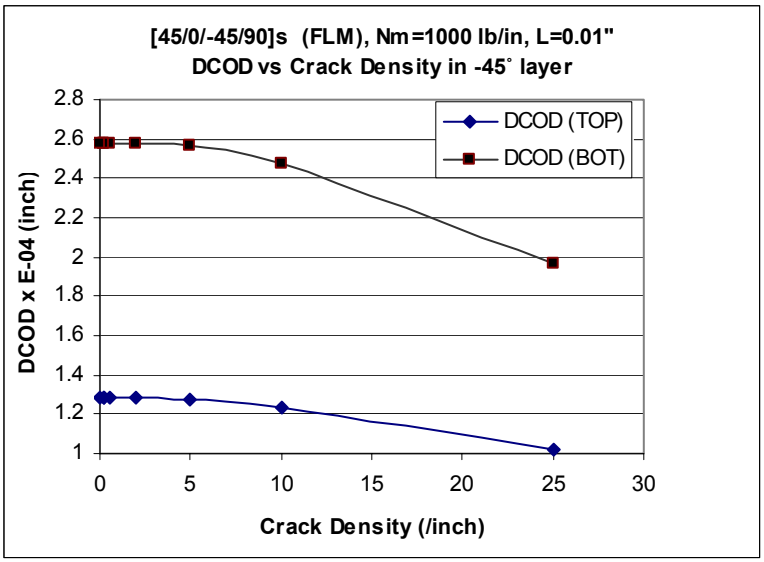

Fig.8.23 $[45/0/-45/90]_s$ laminate with crack in -45˚ layer (FLM) for

N_m = 1000 lb/in and L=0.01”

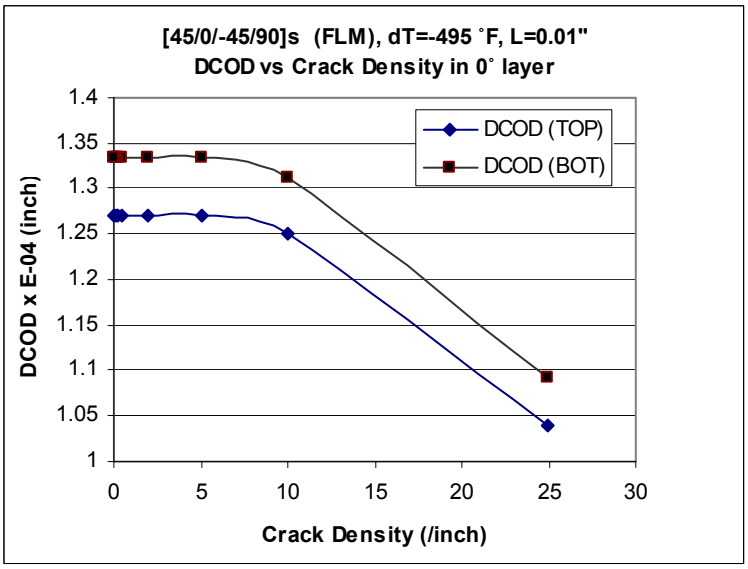

Fig.8.24 $[45/0/-45/90]_s$ laminate with crack in -45˚ layer (FLM) for

ΔT = -495˚F and L=0.01”

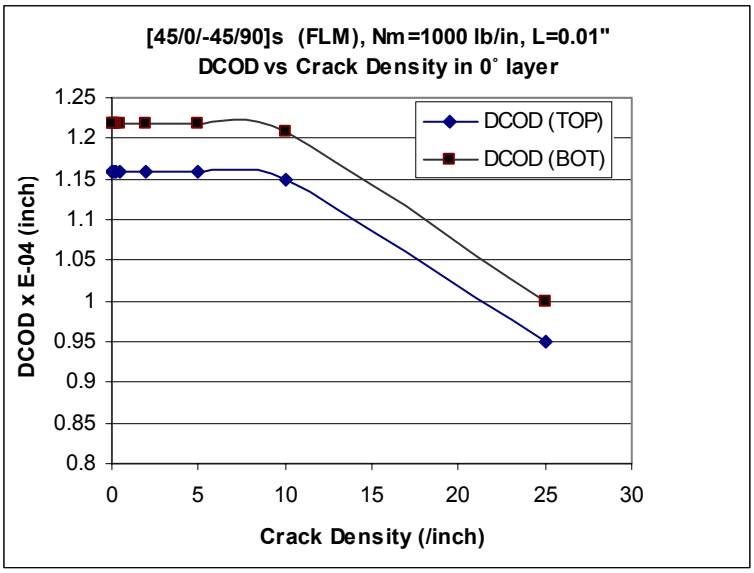

Fig.8.25 $[45/0/-45/90]_s$ laminate with crack in -45˚ layer (FLM) for

N_m = 1000 lb/in and L=0.01”

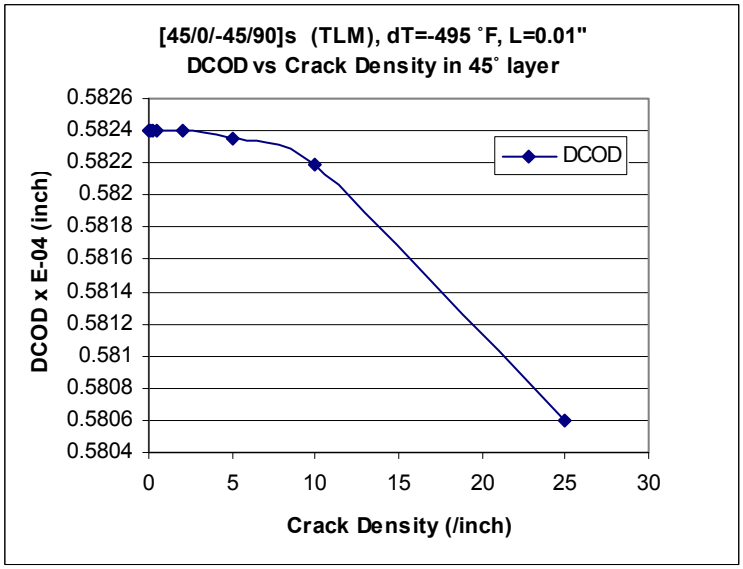

Fig.8.26 $[45/0/-45/90]_s$ laminate with crack in top 45˚ layer (TLM) for

ΔT = -495˚F and L=0.01”

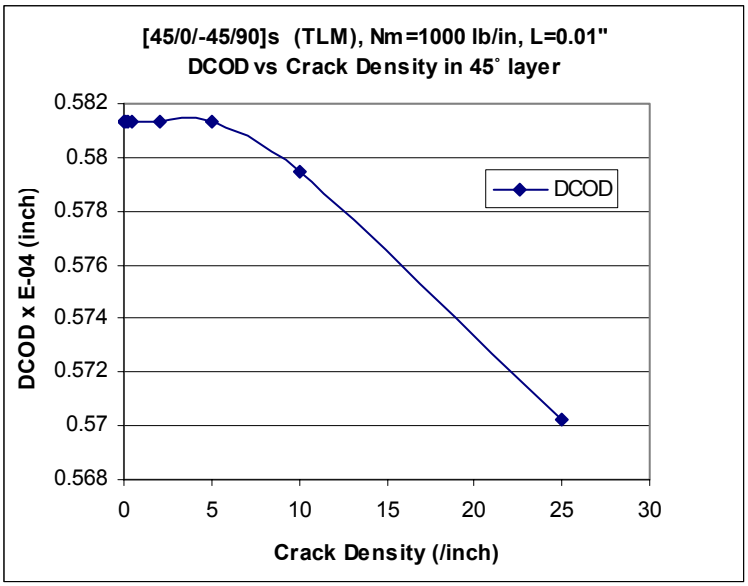

Fig.8.27 $[45/0/-45/90]_s$ laminate with crack in top 45˚ layer (TLM) for

N_m = 1000 lb/in and L=0.01”

8.3 Effect of delamination length on DCOD

Similar to the cases in first part, a $[0/90/0]_s$ configuration is considered using two different sets of crack spacing as S=0.25” and S=2.2” for various delamination lengths L, under a thermal load of -495˚F and mechanical force of 1000 lb/in. Also, another laminate configuration $[45/0/-45/90]_s$ is observed under similar load conditions for different cases of cracks in the 0˚, -45˚ and 45˚ layers separately. Results from Fig.8.28 through Fig.8.41 show that DCOD increases linearly with the increase in delamination length for a given value of crack density and load. This is observed in FLM as well as TLM solutions.

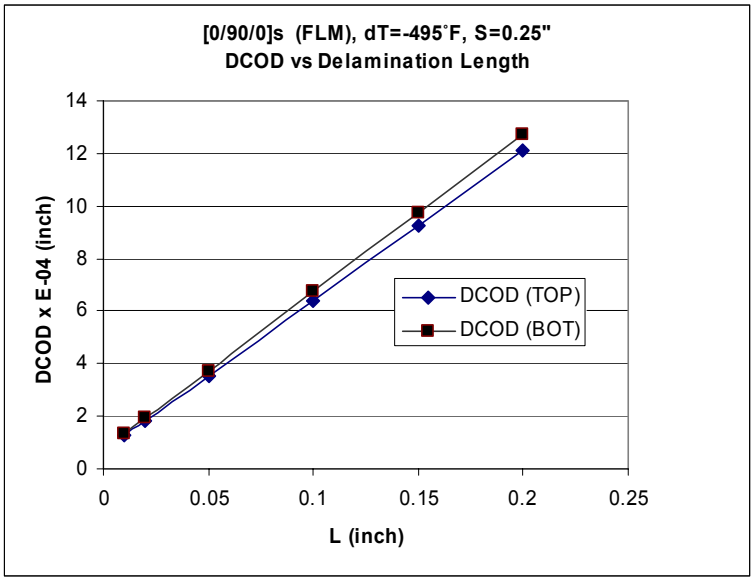

Fig.8.28 $[0/90/0]_s$ laminate with crack in 90˚ layer (FLM) for

ΔT = -495˚F and S=0.25”

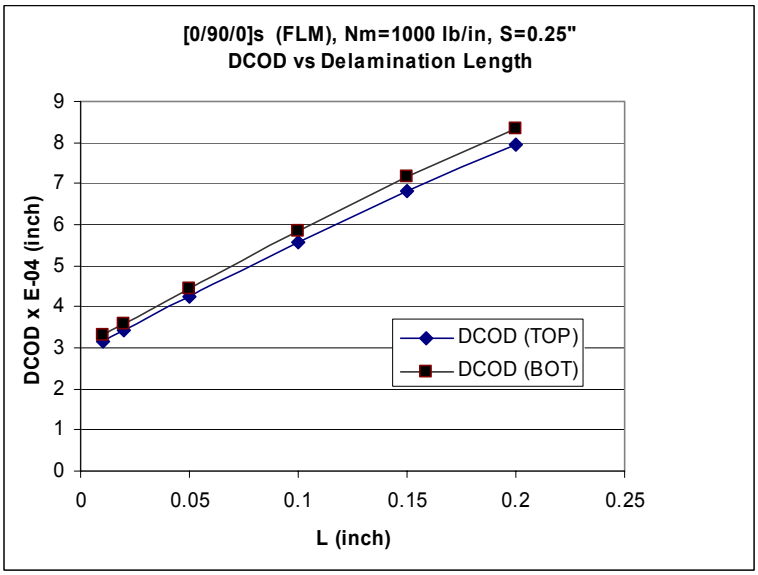

Fig.8.29 $[0/90/0]_s$ laminate with crack in 90˚ layer (FLM) for

N_m = 1000 lb/in and S=0.25”

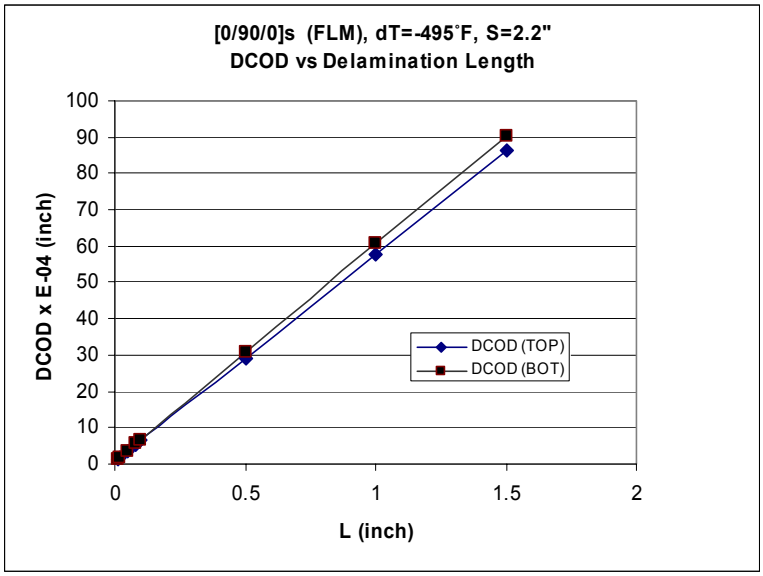

Fig.8.30 $[0/90/0]_s$ laminate with crack in 90˚ layer (FLM) for

ΔT = -495˚F and S=2.2”

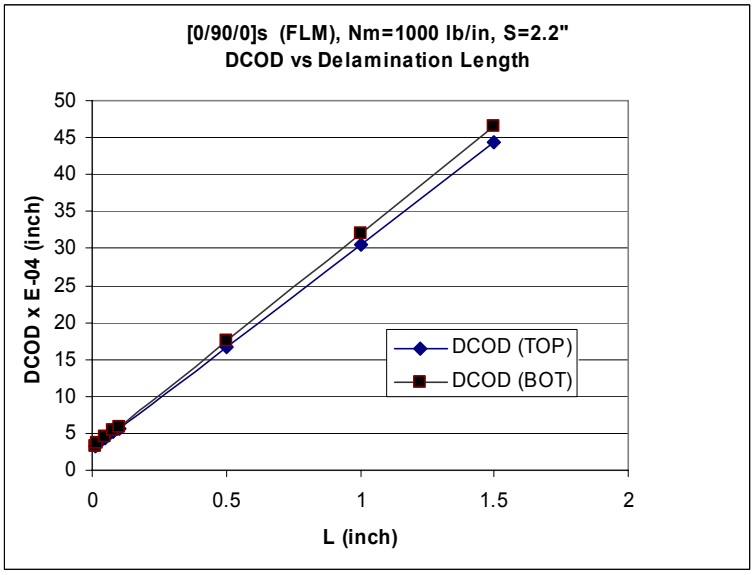

Fig.8.31 $[0/90/0]_s$ laminate with crack in 90˚ layer (FLM) for

N_m = 1000 lb/in and S=2.2”

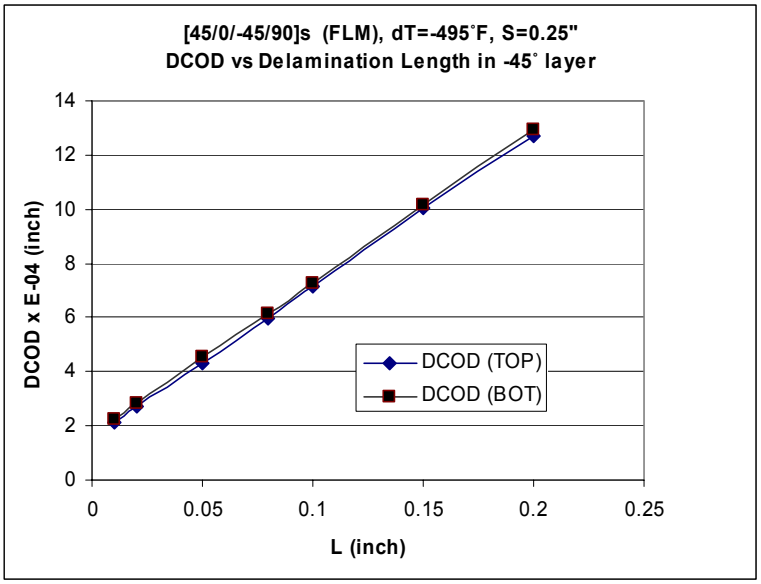

Fig.8.32 $[45/0/-45/90]_s$ laminate with crack in -45˚ layer (FLM) for

ΔT = -495˚F and S=0.25”

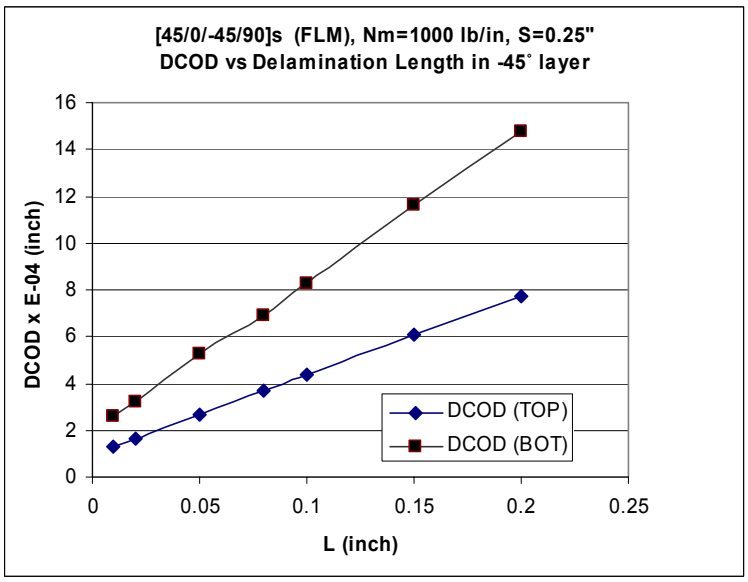

Fig.8.33 $[45/0/-45/90]_s$ laminate with crack in -45˚ layer (FLM) for

N_m = 1000 lb/in and S=0.25”

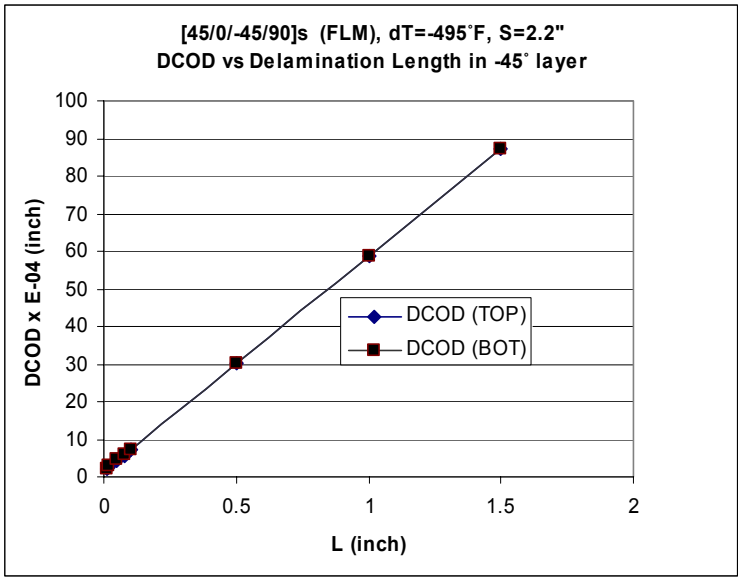

Fig.8.34 $[45/0/-45/90]_s$ laminate with crack in -45˚ layer (FLM) for

ΔT = -495˚F and S=2.2”

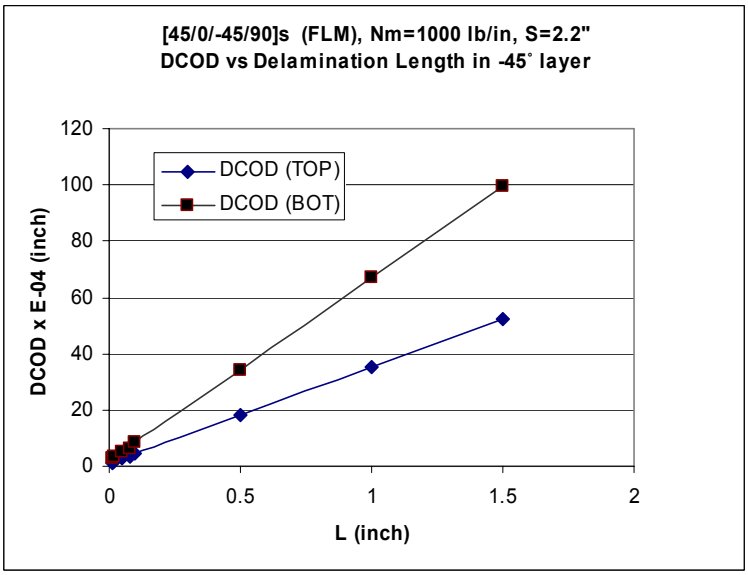

Fig.8.35 $[45/0/-45/90]_s$ laminate with crack in -45˚ layer (FLM) for

N_m = 1000 lb/in and S=2.2”

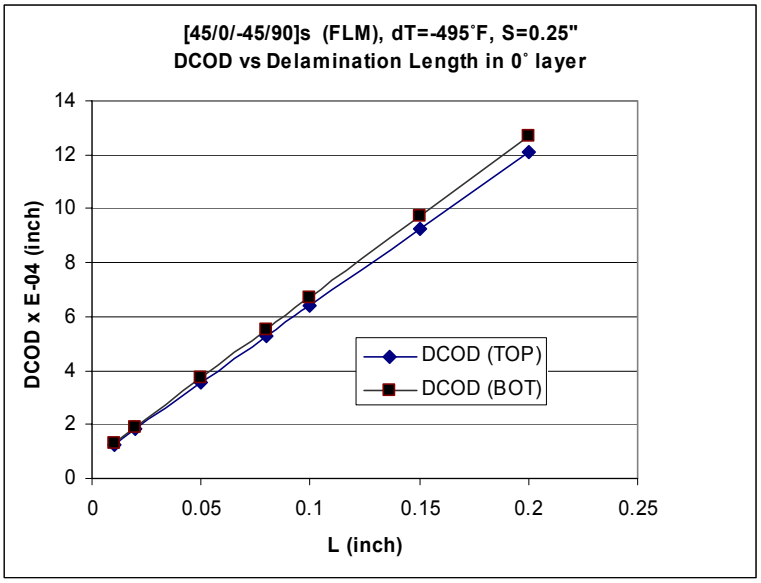

Fig.8.36 $[45/0/-45/90]_s$ laminate with crack in 0˚ layer (FLM) for

ΔT = -495˚F and S=0.25”

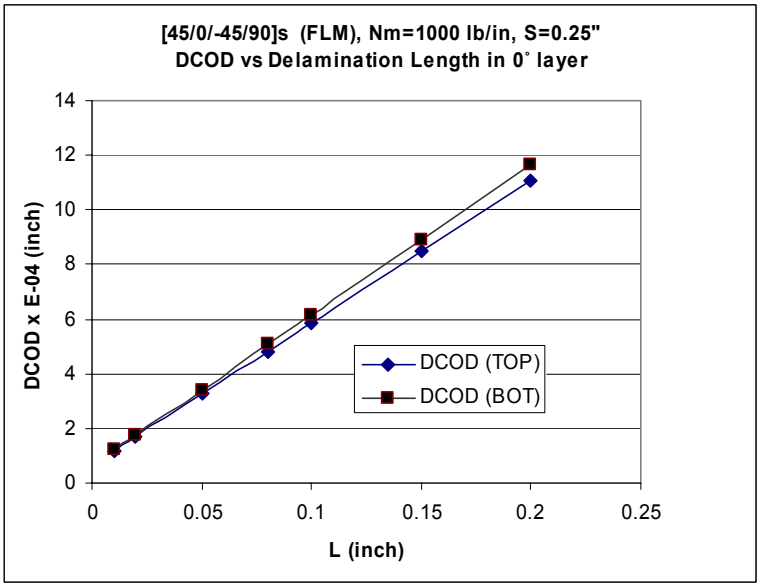

Fig.8.37 $[45/0/-45/90]_s$ laminate with crack in 0˚ layer (FLM) for

N_m = 1000 lb/in and S=0.25”

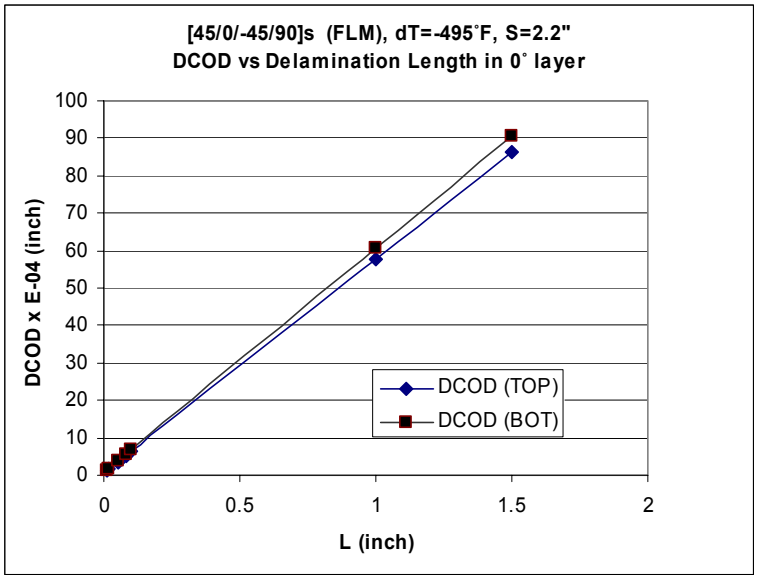

Fig.8.38 $[45/0/-45/90]_s$ laminate with crack in 0˚ layer (FLM) for

ΔT = -495˚F and S=2.2”

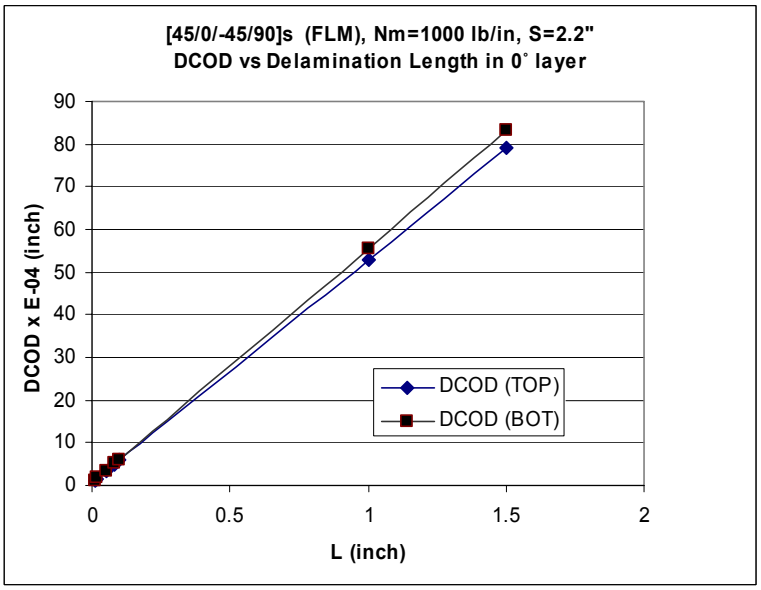

Fig.8.39 $[45/0/-45/90]_s$ laminate with crack in 0˚ layer (FLM) for

N_m = 1000 lb/in and S=2.2”

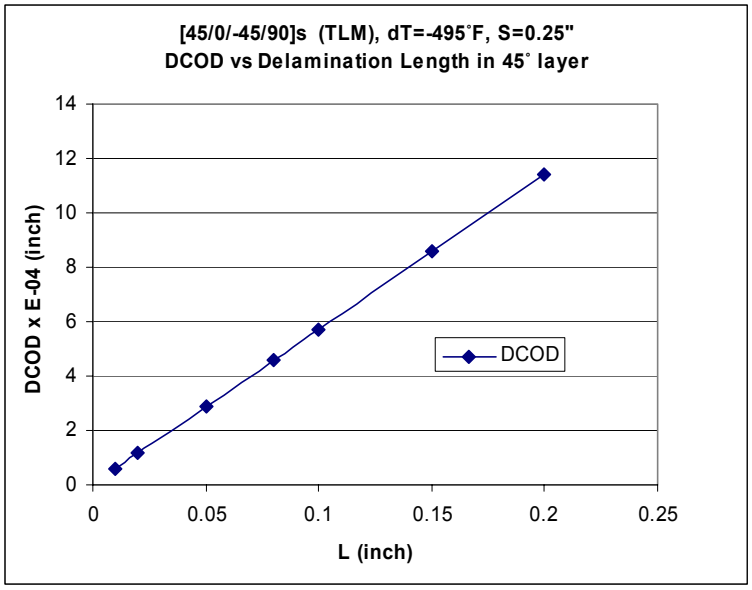

Fig.8.40 $[45/0/-45/90]_s$ laminate with crack in 45˚ layer (TLM) for

ΔT = -495˚F and S=0.25”

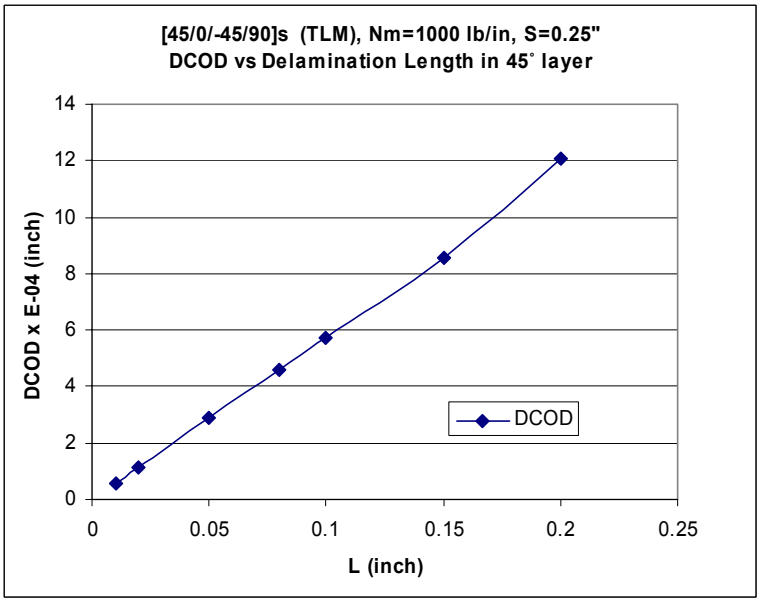

Fig.8.41 $[45/0/-45/90]_s$ laminate with crack in 45˚ layer (TLM) for

N_m = 1000 lb/in and S=0.25”

8.4 Effect of mechanical force on DCOD

A $[45/0/-45/90]_s$ configuration is considered using a set of crack spacing and delamination length as S=0.25” and L=0.01”. A mechanical force of 1000 lb/in is applied on the laminate for different cases of cracks in 0˚, -45˚ and 45˚ layers respectively. Results depicted in Fig.8.42 through Fig.8.44 show that DCOD increases linearly with the increase in mechanical force. This can be seen in FLM as well as TLM solutions. The force is varied from 600 lb/in to 1500 lb/in and is biaxial in nature. The thermal load in this case is zero.

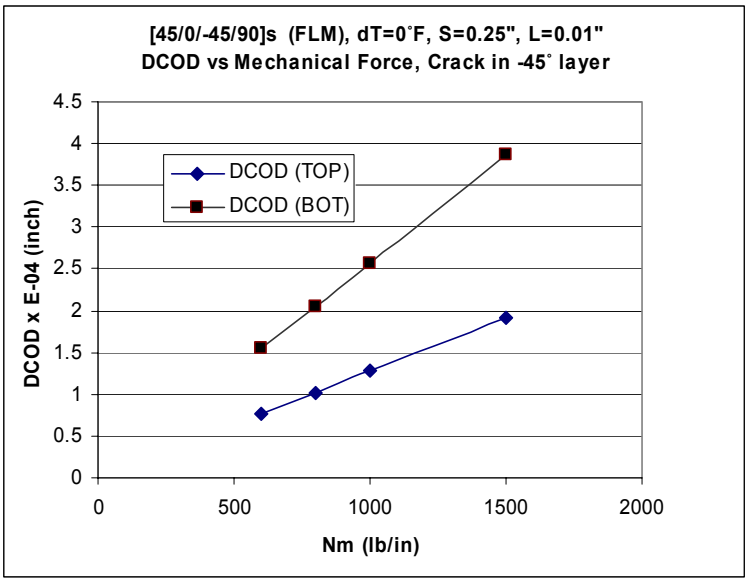

Fig.8.42 $[45/0/-45/90]_s$ laminate with crack in -45˚ layer (FLM) for S=0.25”and L=0.01”, no thermal load

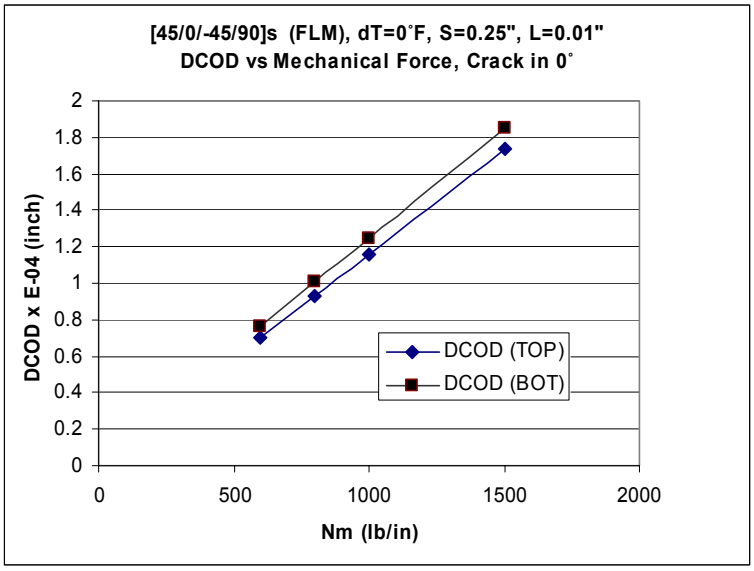

Fig.8.43 $[45/0/-45/90]_s$ laminate with crack in 0˚ layer (FLM) for S=0.25”and L=0.01”, no thermal load

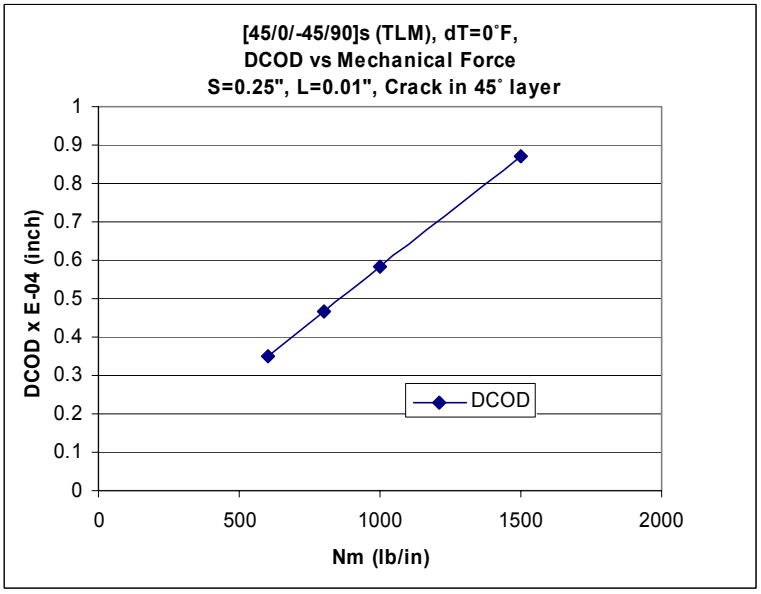

Fig.8.44 $[45/0/-45/90]_s$ laminate with crack in 45˚ layer (TLM) for S=0.25”and L=0.01”, no thermal load

8.5 Effect of temperature difference on DCOD

A $[45/0/-45/90]_s$ configuration is considered using a set of crack spacing and delamination length as S=0.25” and L=0.01”. A thermal load of ΔT = -495˚F is applied on the laminate for different cases of cracks in 0˚, -45˚ and 45˚ layers respectively. Results depicted in Fig.8.45 through Fig.8.47 show that DCOD increases linearly with the increase in temperature difference. This can be seen in FLM as well as TLM solutions. The ΔT is varied from -495˚F to 0˚F. No mechanical force is considered in this case.

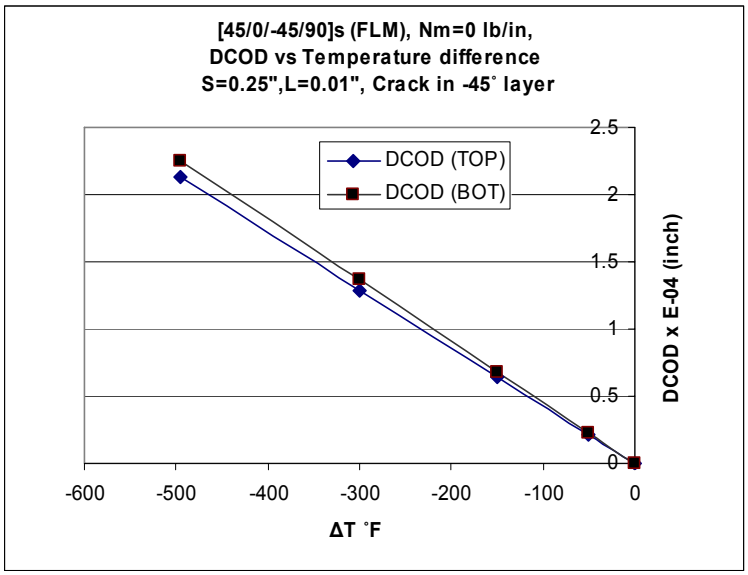

Fig.8.45 $[45/0/-45/90]_s$ laminate with crack in -45˚ layer (FLM) for S=0.25”and L=0.01”, no mechanical load

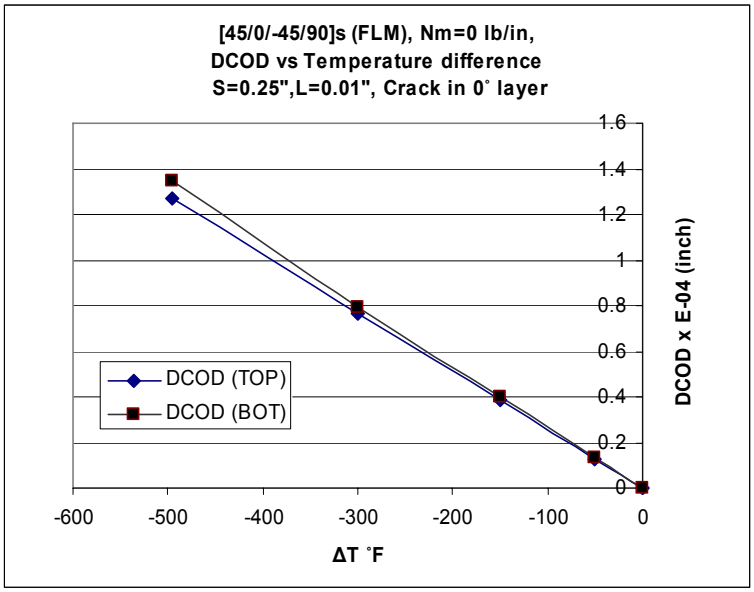

Fig.8.46 $[45/0/-45/90]_s$ laminate with crack in 0˚ layer (FLM) for S=0.25”and L=0.01”, no mechanical load

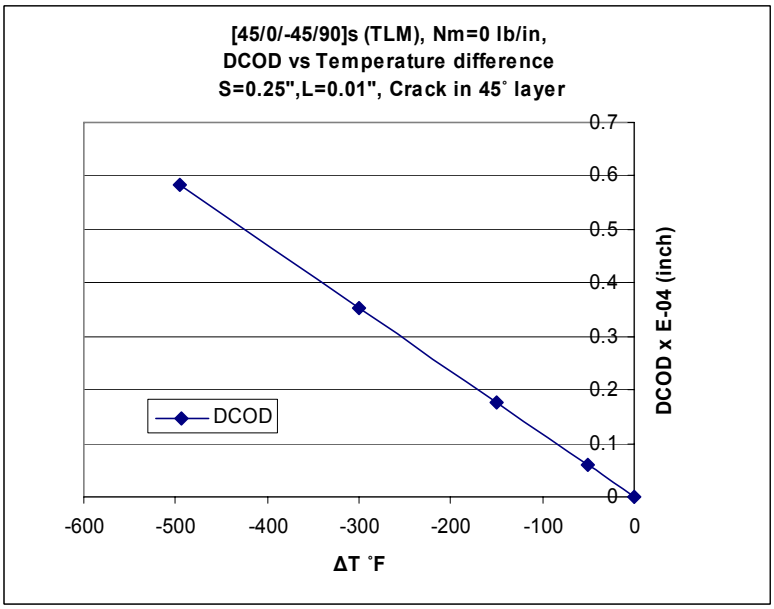

Fig.8.47 $[45/0/-45/90]_s$ laminate with crack in 45˚ layer (TLM) for S=0.25”and L=0.01”, no mechanical load

8.6 Combined effect of mechanical and thermal load on DCOD

A $[45/0/-45/90]_s$ configuration is considered using a set of crack spacing and delamination length as S=0.25” and L=0.01”. A varying thermal load and a mechanical force of 1000 lb/in are applied on the laminate for different cases of cracks in the 0˚, -45˚ and 45˚ layers separately. Results depicted in Fig.8.48 through Fig.8.50 show that DCOD increases linearly with the increase in temperature difference. This can be seen in FLM as well as TLM solutions. The ΔT is varied from -495˚F to 0˚F.

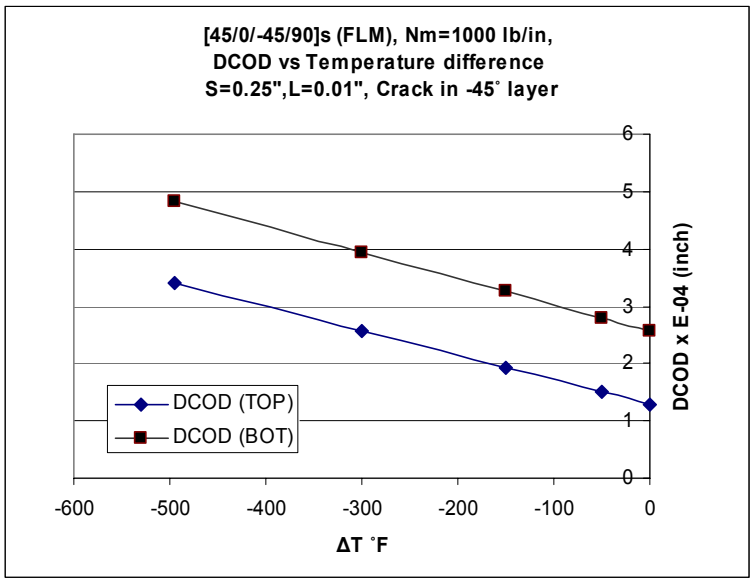

Fig.8.48 $[45/0/-45/90]_s$ laminate with crack in -45˚ layer (FLM) for S=0.25”and L=0.01”, mechanical load N_m=1000 lb/in

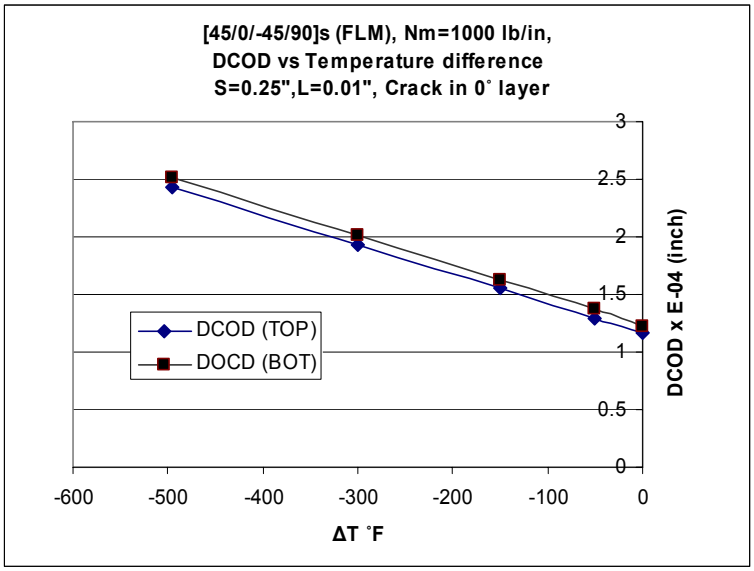

Fig.8.49 $[45/0/-45/90]_s$ laminate with crack in 0˚ layer (FLM) for S=0.25”and L=0.01”, mechanical load N_m=1000 lb/in

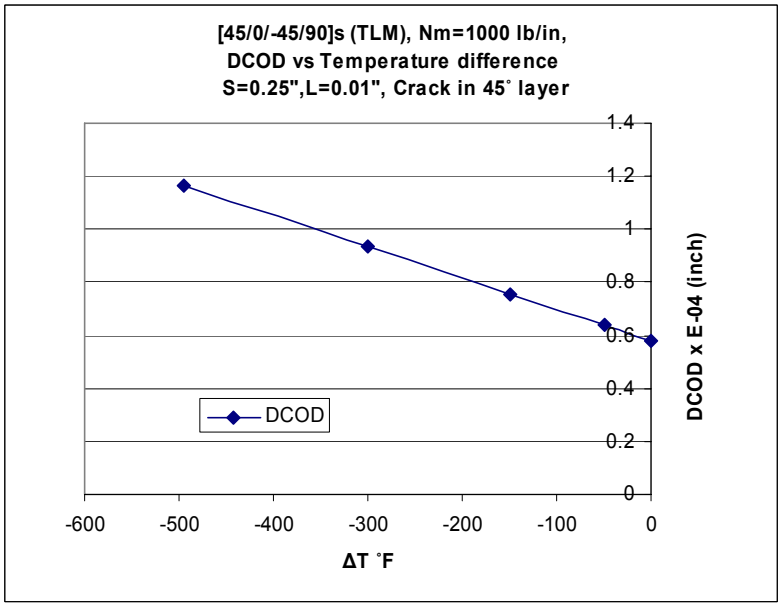

Fig.8.50 $[45/0/-45/90]_s$ laminate with crack in 45˚ layer (TLM) for S=0.25”and L=0.01”, mechanical load N_m=1000 lb/in

8.7 Permeability model results

Using expressions derived by Roy and Benjamin [18] for permeability of composite laminates, permeability of complete laminate can be calculated. A configuration $[45/0/-45/90]_s$ is considered for finding out the permeability under different mechanical and thermal loads and crack spacing values. Results from Fig.8.51 through Fig.8.56 show permeability variation depending upon mechanical load, thermal load, crack spacing, crack opening volume and delamination length.

The effect of adjacent ply cracks is considered negligible in order to superimpose the DCOD values of adjacent layers for calculating normalized permeability, as per Roy and Benjamin [18].

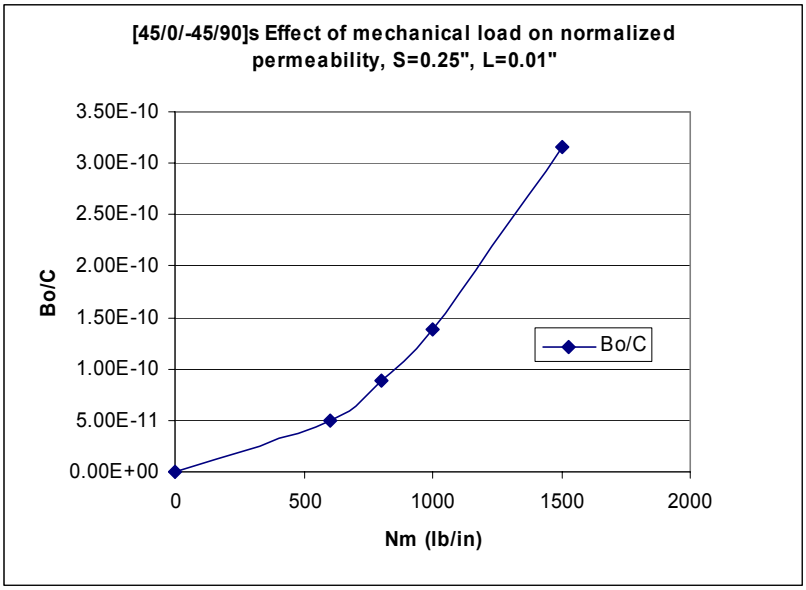

Fig.8.51 $[45/0/-45/90]_s$ laminate S=0.25”and L=0.01”

Effect of mechanical load on normalized permeability

Fig.8.51 shows a parabolic increase in normalized permeability through laminate as the mechanical force increases, due to more delaminated crack opening displacement. Thus, it is clear that increasing DCOD causes higher permeation.

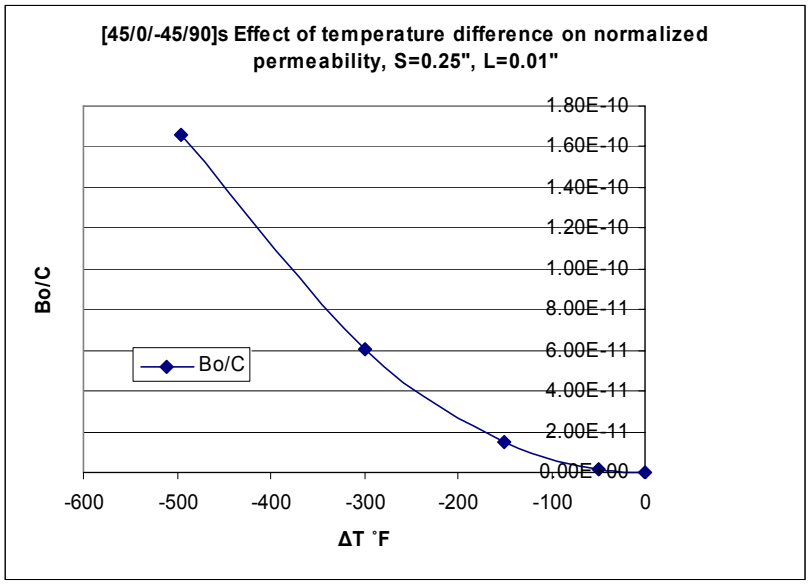

Fig.8.52 $[45/0/-45/90]_s$ laminate S=0.25"and L=0.01"

Effect of thermal load on normalized permeability

Similarly, with more thermal load due to temperature difference, there is more DCOD and thus, increased permeation. This can be seen from Fig.8.52. These trends match with those presented by Roy and Benjamin [18].

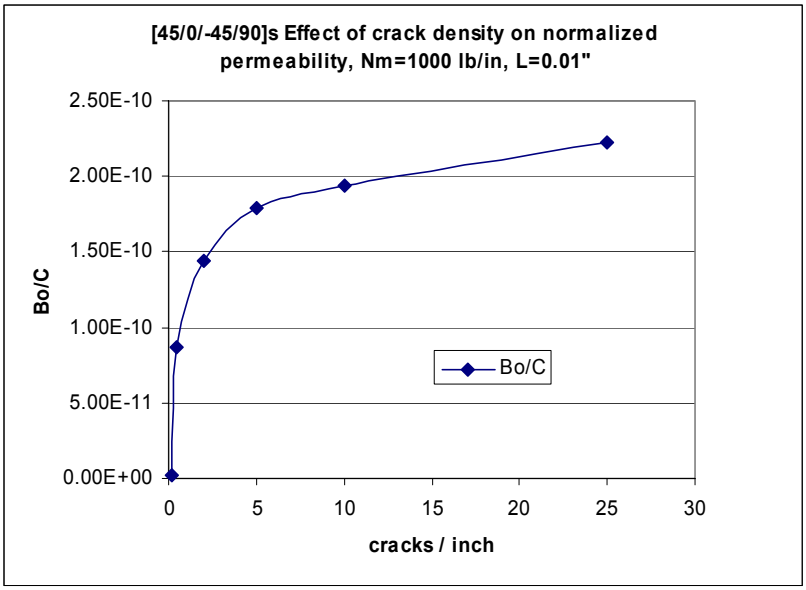

Fig.8.53 $[45/0/-45/90]_s$ laminate L=0.01", N_m=1000 lb/in

Effect of crack spacing on normalized permeability

Fig.8.53 shows that initially, the normalized permeability increases rapidly with increase in crack density. After a certain value of crack density, the rate of increase in normalized permeability is reduced. This can be attributed to the reduction in peak tensile stress in cracked layers which in turn reduce the DCOD values. The same reasoning can be applied to explain the nature of the variation of normalized permeability with an increase in delamination length. Fig.8.55 depicts the variation in normalized permeability due to increase in delamination length. As L increases, normalized permeability also increases initially and rate of increase reduces as delamination length is further increased.

However the normalized permeability still increases, albeit at a slower rate due to the fact that it directly depends on the total crack opening volume, which increases as the crack density increases in a laminate. This can be seen from Fig.8.54.

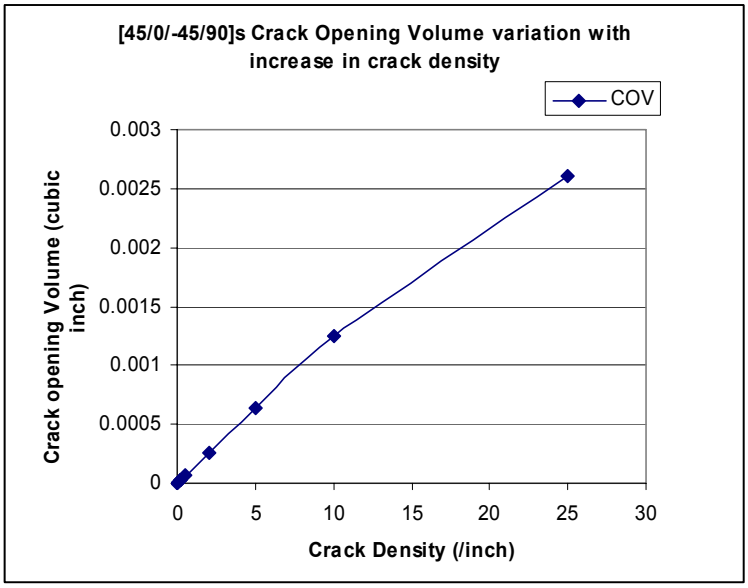

Fig.8.54 $[45/0/-45/90]_s$ laminate L=0.01", N_m=1000 lb/in

Effect of crack density on crack opening volume COV

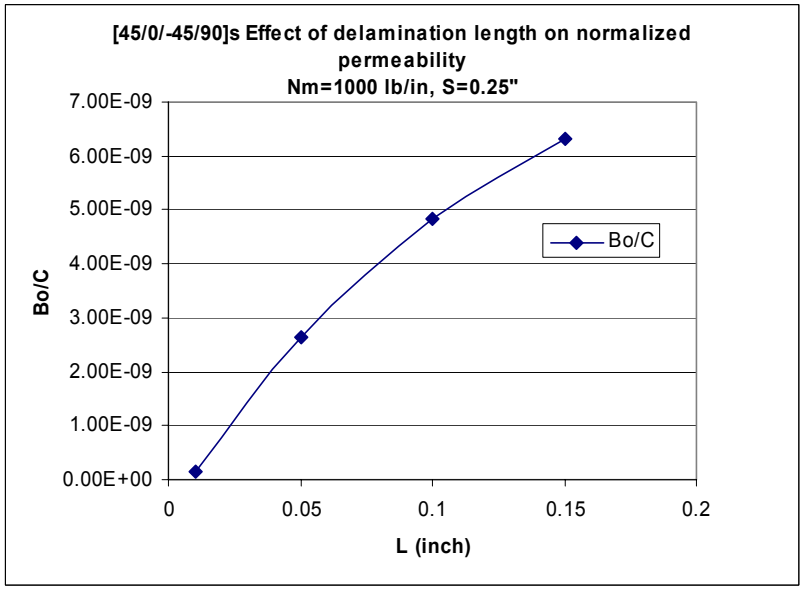

Fig.8.55 $[45/0/-45/90]_s$ laminate S=0.25"

Effect of delamination length on normalized permeability

The reduction in the peak tensile stress values in damaged layers with increase in crack density is depicted in Fig.8.56 for mechanical load of 1000 lb/in.

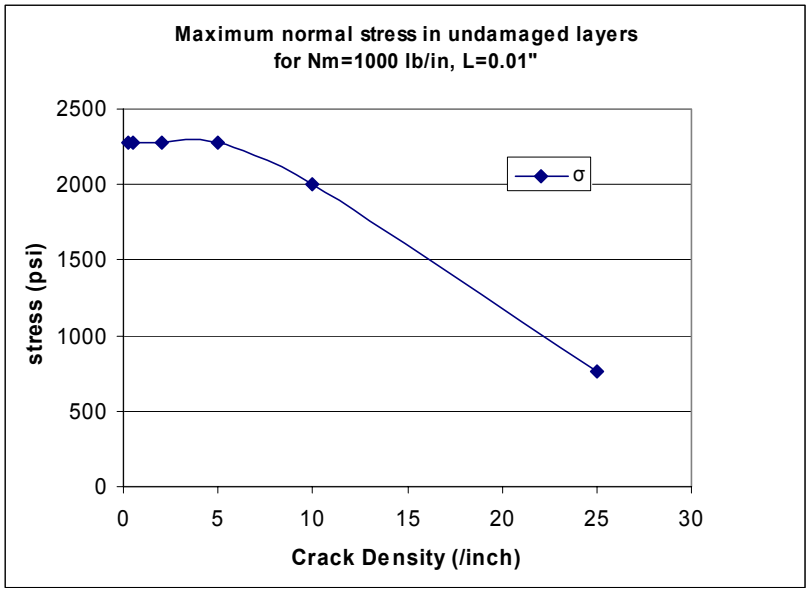

Fig.8.56 $[45/0/-45/90]_s$ laminate L=0.01", N_m=1000 lb/in

Effect of crack density on maximum tensile stress in cracked layer

8.8 Damage growth prediction

Damage growth was also predicted using the model developed. Effect of load on crack density as well as delamination length was observed as shown in Fig. 8.57 through Fig. 8.60. It was observed that as load increases beyond a certain value, crack density increase slows down due to reduction in maximum tensile stress in cracked layer. Delamination length increases almost linearly with increasing load.

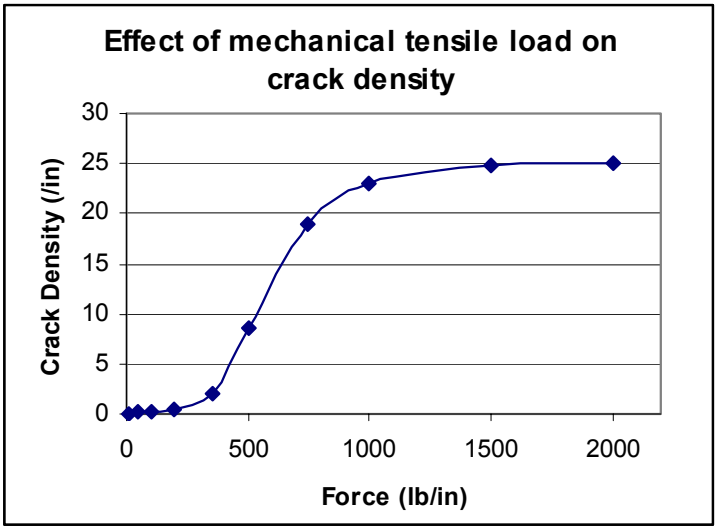

Fig.8.57 Effect of mechanical tensile load on crack density

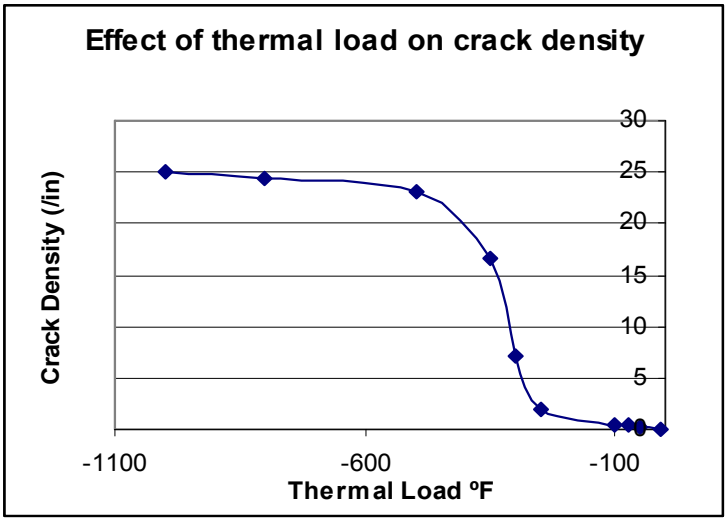

Fig.8.58 Effect of thermal load on crack density

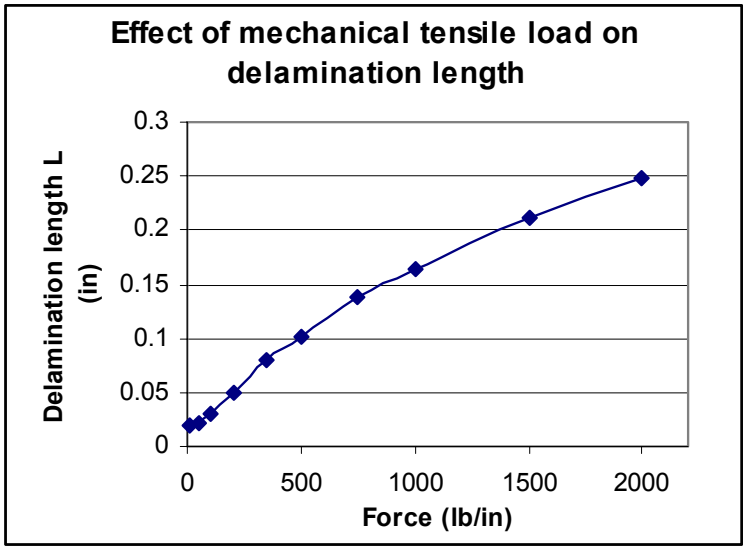

Fig.8.59 Effect of mechanical tensile load on delamination length

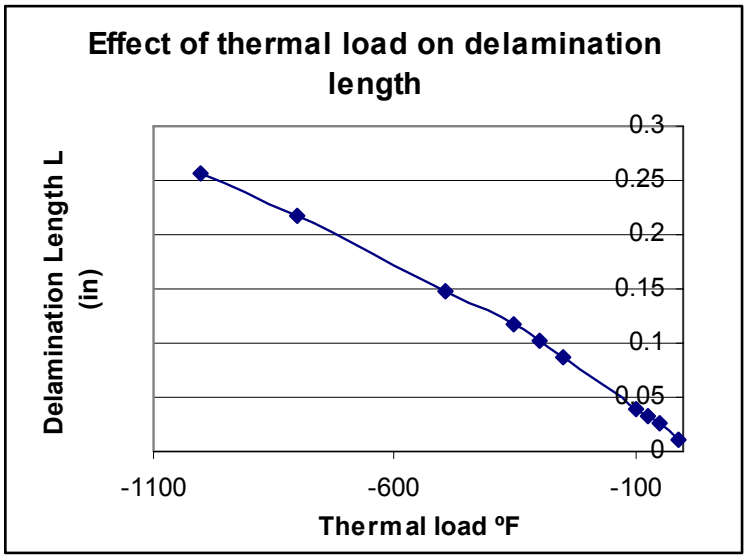

Fig.8.60 Effect of thermal load on delamination length

CHAPTER 9

CONCLUSION

- An analytical model has been developed to find the delaminated crack opening displacement for IM-7/PETI5 graphite epoxy laminates with arbitrary ply orientations. The DCOD solutions are in reasonable agreement with the finite element results and therefore can be used to predict the normalized permeability of any given laminate configuration under given conditions of mechanical biaxial tensile and thermal loads and the state of damage. These observations are limited to IM-7/PETI5 graphite epoxy laminate system.
- Delaminated crack opening displacement of any intermediate layer can be determined using the Five Layer Model solution obtained in this study. The analytical model shows better agreement with 2D FEA results for cross ply laminates. The maximum error observed for [45/0/-45/90]s laminate is approximately 7%.
- Using this analytical model, delaminated crack opening displacement in an individual layer anywhere in the thickness of the laminate can be determined. The

resulting DCOD for all layers then can be used to calculate the normalized permeability of full laminate with arbitrarily oriented plies. This was not possible with the previous model [18], which could be applied to only cross ply laminates.

- Trends in normalized permeability and DCOD are found to be in agreement with those observed by Roy and Benjamin [18]. Normalized permeability is found to increase initially as the crack density and delamination length increase, and then the rate of increase is slow as saturation crack density is approached in laminates. Permeability is seen to increase parabolically with an increase in biaxial tensile mechanical force and thermal loads.
- The model presented here can be applied to predict evolution of matrix cracks and delaminations with increasing load; however, the initial state of damage must be specified as input to the model

REFERENCES

1. McManus, H.L, Park C.H., "Thermally induced damage in composite laminates Predictive methodology and experimental investigation," Composite Science and Technology, Vol. 56, (1996) 1209-1219
2. McManus, H.L., Faust, A. and Uebelhart, S., "Gas Permeability of Thermally Cycled Graphite-Epoxy Composites," American Society for Composites, Paper 092(2001) (CD-ROM)
3. Varna, J., Berglund, L., Talreja, R., and Jacovics, A., "A study of the opening displacement of transverse cracks in cross ply laminates," International Journal of Damage Mechanics, Vol. 2, (1993) 272-289.
4. Hong, C.S., Lim, S.G., "Prediction of transverse cracking and stiffness reduction in cross-ply laminated composites," Journal of Composite Materials, Vol. 23, Issue 7 , (1989) 695-713
5. Hong, C.S., Lim, S.G., "Effect of transverse cracks on the thermomechanical properties of cross-ply laminated composites," Composites Science and Technology, Vol. 34, Issue 2 , (1989) 145-162
6. Nairn, J.A, "The strain energy release rate of composite microcracking: a variational approach," Journal of Composite Materials, Vol. 23, Issue 11, (1989) 1106-1129
7. Nairn, J.A., Hu, S., "The initiation and growth of delaminations induced by matrix microcracks in laminated composites," International Journal of Fracture, Vol. 57, Issue 1, (1992) 1-24

8. Roy, S., Benjamin, M., "Modeling of opening displacement of transverse cracks in graphite epoxy laminates using shear lag analysis," American Society of Composites, Paper 023, Oct 2002. (CD-ROM)
9. Berthelot, J.M., Leblond, P., El Mahi A. and Le Corre J. F., "Transverse cracking of cross-ply laminates: Part 1. Analysis," Composites Part A: Applied Science and Manufacturing, Vol. 27, Issue 10, (1996) 989-1001
10. Berthelot, J.M., Le Corre J. F., "A model for transverse cracking and delamination in cross-ply laminates," Composites Science and Technology, Vol. 60, Issue 7 , (2000) 1055-1066
11. Noah, J., Whitcomb, J., "Effect of laminate design and loads on crack opening volume in laminates used in cryogenic tanks," AIAA paper, AIAA-2002-1415, April 2002. (CD-ROM)
12. Noah, J., Whitcomb, J., "Prediction of delamination growth and opening near intersection of transverse matrix cracks and delaminations," AIAA paper, AIAA-2003-1602, April 2003. (CD-ROM)
13. Zhang, J., Fan, J., and Herrmann, K.P., "Delaminations Induced by Constrained Transverse Cracking in Symmetric Composite Laminates," International Journal of Solids and Structures, Vol. 36,(1999) 813-846.
14. Zhang, J., Fan, J., and Herrmann, K.P., "Stiffness degradation by multilayer intralaminar cracking in composite laminates," Journal of Composites, Part A: Applied Science and Manufacturing, Vol. 30, (1999) 683-706

15. Gates, T., Whitley, K., Grenoble, R., and Bandorawalla, T., "Thermal/Mechanical Durability of Polymer-Matrix Composites in Cryogenic Environments", AIAA paper AIAA-2003-7408, April 2003. (CD-ROM)
16. Bechel, V.T., Mark B. Fredin, M.B., Donaldson, S.L., Camping, J., Kim, R., "Effect of stacking sequence on micro-cracking in a cryogenically cycled carbon-bismaleimide composite," Journal of Composites: Part A, Vol. 34 (2003) 663–672
17. Bechel, V.T., Camping, J., Kim, R., "Cryogenic/elevated temperature cycling induced leakage paths in PMCs," Journal of Composites, Part B: Engineering (2004)
18. Roy, S., Benjamin, M., "Modeling of permeation and damage in graphite/epoxy laminates for cryogenic fuel storage," Composites Science and Technology, Vol. 64, Issues 13-14, (2004) 2051-2065.

APPENDICES

APPENDIX A

FIVE LAYER MODEL LAMINATE ANALYSIS

A.1 Introduction

In this section, an expression for Delaminated Crack Opening Displacement (DCOD) derived based on a two-dimensional first-order shear laminate theory is applied to the five-layer model (FLM) laminate of ply orientation $[\theta_1/\theta_2/90_n]_s$ shown in Fig.A.1. Assuming symmetry of geometry and loading, only one quarter of the five-layer laminate is modeled as shown in Fig.A.2, corresponding to case 1 as discussed earlier. The sublaminates (other than the cracked one) are not considered to be symmetric about their midplanes, due to more than one orientations resulting in the presence of bending extension stiffnesses B_{22}. Transverse matrix cracks are assumed to exist in the 90º plies with uniform crack spacing of 2S. Local delaminations of length 2L are assumed to initiate and grow in a symmetric manner from the tips of each transverse matrix crack

and span the entire width of the laminate. The modeled portion of length S is divided into six sublaminates, three sublaminates in the laminated portion and three sublaminates in the delaminated portion, numbered as shown in Fig.A.2. Plane strain condition is assumed in the width direction (X-direction) of the model. Three local coordinates are used for the model as shown in Fig.A.2.

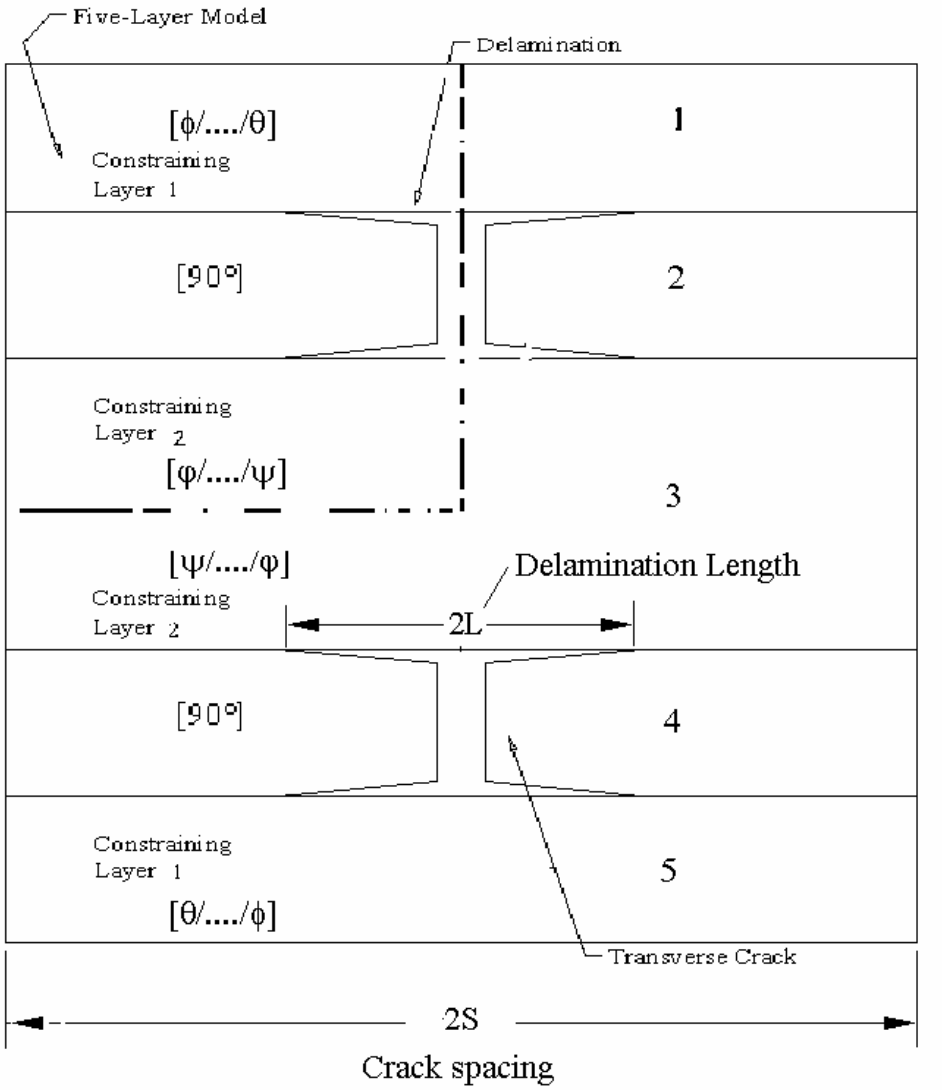

Fig.A.1 Five Layer model for the cracked and delaminated laminates (Case 1)

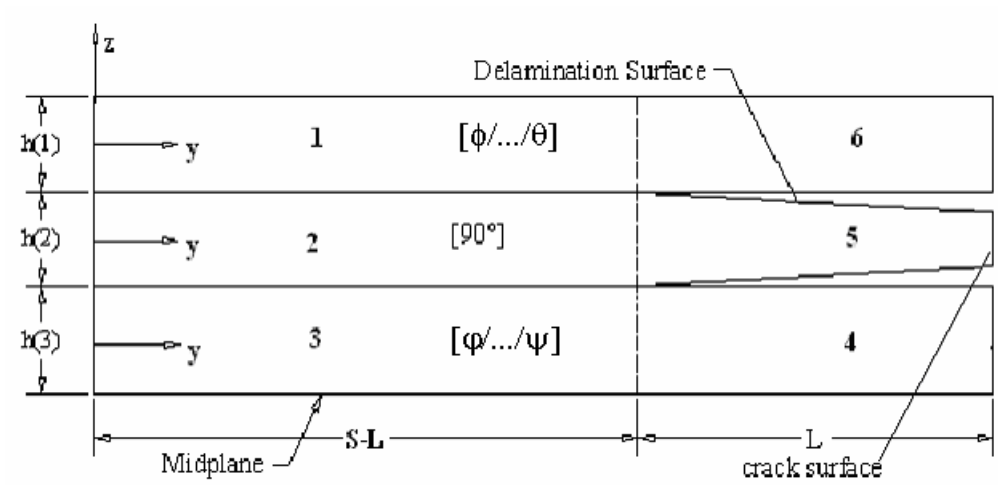

Fig.A.2 Quarter of the repeating interval of the Five Layer model laminate (Case 1)

Assuming that the displacements in y and z directions within each sublaminate can be given by,

$$v(y,z) = V(y) + z\beta(y) \tag{A.1a}$$

$$w = W(y) \tag{A.1b}$$

Where,

V(y) is the y displacement of mid-surface of the sublaminate.

β(y) is the slope of the sublaminate mid-surface in y direction.

W(y) is the z displacement of mid-surface of the sublaminate.

The force and moment equilibrium equations for each sub-laminate are,

$$N_{,y} + T_t - T_b = 0 \tag{A.2a}$$

$$M_{,y} - Q + \frac{h}{2}\left(T_t + T_b\right) = 0 \tag{A.2b}$$

$$Q_{,y} + P_t - P_b = 0 \tag{A.2c}$$

Where N, Q and M are axial force, shear force and bending moment resultants, P and T denote interlaminar peel and shear stresses with subscripts t and b denoting top and bottom surfaces. Combining the strain-displacement relations with Equations (A.1a, A.1b) and the in-plane stress-strain relationships of a lamina, the force-moment relationships of a sublaminate are,

$$N_M = A_{22}V,_y + B_{22}\beta,_y - \bar{Q}_{22}h\int_{T_{ref}}^{T_f} \alpha_y dT \tag{A.3a}$$

$$M_M = B_{22}V,_y + D_{22}\beta,_y - \bar{Q}_{22}h\bar{Z}\int_{T_{ref}}^{T_f} \alpha_y dT \tag{A.3b}$$

$$Q = A_{44}(\beta + W,_y) \tag{A.3c}$$

Where, A_{22}, B_{22}, D_{22} and A_{44} are components of the A, B and D matrix from classical lamination theory. For the two-dimensional orthotropic model the other stiffness components of the anisotropic sublaminate do not appear in the constitutive equations due to the assumption of plane strain with respect to the width of the specimen. h is the thickness of the lamina; $\bar{Z}$ is centroidal distance of the lamina from laminate midplane; α_y is the coefficient of thermal expansion in y-direction and is given by the nonlinear function $C_0+C_1T_f+C_2T_f^2$. In the above equations, non-linear material properties with respect to temperature T_f are used in calculating the thermal forces and moments. The components of A, B, D and $\bar{Q}$ matrix are assumed to be nonlinear functions of temperature T_f. Substitution of Equations (A.3a-A.3c) into Equations (A.2a-A.2c) gives,

$$A_{22}V,_{yy} + B_{22}\beta,_{yy} + T_t - T_b = 0 \tag{A.4a}$$

$$\left(D_{22} - \frac{B_{22}^{\ 2}}{A_{22}}\right)\beta,_{yy} - A_{44}\left(\beta + W,_y\right) + \left(\frac{h}{2} - \frac{B_{22}}{A_{22}}\right)T_t + \left(\frac{h}{2} + \frac{B_{22}}{A_{22}}\right)T_b = 0 \tag{A.4b}$$

$$A_{44}\left(\beta,_{y}+W,_{yy}\right)+P_t-P_b=0 \tag{A.4c}$$

A.2 Laminated Portion: Sublaminates 1, 2 and 3

Modifying the derivation procedure given by Zhang et al [13] and including thermal loading according to Roy and Benjamin [18], the solutions for force, moment, and displacement for sublaminates 1 ,2 and 3 are derived as,

$$\beta^{(i)}=\sum_{j=1}^{3}\alpha_j P_j^{(i)}\sinh(\lambda_j y) \tag{A.5a}$$

Where, i=1, 2 , 3 denotes sublaminates 1, 2 & 3 and constants $P_j^{(i)}$ (j=1, 2, 3) are given as,

$$\begin{Bmatrix} P_j^{(1)} \\ P_j^{(2)} \end{Bmatrix}=\frac{\lambda_j *}{(a_{11}\lambda_j *-A_{44}{}^{(1)})(a_{22}\lambda_j *-A_{44}{}^{(2)})-a_{12}{}^{2}\lambda_j *^{2}}\begin{Bmatrix} a_{13}A_{44}{}^{(2)}-(a_{22}a_{13}-a_{12}a_{23})\lambda_j * \\ a_{23}A_{44}{}^{(1)}-(a_{11}a_{23}-a_{12}a_{13})\lambda_j * \end{Bmatrix} \tag{A.5b}$$

$$P_j^{(3)}=1 \tag{A.5c}$$

Where a_{ij} are functions of the elastic constants of the lamina and given in Zhang [13], $\lambda_j=\sqrt{\lambda_j *}$ and $\lambda_j *$ (j=1, 2, 3) are roots of the equation given below,

$$\begin{aligned}&(a_{11}a_{22}a_{33}+2a_{12}a_{13}a_{23}-a_{33}a_{12}{}^{2}-a_{11}a_{23}{}^{2}-a_{22}a_{13}{}^{2})\lambda *^{3}\\&-(a_{11}a_{22}A_{44}{}^{(3)}+a_{33}a_{22}A_{44}{}^{(1)}+a_{33}a_{11}A_{44}{}^{(2)}-a_{12}{}^{2}A_{44}{}^{(3)}-a_{23}{}^{2}A_{44}{}^{(1)}-a_{13}{}^{2}A_{44}{}^{(2)})\lambda *^{2}\\&+(a_{11}A_{44}{}^{(2)}A_{44}{}^{(3)}+a_{22}A_{44}{}^{(1)}A_{44}{}^{(3)}+a_{33}A_{44}{}^{(2)}A_{44}{}^{(1)})\lambda *-A_{44}{}^{(1)}A_{44}{}^{(2)}A_{44}{}^{(3)}=0\end{aligned} \tag{A.5d}$$

The displacements of the mid-plane of the sublaminates are,

$$V^{(i)} = \sum_{j=1}^{3} \alpha_j \gamma_j^{(i)} \sinh(\lambda_j y) + \alpha_{3+i} y \tag{A.6}$$

The force and moment resultants are,

$$N_M^{(i)} = \sum_{j=1}^{3} \alpha_j \eta_j^{(i)} \cosh(\lambda_j y) + A_{22}^{(i)} \alpha_{3+i} - \bar{Q}_{22}^{(i)} h^{(i)} \int_{T_{ref}}^{T_f} \alpha_y^{(i)} dT \tag{A.7}$$

$$M_M^{(i)} = \sum_{j=1}^{3} \alpha_j \xi_j^{(i)} \cosh(\lambda_j y) + B_{22}^{(i)} \alpha_{3+i} - \bar{Q}_{22}^{(i)} h^{(i)} \bar{Z}^{(i)} \int_{T_{ref}}^{T_f} \alpha_y^{(i)} dT \tag{A.8}$$

Where α_i (i=1, 2…4) are undetermined constants and the remaining constants are given in Zhang et al [13] and Roy and Benjamin [18].

A.3 Delaminated Portion

A.3.1 Sublaminate 4

The peel and shear stresses at top and bottom surface of the sublaminate 4 are given as,

$$T_b^{(4)} = 0 \qquad T_t^{(4)} = 0 \tag{A.9a, b}$$

$$P_t^{(4)} = 0 \tag{A.9c}$$

The symmetry of the laminate implies,

$$W^{(4)}(y) = 0 \tag{A.9d}$$

Substituting Equations (A.9a-e) into Equations (A.4a-c)

$$A_{22}^{(3)} V_{,yy}^{(4)} + B_{22}^{(3)} \beta_{,yy}^{(4)} = 0 \tag{A.10a}$$

$$\left(D_{22}^{(3)} - \frac{(B_{22}^{(3)})^2}{A_{22}^{(3)}} \right) \beta_{,yy}^{(4)} - A_{44}^{(3)} \beta^{(4)} = 0 \tag{A.10b}$$

$$A_{44}{}^{(3)}\beta,_{y}{}^{(4)} = P_b^{(4)} \tag{A.10c}$$

The mid-plane displacement of sublaminate 4 can be given by

$$v^{(4)}(y,z) = V^{(4)}(y) + z^{(3)}\beta^{(4)}(y) \tag{A.11}$$

$$\beta^{(4)} = \psi_1 e^{\omega y} + \psi_2 e^{-\omega y} \tag{A.12a}$$

Where

$$\omega = \sqrt{\frac{A_{44}{}^{(3)}}{\left(D_{22}{}^{(3)} - \frac{(B_{22}{}^{(3)})^2}{A_{22}^{(3)}}\right)}}$$

From Equations (A.10a, c)

$$V^{(4)} = -\frac{B_{22}^{(3)}}{A_{22}^{(3)}}(\psi_1 e^{\omega y} + \psi_2 e^{-\omega y}) + \psi_3 y + \psi_4 \tag{A.12b}$$

Substitution of Equations (A.12a, b) into Equations (A.3a, b) results in,

$$N_M{}^{(4)} = A_{22}{}^{(3)}\psi_3 - \bar{Q}_{22}{}^{(3)}h^{(3)}\int_{T_{ref}}^{T_f} \alpha_y{}^{(3)}dT \tag{A.13a}$$

$$M_M{}^{(4)} = \left(D_{22}^{(3)} - \frac{(B_{22}^{(3)})^2}{A_{22}^{(3)}}\right)\omega(\psi_1 e^{\omega y} - \psi_2 e^{-\omega y}) + B_{22}^{(3)}\psi_3 - \bar{Q}_{22}{}^{(3)}h^{(3)}\bar{Z}^{(3)}\int_{T_{ref}}^{T_f} \alpha_y{}^{(3)}dT \tag{A.13b}$$

Where ψ_k (k=1, 2, 3 & 4) are undetermined constants derived in further section.

A.3.2 Sublaminate 5

The peel and shear stresses at top and bottom surface of the sublaminate 5 are given as,

$$T_b^{(5)} = 0 \qquad T_t^{(5)} = 0 \tag{A.14a, b}$$

$$P_t^{(5)} = 0 \qquad P_b^{(5)} = 0 \tag{A.14c, d}$$

The crack in sublaminate 5 implies,

$$W^{(5)}(y) = 0 \tag{A.14e}$$

Substituting Equations (A.14a-e) into Equations (A.4a-c)

$$A_{22}{}^{(2)} V,_{yy}{}^{(5)} = 0 \tag{A.15a}$$

$$D_{22}{}^{(2)} \beta,_{yy}{}^{(5)} - A_{44}{}^{(2)} \beta^{(5)} = 0 \tag{A.15b}$$

$$A_{44}{}^{(2)} \beta,_{y}{}^{(5)} = 0 \tag{A.15c}$$

The midplane displacement of sublaminate 5 can be given by

$$v^{(5)}(y,z) = V^{(5)}(y) + z^{(2)} \beta^{(5)}(y) \tag{A.16}$$

$$\beta^{(5)} = \theta_1 e^{\omega_1 y} + \theta_2 e^{-\omega_1 y} \tag{A.17a}$$

Where

$$\omega = \sqrt{\frac{A_{44}{}^{(2)}}{D_{22}{}^{(3)}}}$$

From Equations (A.15a, c)

$$V^{(5)} = \theta_3 y + \theta_4 \tag{A.17b}$$

Substitution of Equations (A.17a, b) into Equations (A.3a, b) results in,

$$N_M{}^{(5)} = A_{22}{}^{(2)} \theta_3 - \bar{Q}_{22}{}^{(2)} h^{(2)} \int_{T_{ref}}^{T_f} \alpha_y{}^{(2)} dT \tag{A.18a}$$

$$M_M{}^{(5)} = D_{22}^{(2)}\omega_1(\theta_1 e^{\omega_1 y} - \theta_2 e^{-\omega_1 y}) - \bar{Q}_{22}{}^{(2)} h^{(2)} \bar{Z}^{(2)} \int_{T_{ref}}^{T_f} \alpha_y{}^{(2)} dT \qquad \text{(A.18b)}$$

Where θ_k (k=1, 2, 3 & 4) are undetermined constants derived in next section.

A.3.3 Sublaminate 6

The peel and shear stresses at top and bottom surface of the sublaminate 6 are given as,

$$T_b{}^{(6)} = 0 \qquad T_t{}^{(6)} = 0 \qquad \text{(A.19a, b)}$$

$$P_t^{(6)} = 0 \qquad P_b^{(6)} = 0 \qquad \text{(A.19c)}$$

Substituting Equations (A.13a-e) into Equations (A.4a-c)

$$A_{22}{}^{(1)} V_{,yy}{}^{(6)} + B_{22}{}^{(1)} \beta_{,yy}{}^{(6)} = 0 \qquad \text{(A.20a)}$$

$$\left(D_{22}{}^{(1)} - \frac{(B_{22}{}^{(1)})^2}{A_{22}{}^{(1)}} \right) \beta_{,yy}{}^{(6)} - A_{44}{}^{(1)} (\beta^{(6)} + W_{,y}^{(6)}) = 0 \qquad \text{(A.20b)}$$

$$A_{44}{}^{(1)} (\beta_{,y}{}^{(6)} + W_{,yy}^{(6)}) = 0 \qquad \text{(A.20c)}$$

The midplane displacement of sublaminate 6 can be given by

$$v^{(6)}(y,z) = V^{(6)}(y) + z^{(1)} \beta^{(6)}(y) \qquad \text{(A.21)}$$

Integrating Equation (A.20c),

$$A_{44}{}^{(1)} (\beta^{(6)} + W_{,y}^{(6)}) = \text{constant} \qquad \text{(A.22a)}$$

At y=S,

$$A_{44}{}^{(1)} (\beta^{(6)} + W_{,y}^{(6)}) = Q^{(6)}$$

Also, at y=S, due to symmetry about S, shear stress

$$Q^{(6)} + Q^{(4)} = 0$$

so at y=S, $Q^{(6)} = -Q^{(4)}$ and as $\beta^{(4)}(s) = 0$

constant = - $A_{44}{}^{(3)}(\beta^{(4)}(s)) = 0$

So, $$A_{44}{}^{(1)}(\beta^{(6)} + W'^{(6)}_{y}) = 0 \tag{A.22b}$$

which gives $$W'^{(6)}_{y} = -\beta^{(6)} \tag{A.22c}$$

Therefore from Equation (20b)

$$\left(D_{22}{}^{(1)} - \frac{(B_{22}{}^{(1)})^2}{A_{22}{}^{(1)}} \right) \beta,_{yy}{}^{(6)} = 0 \tag{A.22d}$$

$$\beta^{(6)} = \theta_5 y + \theta_6 \tag{A.23a}$$

$$W^{(6)} = -\frac{\theta_5 y^2}{2} - \theta_6 y + \theta_9 \tag{A.23b}$$

And

$$V^{(6)} = \theta_7 y + \theta_8 \tag{A.23c}$$

Substitution of Equations (A.23 a-c) into Equations (A.3a, b) results in,

$$N_M{}^{(6)} = A_{22}^{(1)}\theta_7 + B_{22}^{(1)}\theta_5 - \bar{Q}_{22}{}^{(1)} h^{(1)} \int_{T_{ref}}^{T_f} \alpha_y{}^{(1)} dT \tag{A.24a}$$

$$M_M{}^{(6)} = B_{22}^{(1)}\theta_7 + D_{22}^{(1)}\theta_5 - \bar{Q}_{22}{}^{(1)} h^{(1)} \bar{Z}^{(1)} \int_{T_{ref}}^{T_f} \alpha_y{}^{(1)} dT \tag{A.24b}$$

Where θ_k (k=5, 6, 7, 8 & 9) are undetermined constants derived in next section.

A.3.4 Determination of the Constants α_i, θ_j and ψ_k

In order to determine the eighteen constants, the same number of independent boundary and continuity conditions has to be described. Assuming the laminate is

subjected to tension force N and thermal load ΔT, the interfacial continuity conditions and boundary conditions are enforced as,

$$N_M{}^{(5)}(S) = 0 \tag{A.25a}$$

$$\beta^{(4)}(S) = 0 \tag{A.25b}$$

$$\beta^{(6)}(S) = 0 \tag{A.25c}$$

$$v^{(5)}(S-L, \frac{h^{(2)}}{2}) = v^{(6)}(S-L, -\frac{h^{(1)}}{2}) \tag{A.25d}$$

$$v^{(5)}(S-L, -\frac{h^{(2)}}{2}) = v^{(4)}(S-L, \frac{h^{(3)}}{2}) \tag{A.25e}$$

$$N_M{}^{(4)}(S) + N_M{}^{(6)}(S) = \frac{1}{2}N \tag{A.25f}$$

$$N_M{}^{(1)}(0) + N_M{}^{(2)}(0) + N_M{}^{(3)}(0) = \frac{1}{2}N \tag{A.25g}$$

$$V^{(1)}(S-L) = V^{(6)}(S-L) \tag{A.25h}$$

$$V^{(2)}(S-L) = V^{(5)}(S-L) \tag{A.25i}$$

$$V^{(3)}(S-L) = V^{(4)}(S-L) \tag{A.25j}$$

$$\beta^{(1)}(S-L) = \beta^{(6)}(S-L) \tag{A.25k}$$

$$\beta^{(2)}(S-L) = \beta^{(5)}(S-L) \tag{A.25l}$$

$$\beta^{(3)}(S-L) = \beta^{(4)}(S-L) \tag{A.25m}$$

$$W^{(6)}(S-L) = 0 \tag{A.25n}$$

$$N_M{}^{(2)}(S-L) = N_M{}^{(5)}(S-L) \tag{A.25o}$$

$$N_M{}^{(3)}(S-L) = N_M{}^{(4)}(S-L) \tag{A.25p}$$

$$M_M{}^{(2)}(S-L) = M_M{}^{(5)}(S-L) \tag{A.25q}$$

$$M_M{}^{(3)}(S-L) = M_M{}^{(4)}(S-L) \tag{A.25r}$$

Substituting Equations (A.17a-q) into Equations (A.5a-A.16b) and solving for the unknowns, the solutions for α_i, θ_j and ψ_k can be derived.

The values of α_i (i=1, 2….6) are derived as,

$$\alpha_4 = \alpha_5 = \alpha_6 = \frac{N + N_T}{A_{22}} \tag{A.26a}$$

Where,

$$N_T = 2\left[\bar{Q}_{22}{}^{(1)}h^{(1)}\int_{T_{ref}}^{T_f}\alpha_y{}^{(1)}dT + \bar{Q}_{22}{}^{(2)}h^{(2)}\int_{T_{ref}}^{T_f}\alpha_y{}^{(2)}dT + \bar{Q}_{22}{}^{(3)}h^{(3)}\int_{T_{ref}}^{T_f}\alpha_y{}^{(3)}dT\right] \tag{A.26b}$$

By solving the three equations given below, the values of α_1, α_2 and α_3 can be derived.

$$\sum_{j=1}^{3}\alpha_j\left\{\cosh(\lambda_j(S-L))\left[\lambda_j - \frac{\eta_j^{(3)}B_{22}^{(3)}}{A_{22}^{(3)}D_{22}^{(3)}}\right]\right.$$

$$\left. -\sinh(\lambda_j(S-L))\left[\frac{\omega(e^{\omega(S-L)} + e^{\omega(S+L)})}{D_{22}^{(3)}(e^{\omega(S-L)} - e^{\omega(S+L)})}\left(D_{22}^{(3)} - \frac{(B_{22}^{(3)})^2}{A_{22}^{(3)}}\right)\right]\right\} = 0 \tag{A.27a}$$

$$\sum_{j=1}^{3}\alpha_j\left[\eta_j^{(3)}\cosh(\lambda_j(S-L))\right] = -\left[\frac{A_{22}^{(2)}(N+N_T)}{A_{22}} - \bar{Q}_{22}^{(2)}h^{(2)}\int_{T_{ref}}^{T_f}\alpha_y{}^{(2)}dT\right] \tag{A.27b}$$

$$\sum_{j=1}^{3}\alpha_j\sinh(\lambda_j(S-L))\left(\gamma_j^{(1)} - \gamma_j^{(2)} - \frac{h^{(2)}}{2}P_j^{(2)} - \frac{h^{(1)}}{2}P_j^{(1)}\right) = 0 \tag{A.27c}$$

The values of ψ_k (k=1, 2, 3) are derived as,

$$\psi_1 = \frac{\sum_{j=1}^{3}\alpha_j\sinh(\lambda_j(S-L))}{(e^{\omega(S-L)} - e^{\omega(S+L)})} \tag{A.28a}$$

$$\psi_2 = -\psi_1 e^{2\omega S} \tag{A.28b}$$

$$\psi_3 = \frac{\sum_{j=1}^{3} \alpha_j \eta_j^{(3)} \cosh(\lambda_j (S-L))}{A_{22}^{(3)}} + \frac{N+N^T}{A_{22}} \tag{A.28c}$$

$$\psi_4 = \sum_{j=1}^{3} \alpha_j \gamma_j^{(3)} \sinh(\lambda_j (S-L)) - \psi_3 (S-L)$$

$$+ \frac{B_{22}^{(3)}}{A_{22}^{(3)}} \psi_1 (e^{\omega(S-L)} - e^{\omega(S+L)}) + \frac{N+N^T}{A_{22}} (S-L) \tag{A.28c}$$

The values of θ_j (k=1, 2…9) are derived as,

$$\theta_1 = \frac{\sum_{j=1}^{3} \alpha_j P_j^{(2)} \sinh(\lambda_j (S-L))}{e^{\omega_1 (S-L)}} - \theta_2 e^{-2\omega_1 (S-L)} \tag{A.28a}$$

$$\theta_2 = \frac{\sum_{j=1}^{3} \alpha_j P_j^{(2)} \left[\omega_1 \sinh(\lambda_j (S-L)) - \lambda_j \cosh(\lambda_j (S-L)) \right] (e^{-2\omega_1 (S-L)})}{2} \tag{A.28b}$$

$$\theta_3 = \left[\frac{\bar{Q}_{22}^{(2)} h^{(2)}}{A_{22}^{(2)}} \int_{T_{ref}}^{T_f} \alpha_y^{(2)} dT \right] \tag{A.28c}$$

$$\theta_4 = \sum_{j=1}^{3} \alpha_j \gamma_j^{(2)} \sinh(\lambda_j (S-L)) + \left[\frac{N+N_T}{A_{22}} - \frac{\bar{Q}_{22}^{(2)} h^{(2)}}{A_{22}^{(2)}} \int_{T_{ref}}^{T_f} \alpha_y^{(2)} dT \right] (S-L) \tag{A.28d}$$

$$\theta_5 = \frac{\sum_{j=1}^{3} \alpha_j P_j^{(1)} \sinh(\lambda_j (S-L))}{-L} \tag{A.28e}$$

$$\theta_6 = -\theta_5 S \tag{A.28f}$$

$$\theta_7 = \frac{-2B_{22}^{(1)} \theta_5 - 2A_{22}^{(3)} \psi_3 + N + N_T - 2\bar{Q}_{22}^{(2)} h^{(2)} \int_{T_{ref}}^{T_f} \alpha_y^{(2)} dT}{2A_{22}^{(1)}} \tag{A.28g}$$

$$\theta_8 = \sum_{j=1}^{3} \alpha_j \gamma_j^{(1)} \sinh(\lambda_j (S-L)) + \frac{A_{22}^{(3)}}{A_{22}^{(1)}} \psi_3 (S-L) + \frac{B_{22}^{(1)}}{A_{22}^{(1)}} \theta_5 (S-L)$$

$$-(S-L)\left[\frac{N + N_T - 2\bar{Q}_{22}^{(2)} h^{(2)} \int_{T_{ref}}^{T_f} \alpha_y^{(2)} dT}{2A_{22}^{(1)}} - \frac{N + N_T}{A_{22}} \right] \quad \text{(A.28h)}$$

$$\theta_9 = -\frac{1}{2} \theta_5 (S^2 - L^2) \quad \text{(A.28i)}$$

All the 18 constants, namely α_i, θ_j and ψ_k (i=1, 2…6; j=1, 2…9; k=1, 2, 3) were solved above and used in the solutions for force, displacement and moment equations. The remaining constants used in the various expressions are given in Zhang [13] and Roy and Benjamin [18].

A.3.5 Delaminated Crack Opening Displacement (DCOD)

The delaminated crack opening displacement (DCOD) calculated at the interface of sublaminate 4 and 5 at y=S for a given delamination length L and crack density 1/2S is given by,

$$DCOD_{top} = v^{(6)}(S, -\frac{h^{(1)}}{2}) - v^{(5)}(S, \frac{h^{(2)}}{2}) \quad \text{(A.29a)}$$

$$DCOD_{bottom} = v^{(4)}(S, \frac{h^{(3)}}{2}) - v^{(5)}(S, \frac{-h^{(2)}}{2}) \quad \text{(A.29b)}$$

Using the above equations, DCOD for any given delamination length, crack density and loading condition (mechanical and/or thermal) can be obtained at any intermediate position of a sublaminate.

APPENDIX B

THREE LAYER MODEL LAMINATE ANALYSIS

B.1 Introduction

In this section, an expression for DCOD derived based on a two-dimensional first-order shear laminate theory is applied to the three-layer model (TLM) laminate shown in Fig.B.1. Assuming symmetry of geometry and loading, only one quarter of the three-layer laminate is modeled as shown in Fig.B.2, corresponding to case 2 as discussed earlier. Transverse matrix cracks are assumed to exist in the 90º plies with uniform crack spacing of 2S. Local delaminations of length 2L are assumed to initiate and grow in a symmetric manner from tips of each transverse matrix crack and span the entire width of the laminate. The modeled portion of length S is divided into four sublaminates as shown numbered in Fig.B.2. Plain strain condition is assumed in the width direction of the model. Two local coordinates are used for the model as shown in Fig.B.2.

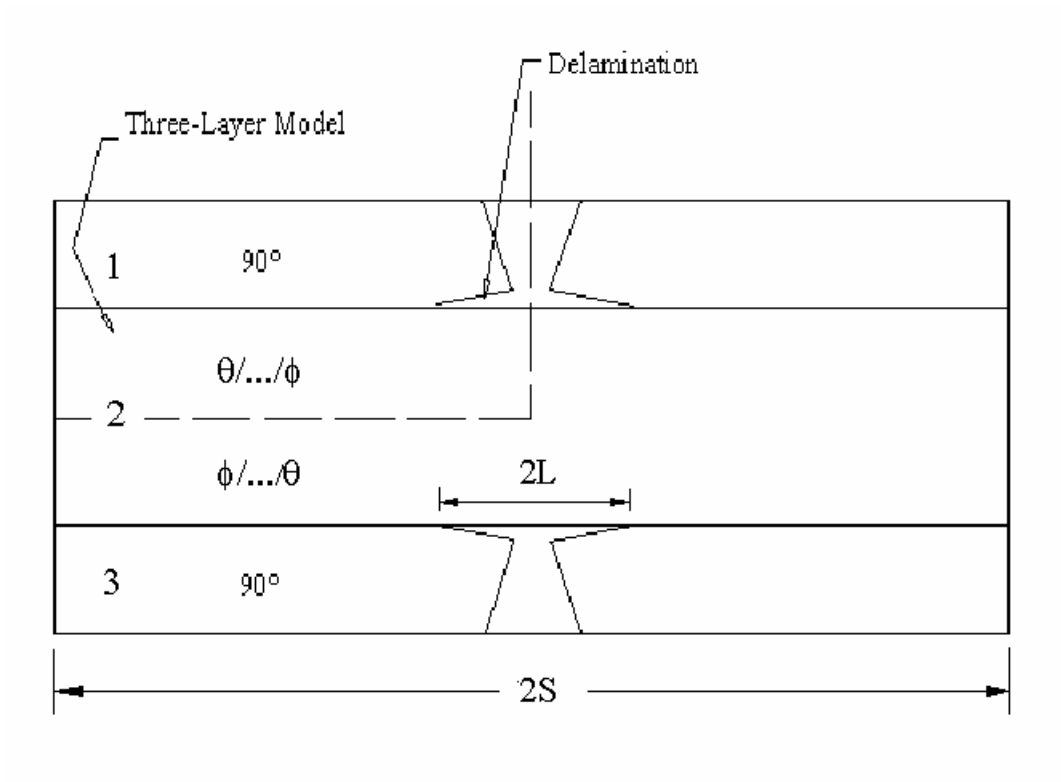

Fig.B.1 Three-layer model for the cracked and delaminated laminates (case 2)

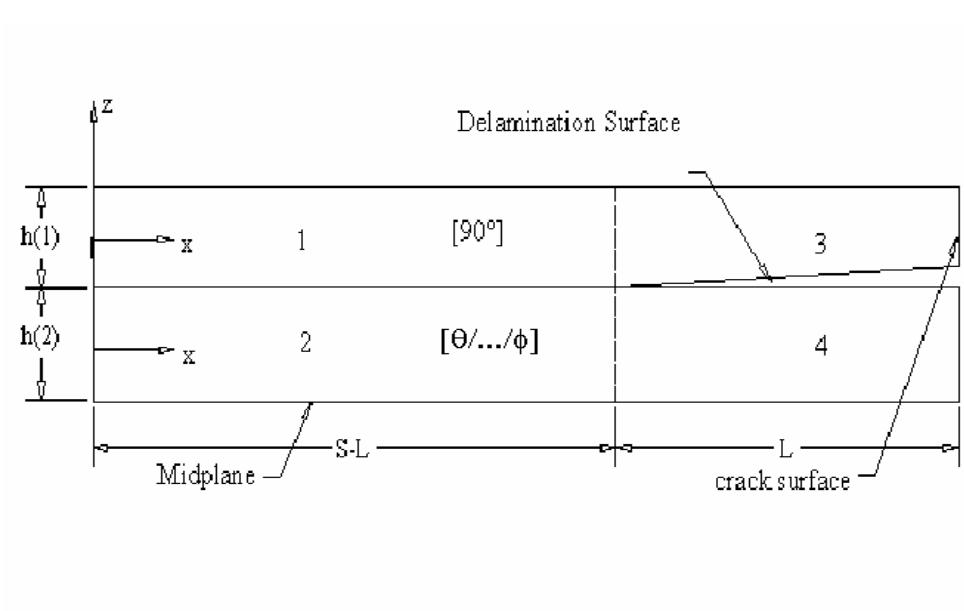

Fig.B.2 one quarter of the repeating interval of the three-layer model laminate (case 2)

Assuming that the displacements in x and z directions within each sublaminate can be given by,

$$u(x,z) = U(x) + z\beta(x) \tag{B.1a}$$

$$w = W(x) \tag{B.1b}$$

Where,

U(x) is the x displacement of mid-surface of the sublaminate.

β(x) is the slope of the sublaminate mid-surface in x direction.

W(x) is the z displacement of mid-surface of the sublaminate.

The force and moment equilibrium equations for each sub-laminate are,

$$N_{,x} + T_t - T_b = 0 \tag{B.2a}$$

$$M_{,x} - Q + \frac{h}{2}\left(T_t + T_b\right) = 0 \tag{B.2b}$$

$$Q_{,x} + P_t - P_b = 0 \tag{B.2c}$$

where N, Q and M are the axial force, shear force and bending moment resultants respectively. P and T denote interlaminar peel and shear stresses with subscripts t and b denoting top and bottom surfaces. Combining the strain-displacement relations with Equations (B.1a, B.1b) and the in-plane stress-strain relationships of a lamina, the force-displacement relationships of a sublaminate are,

$$N_M = A_{11}U_{,x} + B_{11}\beta_{,x} - \bar{Q}_{11}h\int_{T_{ref}}^{T_f} \alpha_x dT \tag{B.3a}$$

$$M_M = B_{11}U_{,x} + D_{11}\beta_{,x} - \bar{Q}_{11}h\bar{Z}\int_{T_{ref}}^{T_f} \alpha_x dT \tag{B.3b}$$

$$Q = A_{44}(\beta + W_{,x}) \tag{B.3c}$$

Where, A_{11}, B_{11}, D_{11} and A_{44} are components of the A, B and D matrix from classical lamination theory. For the two-dimensional orthotropic model the other stiffness components of the anisotropic sublaminate do not appear in the constitutive equations due to the assumption of plane strain with respect to the width of the specimen. h is the thickness of the lamina; $\overline{Z}$ is centroidal distance of the lamina from laminate midplane; α_x is the coefficient of thermal expansion in x-direction and is given by the nonlinear function $C_0+C_1T_f+C_2T_f^2$. In the above equations, non-linear material properties with respect to temperature T_f are used in calculating the thermal forces and moments. The components of A, B, D and $\overline{Q}$ matrix are assumed to be nonlinear functions of temperature T_f. Substitution of Equations (B.3a-B.3c) into Equations (B.2a-B.2c) gives,

$$A_{11}U,_{xx} + B_{11}\beta,_{xx} + T_t - T_b = 0 \tag{B.4a}$$

$$\left(D_{11} - \frac{B_{11}^{\ 2}}{A_{11}}\right)\beta,_{xx} - A_{44}\left(\beta + W,_x\right) + \left(\frac{h}{2} - \frac{B_{11}}{A_{11}}\right)T_t + \left(\frac{h}{2} + \frac{B_{11}}{A_{11}}\right)T_b = 0 \tag{B.4b}$$

$$A_{44}\left(\beta,_x + W,_{xx}\right) + P_t - P_b = 0 \tag{B.4c}$$

B.2 Laminated Portion: Sublaminates 1 and 2

Following the derivation procedure given by Zhang [13] and Roy and Benjamin [18] with modifications for asymmetric sublaminates 2 and 4 resulting in existence of B_{22} for these sublaminates, the solutions for force, moment, and displacement for sublaminate 1 and 2 are given as,

$$\beta^{(1)} = \alpha_1 P_1 \sinh(\lambda_1 x) + \alpha_2 P_2 \sinh(\lambda_2 x) \tag{B.5a}$$

$$\beta^{(2)} = \alpha_1 \sinh(\lambda_1 x) + \alpha_2 \sinh(\lambda_2 x) \tag{B.5b}$$

The displacements of the mid plane of the sublaminates are,

$$U^{(1)} = \alpha_1 \gamma_1^{(1)} \sinh(\lambda_1 x) + \alpha_2 \gamma_2^{(1)} \sinh(\lambda_2 x) + \alpha_3 x \tag{B.6a}$$

$$U^{(2)} = \alpha_1 \gamma_1^{(2)} \sinh(\lambda_1 x) + \alpha_2 \gamma_2^{(2)} \sinh(\lambda_2 x) + \alpha_4 x \tag{B.6b}$$

The force and moment resultants are,

$$N_M^{(1)} = \alpha_1 \eta_1^{(1)} \cosh(\lambda_1 x) + \alpha_2 \eta_2^{(1)} \cosh(\lambda_2 x) + A_{11}^{(1)} \alpha_3 - \bar{Q}_{11}^{(1)} h^{(1)} \int_{T_{ref}}^{T_f} \alpha_x^{(1)} dT \tag{B.7a}$$

$$N_M^{(2)} = \alpha_1 \eta_1^{(2)} \cosh(\lambda_1 x) + \alpha_2 \eta_2^{(2)} \cosh(\lambda_2 x) + A_{11}^{(2)} \alpha_4 - \bar{Q}_{11}^{(2)} h^{(2)} \int_{T_{ref}}^{T_f} \alpha_x^{(2)} dT \tag{B.7b}$$

$$M_M^{(1)} = \alpha_1 \xi_1^{(1)} \cosh(\lambda_1 x) + \alpha_2 \xi_2^{(1)} \cosh(\lambda_2 x) - \bar{Q}_{11}^{(1)} h^{(1)} \bar{Z}^{(1)} \int_{T_{ref}}^{T_f} \alpha_x^{(1)} dT \tag{B.8a}$$

$$M_M^{(2)} = \alpha_1 \xi_1^{(2)} \cosh(\lambda_1 x) + \alpha_2 \xi_2^{(2)} \cosh(\lambda_2 x) + B_{11}^{(2)} \alpha_4 - \bar{Q}_{11}^{(2)} h^{(2)} \bar{Z}^{(2)} \int_{T_{ref}}^{T_f} \alpha_x^{(2)} dT$$

(B.8b)

Where α_i (i=1, 2…4) are undetermined constants and the remaining constants are given in appendix C, which are not exactly same as given by Zhang [13] due to existence of $B_{11}^{(2)}$.

B.3 Delaminated Portion

B.3.1 Sublaminate 3

The symmetry of the laminate and condition of traction-freedom at the upper surface of the sublaminate 3 implies,

$$W^{(3)}(x) = 0 \qquad T_b^{(3)} = 0 \qquad T_t^{(3)} = 0 \qquad P_b^{(3)} = 0 \qquad P_t^{(3)} = 0 \tag{B.9a-e}$$

Applying Equations (B.4a-c) to Equations (B.9a-e),

$$A_{11}{}^{(1)}U,_{xx}{}^{(3)} = 0 \tag{B.10a}$$

$$D_{11}{}^{(1)}\beta,_{xx}{}^{(3)} - A_{44}{}^{(1)}\beta^{(3)} = 0 \tag{B.10b}$$

$$A_{44}{}^{(1)}\beta,_{x}{}^{(3)} = 0 \tag{B.10c}$$

From Equation (B.10c) and Equation (B.10a)

$$\beta^{(3)} = \psi_1 \tag{B.11a}$$

$$U^{(3)} = \psi_2 x + \psi_3 \tag{B.11b}$$

Substitution of Equations (B.11a, b) into Equations (B.3a, b) results in,

$$N_M{}^{(3)} = A_{11}{}^{(1)}\psi_2 - \bar{Q}_{11}{}^{(1)}h^{(1)}\int_{T_{ref}}^{T_f} \alpha_x{}^{(1)}dT \tag{B.12a}$$

$$M_M{}^{(3)} = -\bar{Q}_{11}{}^{(1)}h^{(1)}\bar{Z}^{(1)}\int_{T_{ref}}^{T_f} \alpha_x{}^{(1)}dT \tag{B.12b}$$

B.3.2 Sublaminate 4

The peel and shear stresses at top and bottom surface of the sublaminate 4 are given as,

$$T_b{}^{(4)} = 0 \qquad T_t{}^{(4)} = 0 \tag{B.13a, b}$$

$$P_t^{(4)} = 0 \tag{B.13c}$$

Due to symmetry of laminate,

$$W^{(4)}(x) = 0 \tag{B.13d}$$

Substituting Equations (B.13a-d) into Equations (B.4a-c)

$$A_{11}{}^{(2)}U,_{xx}{}^{(4)} - B_{11}{}^{(2)}\beta,_{xx}^{(4)} = 0 \tag{B.14a}$$

$$\left(D_{11}{}^{(2)} - \frac{(B_{11}{}^{(2)})^2}{A_{11}{}^{(2)}} \right) \beta_{,xx}{}^{(4)} - A_{44}{}^{(2)} \beta^{(4)} = 0 \tag{B.14b}$$

$$A_{44}{}^{(2)} \beta_{,x}{}^{(4)} = P_b^{(4)} \tag{B.14c}$$

From Equations (B.14a-c)

$$\beta^{(4)} = \theta_1 e^{\omega_2 x} + \theta_2 e^{-\omega_2 x} \tag{B.15a}$$

where,

$$\omega_2 = \sqrt{\frac{A_{44}^{(2)}}{\left(D_{11}^{(2)} - \frac{(B_{11}^{(2)})^2}{A_{11}^{(2)}} \right)}}$$

$$U^{(4)} = -\frac{B_{11}^{(2)}}{A_{11}^{(2)}} (\theta_1 e^{\omega_2 x} + \theta_2 e^{-\omega_2 x}) + \theta_3 x + \theta_4 \tag{B.15b}$$

Substitution of Equations (B.15a, b) into Equations (B.3a, b) results in,

$$N_M{}^{(4)} = A_{11}{}^{(2)} \theta_3 - \bar{Q}_{11}{}^{(2)} h^{(2)} \int_{T_{ref}}^{T_f} \alpha_x{}^{(2)} dT \tag{B.16a}$$

$$M_M{}^{(4)} = (\theta_1 e^{\omega_2 x} - \theta_2 e^{-\omega_2 x}) \left(D_{11}^{(2)} - \frac{(B_{11}^{(2)})^2}{A_{11}^{(2)}} \right) \omega_2 + B_{11}^{(2)} \theta_3 - \bar{Q}_{11}{}^{(2)} h^{(2)} \bar{Z}^{(2)} \int_{T_{ref}}^{T_f} \alpha_x{}^{(2)} dT \tag{B.16b}$$

B.4 Determining Constants α_i, θ_j and ψ_k

In order to determine the eleven constants the same number of independent boundary and continuity conditions has to be described. Assuming the laminate is subjected to tension force N and thermal load ΔT, the interfacial continuity conditions and boundary conditions are enforced as,

$$\beta^{(4)}(S) = 0 \tag{B.17a}$$

$$N_M{}^{(4)}(S) = \frac{1}{2} N \tag{B.17b}$$

$$N_M{}^{(1)}(0) + N_M{}^{(2)}(0) = \frac{1}{2}N \tag{B.17c}$$

$$N_M{}^{(3)}(S) = 0 \tag{B.17d}$$

$$u^{(3)}(S-L, -\frac{h^{(1)}}{2}) = u^{(4)}(S-L, \frac{h^{(2)}}{2}) \tag{B.17e}$$

$$U^{(1)}(S-L) = U^{(3)}(S-L) \tag{B.17f}$$

$$U^{(2)}(S-L) = U^{(4)}(S-L) \tag{B.17g}$$

$$\beta^{(1)}(S-L) = \beta^{(3)}(S-L) \tag{B.17h}$$

$$\beta^{(2)}(S-L) = \beta^{(4)}(S-L) \tag{B.17i}$$

$$N_M{}^{(2)}(S-L) = N_M{}^{(4)}(S-L) \tag{B.17j}$$

$$M_M{}^{(1)}(S-L) = M_M{}^{(3)}(S-L) \tag{B.17k}$$

$$M_M{}^{(2)}(S-L) = M_M{}^{(4)}(S-L) \tag{B.17l}$$

Substituting Equations (B.17a-l) into Equations (B.5a-B.16c) gives,

$$\theta_1 e^{\omega_2 S} + \theta_2 e^{-\omega_2 S} = 0 \tag{B.18a}$$

$$A_{11}{}^{(2)}\theta_3 - \bar{Q}_{11}{}^{(2)}h^{(2)}\int_{T_{ref}}^{T_f} \alpha_x{}^{(2)}dT = \frac{1}{2}N \tag{B.18b}$$

$$A_{11}{}^{(1)}\alpha_3 + A_{11}{}^{(2)}\alpha_4 = \frac{1}{2}N + \frac{1}{2}N_T \tag{B.18c}$$

Where, $$N_T = 2\left[\bar{Q}_{11}{}^{(1)}h^{(1)}\int_{T_{ref}}^{T_f} \alpha_x{}^{(1)}dT + \bar{Q}_{11}{}^{(2)}h^{(2)}\int_{T_{ref}}^{T_f} \alpha_x{}^{(2)}dT\right]$$

$$A_{11}{}^{(1)}\psi_2 - \bar{Q}_{11}{}^{(1)}h^{(1)}\int_{T_{ref}}^{T_f} \alpha_x{}^{(1)}dT = 0 \tag{B.18d}$$

$$\alpha_1\gamma_1{}^{(1)}\sinh(\lambda_1(S-L)) + \alpha_2\gamma_2{}^{(1)}\sinh(\lambda_2(S-L)) + \alpha_3(S-L) = \psi_2(S-L) + \psi_3 \tag{B.18e}$$

$$\alpha_1\gamma_1^{(2)}\sinh(\lambda_1(S-L))+\alpha_2\gamma_2^{(2)}\sinh(\lambda_2(S-L))+\alpha_4(S-L)$$

$$=-\frac{B_{22}^{(1)}}{A_{22}^{(1)}}(\theta_1 e^{\omega_2(S-L)}+\theta_2 e^{-\omega_2(S-L)})+\theta_3(S-L)+\theta_4 \tag{B.18f}$$

$$\alpha_1 P_1\sinh(\lambda_1(S-L))+\alpha_2 P_2\sinh(\lambda_2(S-L))=\psi_1 \tag{B.18g}$$

$$\alpha_1\sinh(\lambda_1(S-L))+\alpha_2\sinh(\lambda_2(S-L))=(\theta_1 e^{\omega_2(S-L)}+\theta_2 e^{-\omega_2(S-L)}) \tag{B.18h}$$

$$-\alpha_1\eta_1^{(2)}\cosh(\lambda_1(S-L))-\alpha_2\eta_2^{(2)}\cosh(\lambda_2(S-L))+A_{11}^{(2)}\alpha_4=A_{11}^{(2)}\theta_3 \tag{B.18i}$$

$$\alpha_1\xi_1^{(1)}\cosh(\lambda_1(S-L))+\alpha_2\xi_2^{(1)}\cosh(\lambda_2(S-L))=0 \tag{B.18j}$$

$$\alpha_1\xi_1^{(2)}\cosh(\lambda_1(S-L))+\alpha_2\xi_2^{(2)}\cosh(\lambda_2(S-L))+B_{11}^{(2)}\alpha_4$$

$$=(\theta_1 e^{\omega_2(S-L)}-\theta_2 e^{-\omega_2(S-L)})\left(D_{11}^{(2)}-\frac{(B_{11}^{(2)})^2}{A_{11}^{(2)}}\right)\omega_2+B_{11}^{(2)}\theta_3 \tag{B.18K}$$

From Equation (B.18a)

$$\theta_2=-\theta_1 e^{2\omega_2 S} \tag{B.19a}$$

From Equation (B.18b)

$$\theta_3=\frac{N-2\bar{Q}_{11}^{(2)}h^{(2)}\int_{T_{ref}}^{T_f}\alpha_x^{(2)}dT}{2A_{11}^{(2)}} \tag{B.19b}$$

From Equation (B.18c)

$$\alpha_3=\alpha_4=\frac{N+N_T}{A_{11}} \tag{B.19c}$$

From Equation (B.18d)

$$\psi_2=\frac{\bar{Q}_{11}^{(1)}h^{(1)}\int_{T_{ref}}^{T_f}\alpha_x^{(1)}dT}{A_{11}^{(1)}} \tag{B.19d}$$

Substituting Equation (B.19a) in Equation (B.18h) gives,

$$\theta_1 = \frac{\left[\alpha_1 \sinh(\lambda_1(S-L)) + \alpha_2 \sinh(\lambda_2(S-L))\right]}{(e^{\omega_2(S-L)} - e^{\omega_2(S+L)})} \qquad \text{(B.19e)}$$

Substituting Equation (B.19e) in Equation (B.18k) gives,

$$\alpha_1 \sinh(\lambda_1(S-L))\left[\gamma_1^{(2)} + \frac{h^{(2)}}{2} - \gamma_1^{(1)} + \frac{h^{(1)}}{2} P_1\right]$$

$$+\alpha_2 \sinh(\lambda_2(S-L))\left[\gamma_2^{(2)} + \frac{h^{(2)}}{2} - \gamma_2^{(1)} + \frac{h^{(1)}}{2} P_2\right] = 0 \qquad \text{(B.19f)}$$

Equation (B.18i) can be modified as,

$$\alpha_1 \eta_1^{(2)} \cosh(\lambda_1(S-L)) + \alpha_2 \eta_2^{(2)} \cosh(\lambda_2(S-L)) = A_{11}{}^{(2)}(\theta_3 - \alpha_4) \qquad \text{(B.19g)}$$

Equation (B.19f) and Equation (B.19g) can be solved for α_1 and α_2 as shown below,

$$\alpha_1 = \frac{-\alpha_2 Q}{P} \qquad \text{(B.19h)}$$

$$\alpha_2 = \frac{-PA_{11}{}^{(2)}(\theta_3 - \alpha_4)}{RQ - PS} \qquad \text{(B.19i)}$$

Where, $$P = \sinh(\lambda_1(S-L))\left[\gamma_1^{(2)} + \frac{h^{(2)}}{2} - \gamma_1^{(1)} + \frac{h^{(1)}}{2} P_1\right]$$

$$Q = \sinh(\lambda_2(S-L))\left[\gamma_2^{(2)} + \frac{h^{(2)}}{2} - \gamma_2^{(1)} + \frac{h^{(1)}}{2} P_2\right]$$

$$R = \eta_1^{(2)} \cosh(\lambda_1(S-L))$$

$$S = \eta_2^{(2)} \cosh(\lambda_2(S-L))$$

From Equation (B.18g)

$$\psi_1 = \alpha_1 P_1 \sinh(\lambda_1(S-L)) + \alpha_2 P_2 \sinh(\lambda_2(S-L)) \qquad \text{(B.19k)}$$

From Equation (B.18e)

$$\psi_3 = \alpha_1 \gamma_1^{(1)} \sinh(\lambda_1(S-L)) + \alpha_2 \gamma_2^{(1)} \sinh(\lambda_2(S-L)) + (\alpha_3 - \psi_2)(S-L) \qquad \text{(B.19l)}$$

From Equation (B.18f)

$$\theta_4 = \alpha_1 \gamma_1^{(2)} \sinh(\lambda_1(S-L)) + \alpha_2 \gamma_2^{(2)} \sinh(\lambda_2(S-L)) + (\alpha_4 - \theta_3)(S-L)$$

$$+ \frac{B_{22}^{(1)}}{A_{22}^{(1)}} (\theta_1 e^{\omega_2(S-L)} + \theta_2 e^{-\omega_2(S-L)}) \qquad \text{(B.19m)}$$

All the 11 constants, namely α_i, θ_j and ψ_k (i=1, 2…4; j=1, 2…4; k=1, 2, 3) were solved above and used in the solutions for force, displacement and moment equations.

B.5 Delaminated Crack Opening Displacement (DCOD)

The delaminated crack opening displacement (DCOD) calculated at the interface of sublaminate 3 and 4 at y=S for a given delamination length L and crack density 1/2S is given by,

$$DCOD = u^{(4)}(S, \frac{h^{(2)}}{2}) - u^{(3)}(S, \frac{-h^{(1)}}{2}) \qquad \text{(B.20a)}$$

Using the above equations, DCOD for any given delamination length, crack density and loading condition (mechanical and/or thermal) can be found.

APPENDIX C

CONSTANTS IN THREE LAYER MODEL LAMINATE ANALYSIS

C.1 List of Constants in Three-Layer Model Laminate Analysis

$$A_{11} = 2(A_{11}{}^{(1)} + A_{11}{}^{(2)}) \tag{C.1}$$

$$\chi = \frac{A_{11}{}^{(2)}}{A_{11}{}^{(1)}} \tag{C.2}$$

$$a_{22} = D_{11}{}^{(2)} - \frac{B_{11}{}^{(2)^2}}{A_{11}{}^{(2)}} + \frac{(-2B_{11}{}^{(2)} + h^{(2)}A_{11}{}^{(2)})A_{11}{}^{(1)}}{2A_{11}{}^{(1)^2}A_{11}} \tag{C.3}$$

$$a_{12} = a_{21} = \frac{h^{(1)}(h^{(1)}A_{11}^{(2)} - 2B_{11}^{(2)})A_{11}{}^{(1)}}{2A_{11}} \tag{C.4}$$

$$a_{11} = D_{11}{}^{(1)} + \frac{h^{(1)2}A_{11}{}^{(2)}A_{11}{}^{(1)}}{2A_{11}} \tag{C.5}$$

$$\lambda_1{}^2, \lambda_2{}^2 = \frac{-b \pm \sqrt{b^2 - 4ac}}{2a} \tag{C.6}$$

Where,

$$a = a_{11}a_{22} - a_{12}{}^{2}$$

$$b = -(a_{11}A_{44}{}^{(2)} + a_{22}A_{44}{}^{(1)})$$

$$c = A_{44}{}^{(1)}A_{44}{}^{(2)})$$

For j=1 and 2, the constants are,

$$P_j = -\frac{a_{12}\lambda_j{}^{2}}{a_{11}\lambda_j{}^{2} - A_{44}{}^{(1)}} \tag{C.7}$$

$$\gamma_j{}^{(1)} = \frac{P_j(h^{(1)}A_{11}{}^{(2)} + h^{(2)}A_{11}{}^{(2)} - 2B_{11}{}^{(1)})}{A_{11}} \tag{C.8}$$

$$\gamma_j{}^{(2)} = -\frac{P_j(h^{(1)}A_{11}{}^{(1)}) + 2B_{11}{}^{(1)} + h^{(2)}A_{11}{}^{(1)}}{A_{11}} \tag{C.9}$$

$$\eta_1^{(1)} = (A_{11}{}^{(1)}\gamma_1{}^{(1)})\lambda_1 \tag{C.10}$$

$$\eta_2^{(1)} = (A_{11}{}^{(1)}\gamma_2{}^{(1)})\lambda_2 \tag{C.11}$$

$$\eta_1^{(2)} = (B_{11}{}^{(2)} + A_{11}{}^{(2)}\gamma_1{}^{(2)})\lambda_1 \tag{C.12}$$

$$\eta_2^{(2)} = (B_{11}{}^{(2)} + A_{11}{}^{(2)}\gamma_2{}^{(2)})\lambda_2 \tag{C.13}$$

$$\xi_j{}^{(1)} = (D_{11}{}^{(1)}P_j + B_{11}{}^{(1)}\gamma_j{}^{(1)})\lambda_j \tag{C.14}$$

$$\xi_j{}^{(2)} = D_{11}{}^{(2)}\lambda_j \tag{C.15}$$

VITA

Abhijeet Utturkar

Candidate for the Degree of

Master of Science

Thesis: PERMEABILITY MODELING OF SYMMETRIC GRAPHITE EPOXY LAMINATES WITH ARBITRARY PLY ORIENTATIONS

Major Field: Mechanical Engineering

Biographical:

Personal data: Born in Pune, India, On April 04, 1980, the son of Vikas and Supriya Utturkar.

Education: Received Bachelor of Engineering degree in Mechanical Engineering from University of Pune, India in June 2001. Completed requirements for Master of Science degree with a major in Mechanical and Aerospace Engineering at Oklahoma State University in May 2005.

Experience: Graduate Research Assistant in Mechanical and Aerospace Engineering Department, Oklahoma State University, Stillwater, Oklahoma, August, 2003 – December, 2004. Graduate Teaching Assistant in Mechanical and Aerospace Engineering Department, Oklahoma State University, Stillwater, Oklahoma, August, 2002 – December, 2004.

Name: Abhijeet Utturkar Date of Degree: May, 2005

Institution: Oklahoma State University Location: Stillwater, Oklahoma

Title of Study: PERMEABILITY MODELING OF SYMMETRIC GRAPHITE EPOXY LAMINATES WITH ARBITRARY PLY ORIENTATIONS

Pages in Study: 108 Candidate for the Degree of Master of Science

Major Field: Mechanical Engineering

Scope and Methodology of Study: Composites are extensively used for various aerospace applications and one of the important uses is as cryogenic fuel tank materials for RLV and ELV. Composites offer high strength to weight ratio and therefore are preferred to many other materials. In number of cases, arbitrarily orientated ply laminates are used to optimize various desirable properties and weight of the structure. However under structural mechanical loads and/or thermal loads due to change in temperature conditions, transverse micro-cracks are developed in the polymer matrix. These cracks along with interlaminar delaminations produced at the crack tips, lead to passage of cryogenic fuel permeation through the laminates. In this thesis, a mathematical model has been developed to find the delaminated crack opening for each ply throughout the thickness of laminate and permeability of symmetric arbitrarily orientated ply graphite epoxy laminates subjected to different load conditions.

Findings and Conclusions: In this thesis, an expression for predicting delaminated crack opening displacement in symmetric arbitrarily oriented ply graphite epoxy laminates has been derived using first order shear deformation theory applied to five layer and three layer models. This expression for DCOD depends on crack length, delamination length, crack spacing and load conditions. The DCOD predicted by mathematical model showed good agreement with finite element analysis results. These predicted DCOD values are used to find out permeability of given laminate using Darcy's law of isothermal, viscous fluid flow of gases through porous media. Permeability can be predicted for more general symmetric ply laminate configurations with $[\theta_1/\theta_2/\theta_3/\theta_4]_s$, various orientations and thickness. These observations have been made for IM7/PETI-5 graphite epoxy laminate system and conclusions may not be transferable to other types of laminates.